Università Campus Bio-Medico di Roma

PhD Course in Science and Engineering for Humans and the Environment

XXXVII Cycle

a.a. 2021/2022

CO_2 Methanation

From micro to macro scale

Coordinator

Prof. Giulio Iannello

Supervisor

Prof. Marcello De Falco

Co-supervisor

Prof. Mauro Capocelli

Ph.D. Candidate

Marco Facchino

Department of Science and Technology
for the Sustainable Development and One Health
Unit of Process Engineering

Summary

List of Figures

List of Tables

Preface

More than any other time in human history, society is experiencing a systemic and multi-facet crisis that is threatening its existence on Earth. From the institution and academic perspective, the pandemic crisis and the ongoing conflicts in Eastern Europe and in the Middle East exacerbated the magnitude of the unsolved issues of inequality, development and environmental mitigation, constituting the so-called Global Energy Trilemma (GET) [1,2].

Since the onset of the Industrial Revolution, atmospheric carbon dioxide (CO_2) concentrations have risen prominently, from approximately 277 ppm in 1750 to 422.5 ppm in 2024, representing an increase of over 50% [3]. The threats behind the presence of high CO_2 concentrations in the atmosphere emerged way after the discovery of the greenhouse effect by Jean-Baptiste in 1824 [4], with first investigations performed by John Tyndall [5] pointing out that water vapour was the main *blanket* which trapped solar radiations inside the atmosphere. The prominent role of CO_2 in this phenomenon was first assessed by Svante Arrhenius [6]in 1896, who also correlated the average Earth temperature to CO_2 concentrations and outlined potential increases of about 5 °C in case the concentration would have double. Later, the *Carbon Dioxide Theory* of Plass, published in 1956, confirmed that the continue emissions of CO_2 from industries using fossil fuels as either energy sources or feedstock would have led to a 1.1 °C increase in the mean global temperature each century. Since then, concerns on climate change and discussion on how to fight it began, and in 1981 Wigley and Jones [7] stated that "[...] *atmospheric CO_2 concentration will probably become sufficiently high (and we will be committed to further increases) that a climatic change significantly larger that any which has occurred in the past century could be unavoidable*". In those years, the scientific community reached a wider agreement on the role of CO_2 as the main greenhouse gas (GHS), as well as on the role of industrial emitters and on the threats posed by climate change on economic growth and human well-being. In 1988, the United Nations Environment Programme (UNEP) established the Intergovernmental Panel on Climate Change (IPCC) to closely monitor climate change trends and promote knowledge and understanding of the phenomenon, thereby guiding policymakers in developing appropriate strategies. In 1990, the IPCC First Assessment Report [8]identified human-driven GHGs emissions as the main driver of the current rate of climate change and concluded that keeping the current rate of CO_2 emissions would have led to an average global temperature increase of 0.2 °C per decade. Amid rising awareness of the hiding costs of fossil fuels (e.g., inequitable global distribution, third-party dependency and security issues) and increasing geopolitical tension in the energy sector (e.g., the oil crises of 1969 and 1973) [9], Western governments pushed for a common paradigm shift at the United Nations Conference on Environment and Development (UNCED) held in Rio De Janeiro in 1992. Building on the IPCC report, after the Rio Summit the United Nations (UN) launched the UN Framework Convention on Climate Change (UNFCCC), alongside related conventions on biodiversity

and desertification. Over time, the UNFCCC has established several mechanisms based on scientific evidence, including the formulation of explicit objectives to stabilize GHGs concentrations. This facilitated a transition shift towards an intergovernmental approach that is grounded in scientific understanding of the interconnected nature of climate, ecosystems and society and resulted in the signing of legally binding agreements, including the Paris Agreement in 2015 [10]. The Paris Agreement aimed at strengthening the global action with respect to climate change by setting the binding target of "*holding the increase in the global average temperature well below 2 °C above pre-industrial levels*", mandating signatories to pursue "*efforts to limit the temperature increase to 1.5 °C above pre-industrial levels*". The obligations agreed in the Paris Climate Agreement increased the pressure to implement synergistic strategies and policies aimed at supply societies with climate-neutral energy and fostering a shift towards a sustainable economic system. The signatories started to announce pledges to achieve a Net Zero Emission (NZE) scenario by 2050, as summarised by the International Energy Agency (IEA) in its first *Roadmap for the Global Energy Sector* [11] released in 2021, where a thorough analysis of the energy transition pathways was proposed. At the time, the energy sector represented nearly 75% of GHGs emission, and there was a general agreement that the path to NZE would have required an "*immediate and massive deployment of all available clean and efficient technologies*". In the meantime, the European Union (EU) presented the European Green Deal in 2019, which set the target for EU to become the first climate-neutral bloc by 2050 though the implementation of measures aimed at the proliferation of renewable energy sources (RES), enhancements in energy efficiency and replacement of fossil fuels. The targets proposed within the European Green Deal [12] have since become legally binding in the face of the enactment of the European Climate Law [13], which also enshrines a commitment to reduce net effect gas emissions by at least 55% by 2030 compared to 1990 levels. Moreover, the recent issuance of the RePowerEU plan was focused on the need to put in place measures to save energy through process efficiency and measures to diversify sources of supply, mainly related to natural gas, hydrogen and liquefied natural gas (LNG) supplies. In addition, the European Commission (EC) proposed to set the renewables target for 2030 at 45%, thus emphasizing the need to increase solar photovoltaic capacity, as well as hydrogen and biomethane production [14].

Despite all these efforts, in 2024, global energy-related CO_2 emissions reached a historic high of 37.8 Gton, marking a 0.8% increase from the previous year [3]. Recent estimations suggest that up to 75% of the global GHGs emissions should be cut to achieve the target of the NZE, while some studies anticipate a potential rise in CO_2 concentration up to 600-1550 ppm in the next decades [15]. This escalation underscores the persistent reliance on fossil fuels and highlights the challenges in curbing emissions despite international climate commitments. The proposed *phase out of fossil fuels* has been replaced with a softer *transition away from fossil fuels*, given the absence of international consensus and the technological gaps that still need to be solved. This shift necessitates the implementation of transitional decarbonization pathways that permit continued fossil fuel use but with a more conscious approach aimed at mitigating the associated environmental externalities. This is accompanied by a particular socio-political responsibility that more

developed countries must assume in pursuing green and sustainable chemistry approaches to mitigate the effects of global warming.

The massive roll-out of RES necessitates the simultaneous deployment of Long Duration Energy Storage (LDES) to effectively enable their integration in the energy system without causing detrimental effects on the stability and safe functioning of the electricity grid, given the inherent volatility of sources such as solar and wind [16]. On the other hand, the establishment of a hydrogen economy is unviable from both the technical and financial perspective [17], whereas the development of a Power-to-Fuel (PtF) framework could enable this transition while representing a cross-sectoral integration strategy. Indeed, PtF technologies are also part of the Carbon Capture Utilization and Storage (CCUS) framework, aimed at selectively removing CO_2 from both flue gas streams and the atmosphere to later use it as a building block of the PtF routes or permanently store it underground [18–20]. Among the different routes, Power-to-Methane (PtM) has emerged as a critical technology to seamlessly integrate the electricity and gas network and fully exploit the existing infrastructures devoted to transport and distribution. The full development of PtM is anticipated to play a major role in the advancements towards a more sustainable, affordable, and reliable energy system, as it leverages system integration to support the deployment of RES and foster the decarbonisation of natural gas (NG) consumers [21,22].

Synthetic Natural Gas (SNG) produced through the catalytic hydrogenation of CO_2, therefore, represents one of the potential routes to support a just and effective transition. SNG offers the advantage of leveraging the existing NG infrastructure while simultaneously enabling the penetration of the other low-emission technologies [23]. Therefore, SNG can act as an enabler of system-wide decarbonisation, though its adoption still faces significant technical and economic challenges, these being:

- The process is heavily reliant on the performance of the catalyst [15,24]. While nickel (Ni) based catalysts have already reached commercial application due to their favourable cost-performance trade-off, these systems are still far from optimal. Further advancements are needed to enhance their activity, selectivity, and stability, which requires a combined streamline of synthesis techniques, supports and promoters. Furthermore, the broader economic and environmental implication of these catalysts, which should drive innovation in this field, remain insufficiently addressed in the scientific literature, while issues such as the actual economic and environmental implications of these catalysts on the process should represent a driver for further advancements, these are scarcely addressed in literature.
- A fundamental challenge arises from the highly exothermic nature of the methanation reaction [25,26], which leads to the formation of thermal hot spots and causes catalyst deactivation by sintering. Therefore, reactor design and thermal management strategies are critical for ensuring stable, efficient and safe operation, particularly at larger scales. Simple and cost-effective reactor configurations are needed to overcome these limitations and enable the scale up of the process

- The wide adoption of PtM technologies is also hindered by their current high costs [27,28], which stem from the high resource and energy-intensive production process of electrolytic hydrogen, and from the complex plant architectures that increase capital expenditure. To reduce these costs, progress in plant design and component integration are required.

Scope of this research

The present dissertation undertakes a comprehensive investigation of the CO_2 methanation process, addressing it holistically across scales, *from micro to macro*, describing the intimate connections between the disciplines of catalysis and chemical engineering. The thesis starts from the micro-scale, concerning with the design, synthesis and functional assessment of heterogeneous catalysts to then deal with reactor modelling and design, representing a meso-scale, and a plant-scale investigation of the techno-regulatory viability of the methanation plant. The adoption of a multi-scale logic is grounded in the need to foster the adoption of multi-disciplinary and complementing approaches to respond to the challenges posed by the energy transition and the overall decarbonisation efforts.

The fundamental insights into catalyst design and assessment, representative of the micro-scale level of the present dissertation, are based on a concise yet strategically significant experimental campaign that was conducted at the Institute for Advanced Energy Technologies "Nicola Giordano" of the Italian National Research Council (CNR-ITAE). The campaign was carried out under the expert supervision of Dr. Antonio Vita and Dr. Cristina Italiano, within the Hydrogen Production Technologies and Catalytic Materials (FPMAT) research group and was focused on the testing of a Ni/CeO_2-ZrO_2 catalysts for CO_2 methanation. On the other hand, the methodological framework devised by Professors Marcello De Falco and Mauro Capocelli of the Process Engineering Research Unit at Università Campus Bio-Medico di Roma is at the base of the entire pathway from the micro- to the macro- scale. This framework encompasses system modelling and simulation, economic and environmental assessment and its application throughout the entire dissertation demonstrates the inherent versatility across scales and application contexts, confirming its pivotal role in identifying optimal pathways towards a sustainable, low-carbon economy model [29]. The thesis is divided into four chapters, briefly described below:

- **Chapter 1** provides a comprehensive overview of the historical development of the methanation process, identifying the main drivers and the strategic relevance in energy transition scenarios. The chapter positions methanation within the broader landscape of sustainable energy technologies, emphasising its role as an Energy Storage Technology. The fundamental thermodynamic principles of the methanation process are discussed to properly understand the main challenges faced in the development of the process.
- **Chapter 2** focuses on the preparation, the characterization and the testing of a Ni/CeO_2-ZrO_2 catalyst prepared through Solution Combustion Synthesis (SCS), capable to operate under mild operating conditions for a prolonged period. CO_2 methanation tests were performed in a FBR equipped with

the 25 wt.% Ni/20 wt.% CeO_2-55 wt.% ZrO_2 catalyst in powder form (50–70 mesh, ~250 μm) diluted with inert quartz particles of similar size (1:9 ratio of approximately 1:1 by weight) to prevent hot spots formation and operate in isothermal conditions. The activity tests were performed in the temperature range between 175 °C and 400 °C and at pressures ranging from 1 to 10 bar. The activities herein discussed served as a precursor to a broader investigation aimed at determining the intrinsic kinetics of the reaction. The chapter also proposes an extension of the catalyst assessment to encompass its environmental footprint during manufacture and operation through a pre-commercial Life Cycle Assessment (LCA).

- **Chapter 3** addresses the challenge of managing the significant exothermicity of the methanation reaction through the conceptualisation, modelling and simulation of a Multi Tubular Heat Exchange Reactor (MT-HER), designed to maintain control over temperature gradients and avoid localised hot spots. The MT-HER has been designed as a potential candidate technology for large-scale SNG production, with an estimated output of approximately 1,000 $Nm^3\ h^{-1}$. Therefore, the developed model has been therefore integrated into a plant-scale simulation aimed at assessing the feasibility of deploying a streamlined and compact methanation plant to produce pipeline-grade SNG. The discussion encompasses state-of-the-art reactor modelling and plant designs, beside the role of process intensification strategies to advance the technical maturity of certain solutions.
- **Chapter 4** synthesises the findings of the preceding chapters, thereby articulating the contributions of this research to advancing CO_2 methanation technologies across scales. Furthermore, the chapter provides a more extensive reflection on the implications of the methanation process and the replacement of fossil NG with SNG, outlining potential roads for future research and development.

The **Annex** constitutes a compendium of detailed materials that complement and enrich the main body of the dissertation, providing both broader context and deeper technical understanding. The overall methodological framework employed in the research is further elaborated, including a section devoted to the LCA methodology. Beyond this methodological contribution, the section includes additional notes and observations on SNG grid compliance requirements.

Chapter 1. The Process

Among fossil fuels, natural gas (NG) is set to remain as a driver of the energy transition. Indeed, the International Energy Agency (IEA) reported that the NG demand increased by 2.8% in 2024, corresponding to roughly 115 billion cubic metres (bcm). Moreover, the demand for NG is anticipated to continue its growth with a 1.5% increase in 2025 [30]. The chance of considering NG as a transition fuel rise the fossil fuel featured by the lowest carbon footprint and can help in reducing greenhouse gases (GHGs) emissions in the short-to-medium term. A recent investigation performed by Gürsan and de Gooyert [31] backed the consideration of NG as a transition fuel but outlined that the major threat behind this approach would be that of diverting investments from clean technologies generating unintended delays to the actual transition.

According to the latest Eurostat estimates, NG represented the second largest source of gross energy availability in the European Union (EU), contributing to satisfy nearly 20.4% of the supply (34.8% in Italy) [32]. The use of NG diminished through the last years due to the ongoing conflicts, as the major issue with its supply is the third import dependency rate, these being of 85.6% at the EU level and of 95.6% at the Italian level. Therefore, to overcome the challenge of third-party dependence and prompt the achievement of climate neutrality goals, the EU set ambitious targets for the deployment of Renewable Energy Sources (RES). These sources accounted for 24.5% of the total energy consumption in the region in 2023 (with Italy accounting for 19.6%). Nonetheless, their inherent volatility hinders their further deployment, which could cause severe grid issues if the threshold of 60% for electricity generation is exceeded [33].

The IEA has therefore underscored the pivotal function of NG in providing backup power and facilitating the development of a robust energy system by offering seasonal and short-term energy storage solutions [30]. Concurrently, the agency emphasised the necessity of diversifying procurement pathways, prioritising routes that do not necessitate substantial investments in infrastructure retrofitting. Indeed, while the substantial transition towards Liquefied Natural Gas (LNG) necessitates the establishment of supplementary receiving terminals to accommodate the influx of LNG into Europe from the United States and Qatar, alternative low-emission gases can fulfil this requirement. This umbrella term encompasses a variety of fuels, including biomethane, low-emission hydrogen, and *e*-methane, also referred to as synthetic natural gas (SNG). *e*-methane is indeed an electro fuel (*e*-fuel), a term which refers to a broad set of synthetic fuels (e.g., e-kerosene, e-methanol, e-diesel, etc.) that are produced using hydrogen generated through electrolysis and a carbon source as feedstocks [34]. *e*-fuels fall in the scope of the Power-to-Fuel (PtF) framework, figuring as potential storage pathways and a bridge between different sectors. Indeed, as *e*-fuels are produced to resemble their fossil-based counterpart, these are promoted as substitutes of conventional fossil fuels in the transport and industrial sectors [35–37]. Among *e*-fuels, *e*-methane stems as

the most easily integrable solution, given the chance of exploiting the branched and well-established NG infrastructure. Power-to-Methane (PtM) is therefore regarded as a crucial enabler of the transition, as it effectively represents a bridge between two seamlessly interconnected networks and enable a system-wide decarbonization [38]. Germany and Italy represent a compellent case for PtM deployment, as their gas-grid is branched (500,000 km and 269,000 km, respectively) and backed by a substantial NG storage capacity (260 TWh and 180 TWh, respectively). Nonetheless, the IEA reported that the interchangeability of *e*-methane with NG has also attracted attention outside Europe, where the technology was developed. For example, Japan's Seventh Strategic Energy Plan set an ambitious target of a 1% share for e-methane by 2030, considering it crucial to achieving a 65% reduction in emissions by that time [30].

Besides, Götz et al. [38] stressed the role of SNG/*e*-methane an enabler of the hydrogen economy, acting as green hydrogen carrier by providing safe distribution and storage facilities and opening the use of hydrogen to a wide range of end-use possibilities, spanning from the energy to the industrial sector. Moreover, *e*-methane is one of the most cost-effective technologies to enable the transport of hydrogen, outpacing the pathways of liquefaction and conversion into ammonia, which is also featured by issues related to the transport phase given the corrosive properties and toxicity. The IEA has also emphasised the potential of *e*-methane as storage medium, leveraging the already established practice of seasonal storage in salt caverns, porous formation, or tanks (both in the gaseous and liquid form as LNG).

Building on this evidence, NG must be considered as a transition fuel in a broader sense, and as an effective enabler of the pathway towards the achievement of the ambitious goals set by the European Green Deal. Indeed, SNG production also contributes to the advancement of the Carbon Capture Utilization and Storage (CCUS) value chain, a further pillar of the EU climate strategy [13]. Furthermore, SNG production has the potential to reduce dependence on third-party suppliers and mitigate reliance on extraction from oil and gas fields, whose reserves are estimated to last only 40–60 years [39].

The objective of this chapter is to facilitate a fundamental comprehension of the SNG production process and its function in the context of the energy transition. The chapter begins with a concise synopsis of the historical progression of the process, encompassing its initial discovery by Sabatier and its current state, with the objective of understanding the drivers of its evolution (**Section 1.1**). The PtM framework is then explained and discussed in **Section 1.2**, including a short discussion on the limitations of the hydrogen economy and the advantages of SNG. Finally, the thermodynamic characteristics of the Sabatier reaction are outlined in **Section 1.3** to define the scope and boundaries of the work presented in the following chapters.

1.1 Historical Evolution

Synthetic natural gas (SNG) is a gas mixture with a composition resembling that of natural gas (NG) that could be obtained through both the gasification of carbon sources (e.g., coal and biomass) or via the

chemical conversion of carbon oxides through the so-called Sabatier reaction [40]. SNG has therefore the potential to contribute to the efforts in decarbonizing the gas network without the need for expensive and long-lead time retrofitting of the existing infrastructure (e.g., LNG receiving terminals, LNG tankers, gas pipelines, and consumer gas equipment).

The development of the catalytic process for CO_2 methanation began in 1873, when Sir Benjamin Brodie first documented the slow-rate formation of methane (CH_4) through the application of an electric discharge to a syngas stream, setting a precedent for the exploration of carbon oxides reduction pathways [41]. Leveraging those findings, the French chemists Paul Sabatier and Jean-Baptiste Senderens investigated the thermochemical route for methanation, successfully testing the use of nickel (Ni)-based catalysts in 1902 [40]. The demonstrated efficacy of heterogeneous catalyst setting in promoting the formation of methane at moderated temperatures (i.e., 200-300 °C) paved the way for modern methanation processes, while the pioneering role of Sabatier was awarded with the Noble Prize in Chemistry in 1912 “for his method of hydrogenating organic compounds in the presence of finely disintegrated metals” [22]. For these reasons, the methanation reaction still brings the name of Sabatier, being his work a cornerstone of the evolution of the process.

Nonetheless, Sabatier himself emphasized the need to deepen the comprehension of the reaction mechanisms and of the role of operating conditions to streamline the process and enhance the overall effectiveness of the process. Moreover, SNG production was not economically competitive with fossil fuels, so research into methanation only surged in the 1950s when issues with energy procurement arose and SNG began to be considered a valuable alternative to fossil NG, given its potential to increase energy security and independence. In a first phase, industrial-scale projects were focused on CO methanation, as the process was meant to purify syngas streams deriving from coal-gasification, as the case for the Great Plains Synfuels Plant in Beulah (North Dakota, United States, US), operational since 1984. The plant, equipped with a Lurgi reactor, was intended to produce nearly 5 million cubic meters (mcm) of SNG from lignite and inject it into the Northern Border pipeline. One of the first post-assessment on SNG technologies was realized by Kopyscinski et al. [42] with the aim of tracking the processes in production technologies handing coal and biomass as feedstocks. The authors reported a coal/biomass-to-SNG chemical efficiency up to 65% (wood-to-SNG), and outlined a general scheme of the process comprising: 1) a gasification section to generate *syngas*; 2) a gas cleaning and conditioning section to abate impurities; and 3) the methanation reactor, designed as either a fixed bed-reactor (FBR), isothermal reactor, fluidized bed and other types. The authors underscored that, given the highly exothermic nature of SNG production, most of the industrial systems employed a series of methanation reactors with intermediate cooling and product-gas recycling. Those arrangements were meticulously designed to ensure robust thermal control, enhance productivity, and avoid the release of unconverted CO_2 (and CO) into the atmosphere.

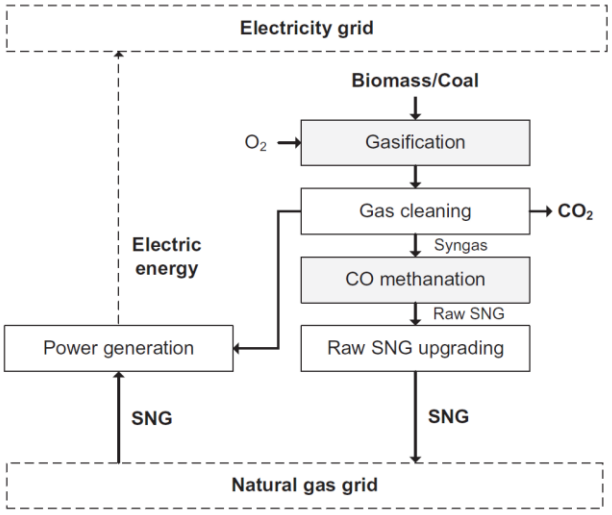

Figure 1 Schematic representation of a biomass/coal-to-SNG plant [43].

On the other hand, studies on CO_2 methanation commenced in the 1980s and considered the process as a downstream treatment for either biogas upgrading or blast furnace gas cleaning, with a first bench of concepts reaching the commercial scale and spreading across the US, Germany, United Kingdom (UK) and Japan in the following years. Rönsch et al. [43] Evolving from the process proposed by Hashimoto et al. who considered the integration of seawater electrolysis and CO_2 methanation, Sterner identified CO_2 methanation as both a climate mitigation and an energy storage technology . Germany led the development of the current architecture as a part of *Energiewende* (Energy Transition) research project commenced in 2010 and focused on the use of the NG infrastructure as a storage intermedium. The project led to the start-up of the Audi e-gas plant, the first full-scale CO_2 methanation demonstrator operational since 2013 and located in Wertle, Germany. Beside the successful deployment of the first industrial methanation facility, the Audi e-gas plant demonstrated the chance of integrating methanation as an upgrading technology for biogas coming from anaerobic digestion, obtaining a 54% conversion efficiency from biogas to methane by adopting heat integration strategies [44].

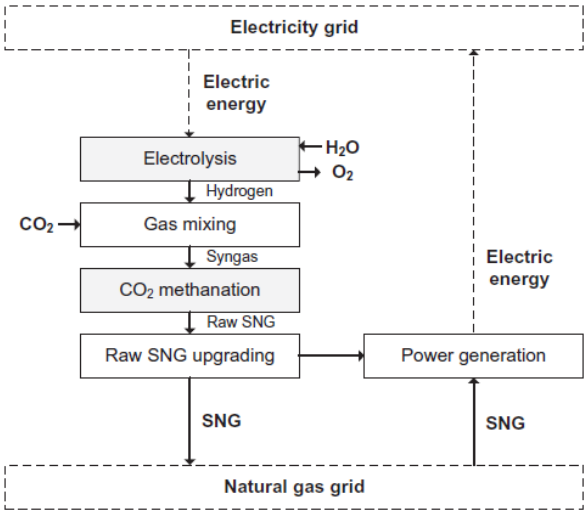

Figure 2 Schematic representation of a electricity-to-SNG plant [43].

As will be further detailed in **Section 3.1.1**, several pilot projects were executed after the successful demonstration of the Audi e-gas plant, aimed at evaluating the potential usage routes for SNG and at advancing the technological maturity of the methanation process. As reported by Rönsch et al. [43], most large-scale CO methanation projects are in Asia (mostly China) and were developed in the framework of coal-to-SNG. On the other hand, Europe (mostly Germany) led the development of CO_2 methanation, as the technology has been developed to enhance the flexibility of the energy system.

The ongoing debate on sustainable energy supply has led to intensified research efforts on methanation, with substantial advancements in the development of both the catalytic and the biological route [15]. Though the former represents the most mature technology and detains a higher deployment potential soon, several studies and projects have been made to advance the biological process, starting from the first deployment in Allendorf (Eder, Germany), in 2015. Biological methanation (BM) uses microorganisms together with a nutrient source to convert the reactants into methane [45]. BM is widely applied for the upgrading of biogas and deals with the use of some specific microorganism (archaea) as biocatalysts. The latter are indeed able to anaerobically metabolize the reactants and generate methane operating at low temperatures (30-60°C) and atmospheric pressure. The process is commonly performed in either stirred tank reactors (STR) or trickle-bed reactors (TBR). The biological route can be performed both *in-situ* and *ex-situ* depending on where the reaction takes place (within the digester or in a separate methanation reactor, respectively). *In-situ* BM represented a cost-reduction opportunity for market players in the field of biogas and biomethane, as it provides the chance to avoid a separated upgrading step to remove CO_2 from the product gas coming from the anaerobic digestors [46].

Both processes have gained interest from scientists, academics, institutions, and industries, since the production of either SNG and biomethane represent a valuable means to leverage the branched and robust NG network (i.e., transportation, distribution, and usage infrastructures) while pursuing decarbonization

objectives. As outlined by Rönsch et al. [43], one of the main drivers of the recent advancements in this field has been the necessity to adapt and streamline state-of-the-art technologies to ensure compliance with the changed requirements of a decentralized energy system. Indeed, focusing on the catalytic route, this solution is appealing due to the declination of SNG into *e*-methane, this being entailed in the framework of *e*-fuels. In this prospective, SNG is integrated into both energy storage processes and carbon valorisation ones.

1.2 Methanation as an Energy Storage Technology

The global roadmap for climate neutrality envisions the widespread adoption of clean energy generation technologies, primarily driven by Intermittent Renewable Energy Sources (i-RES) such as solar and wind power. Nonetheless, the inherent volatility and intermittency of these energy sources, alongside the remote locations of the generation plants, pose significant challenges in terms of dispatchability and compliance with the pillars of the energy trilemma [2]. The latter is a framework introduced by the World Energy Council (WEC) [1] to guide the assessment of the status of the global energy systems and the design of their future structure. In this perspective, the performance of the energetic infrastructure should be evaluated in terms of security, equity, and environmental sustainability, and a proper balance among these three dimensions must be maintained while facing the shift towards the novel system. The current practice to cope with the unbalance between supply and demand foresees the curtailment of surplus electricity that cannot be injected into the grid for safety and stability reasons [47–49]. Moreover, the variability in generation patterns adds another layer of uncertainty to the evolution of the electricity market, driving volatility in electricity prices and, consequently, affecting access to electricity for certain customer groups.

To cope with reliability issues (i.e., secure a match between generation and demand), substantial efforts have been devoted to developing energy storage systems, which emerged as a critical enabler for the seamless integration of i-RES into electricity networks. By providing the flexibility to store surplus energy and release it during periods of high demand or low generation, these technologies minimize the need for curtailment while enhancing grid reliability. Besides, energy storage solutions unlock additional value generation by optimizing the supply of IRES, paving the way for their penetration into the grid and the achievement of grid shares objectives. Prominent academics, sectoral associations and institutions recently pointed out that with an increase in IRES share the current European grid infrastructure could potentially collapse without an adequate deployment of energy storage solutions at both distributed and local scales. The EU Commission stated that beyond 25% of IRES penetration it will become mandatory to curtail the energy generated during low-demand periods to avoid grid perturbation and congestion. On the other

[1] Founded in 1923, the World Energy Council (WEC) brings together key stakeholders in the energy sector to promote solutions that accelerate the transition to sustainable energy systems. Accredited by the United Nations, the Council operates in over 100 countries and represents more than 3,000 members, including governments, industries, academics, and other institutions.

hand, the current network management practice includes the activation of fossil-fuel driven backup power generation to meet user demand in cases of low IRES generation, with modern natural gas combined cycle (NGCC) power plants become extremely flexible to enable a rapid shift towards higher and lower production rates synchronously with the grid. However, this can lead to an i-RES maximum penetration level lower than 40%. In general terms, previous studies such that of Sterner and Specht [50]outline the main issues arising from a massive deployment of i-RES, these being: (1) the electricity grid represents a potential storage site, but it allows for the spatial balance of surplus electricity rather than for load shifting and temporal management; (2) demand side management can reduce the need for time flexibility and storage, but it cannot completely replace them; (3) flexible electricity generation can partially balance weather-dependent energy production, but only by using further fossil resources; (4) energy storage is the least efficient but still the cheapest solution at the system level for balancing the electricity system over time.

As for the last point, the large-scale deployment of energy storage technologies is currently hindered by both technical and practical challenges related to storage duration and storage capacities [51]. Commercially available energy storage technologies, such as Lithium-Ion Batteries, are intended to intra-day energy storage needs, with few of them being classifiable as Long Duration Energy Storage (LDES) technologies. Among these, Pumped Hydro Storage (PHS) is the most suitable solution for seasonal storage, though its adoption is topographically limited and the existing (and potential) capacities are not comparable to the actual needs [48]. To overcome the inherent challenges of commercial energy storage solutions, research on innovative routes for energy storage led to the development of the Power-to-Gas (PtG) and Power-to-Liquid (PtL) concepts [18]. These technologies concern the electrochemical conversion of surplus from renewable energies into gaseous energy carriers such as hydrogen, which can be subsequently converted into valuable fuels and chemicals at the gaseous or liquid state. The PtG chain could end with the production, transportation, storage, and usage of hydrogen, but there exist significant barriers that hinders this route, such as the absence of an adequate infrastructure for transportation and distribution and stringent end-user requirements.

The Hydrogen Economy

In contrast to conventional fuels, and in a similar manner to electricity, hydrogen functions as an energy vector rather than as a source of energy, and as such it must be produced. Hydrogen is characterised by several distinctive physical properties which collectively make it a promising fuel for various energy applications. In 1970, during a talk given by John O'M. Bockris at the General Motors technical centre, the term *hydrogen economy* was first coined. Though the concept was proposed earlier by geneticist J.B.S. Haldane, Bockris published its book, *Energy: The Solar-Hydrogen Alternative*, in 1975, describing his idea of United States' cities supplied with solar energy [52,53]. The development of a hydrogen economy entailed that carbon containing fuels should have been completely replaced by hydrogen, and the idea was timing considering that the oil crisis caused by the OPEC oil embargo made mandatory to look for alternative fuels. At the time, however, scientists and policy makers supposed that the only alternatives to zero gasoline dependence were natural gas and coal. Therefore, aiming at looking for feasible and economically viable solutions, the International Energy Agency (IEA) was established in 1977, and the United States Department of Energy (DOE) being created. Later, in 1996, the IEA established the Hydrogen Storage Task Force looking for innovative hydrogen storage methods and materials, while the United States Department of Energy (DOE) developed a long-term hydrogen strategy setting a standard for this discussion considering both economic and environmental parameters. Indeed, the full development of a hydrogen economy is mainly hindered by the issue of storing it, since while the gravimetric density is the highest among all fuels (120 MJ kg^{-1}), the volumetric density of hydrogen at standard conditions is the lowest (12 MJ Nm^{-3}) (see **Table 1**). Therefore, substantial efforts are undergoing to meet the needs of the most demanding consumer applications, such as Fuel Cell Vehicles (FCVs), whose development has prompted the advancements in the field of both gaseous hydrogen storage and solid-state storage, a route that foresees the physisorption of hydrogen as dihydrogen molecule or more strongly chemically bound as monoatomic hydrogen. Beyond necessitating onboard storage systems capable of withstanding extremely high pressures, often exceeding 5,000 to 10,000 psi, FCEVs demand hydrogen of an ultra-high purity, which can only be obtained through a limited number of production routes or via sophisticated purification systems downstream of the production unit [54]. Most of the global production of hydrogen is still based on conventional methods such as Steam Methane Reforming (SMR), either abated (the so-called blue hydrogen) or unabated (the so-called grey hydrogen) [55]. The Global Hydrogen Review 2024, published by the International Energy Agency (IEA), has reported that of the 97 Mton of hydrogen produced in 2023, less than 1% could be classified as low emissions. Consequently, the production of hydrogen resulted in the release of 920 Mton of CO_2, with unabated SMR accounting for almost 67% of this total [55]. As reported by De Cata et al. [56], SMR could be decarbonised through electrification, leveraging the increasing share of renewable energy sources (RES) into the electric grid. The electrified Steam Methane Reforming (eSMR) process could represent a promising alternative in a mid-term scenario while waiting for a more consolidated scale up and validation of the green hydrogen route, which entails hydrogen production by means of electrolysis [57,58]. Indeed, while the current landscape is featured by a wide range of hydrogen production processes, spanning from thermochemical processes to biological ones, electrolysis is widely regarded as the main production route in future scenarios, as it is solely supplied by electricity and water and generates hydrogen and oxygen as by-product [59]. Three main electrolysis technologies have led the technological development up to date, these being Alkaline Electrolysis (ALK), Polymer Electrolyte Membrane (PEM) and Solid Oxide Electrolysis (SOEC) [60]. On the other hand, the establishment of a reliable hydrogen distribution network remains a critical infrastructural challenge given the prominent risks of hydrogen embrittlement (HE) and the threat of structural damages. Indeed, given the small size

and high diffusivity of the hydrogen molecule, it can enter within the crystalline structure of stainless and carbon steel pipelines and modify their ductility, fracture resistance, and fatigue properties [61]. Indeed, while the use of the existing NG infrastructure has been proposed given their well-established presence, the peculiar features of hydrogen make this route unsuitable given the complexity of technical adaptation and the high associated costs. However, a promising solution lies into the usage of hydrogen to enrich methane streams, therefore leveraging the existing NG infrastructure without requiring substantial retrofitting. Enriched methane consists of a methane stream comprising a certain amount of hydrogen (ranging from 10 to 30 vol.%) and it is intended to partially decarbonise the combustion processes. The pioneering work of De Falco et al. [62] provided one of the first overview of the entire value chain of enriched methane, from production to end-use in Internal Combustion Engines (ICEs) and Gas Turbines (GT). The authors provided a preliminary estimation of the environmental benefits in terms of emissions reduction, stating that a 30 vol.% hydrogen blending could bring down CO_2 equivalents emissions of about 11%. Nonetheless, the presence of hydrogen in the NG stream alters both distribution and combustion dynamics while hydrogen as a Higher Heating Value (HHV) that is more than twice that of methane, its low density significantly influences the WI, affecting both heat delivery capacity and combustion behaviour. The actual interchangeability of NG and hydrogen-enriched NG streams was thoroughly addressed by Franco and Rocca [63], who introduce an innovative thermodynamic framework for evaluating hydrogen–methane fuel blends, grounded in the Wobbe Index (WI). Through rigorous analysis, they confirm that the current industrial infrastructure, particularly burners used in high-temperature (> 750 °C) applications, can tolerate hydrogen additions of up to 20 vol. %. Moreover, the authors demonstrate that beyond approximately 25 vol.% hydrogen, the WI declines to a point where heat delivery becomes inefficient and system compatibility breaks down, rendering further hydrogen blending counterproductive. Nonetheless, it is important to stress that the main parameters used to assess the interchangeability of gases is the WI, and it is therefore sufficient to proceed with the blending while keeping the gas quality required by the technical rules of each country. The exploitation of pipelines to store and transport hydrogen is regarded as a strategic element of the pan-European hydrogen infrastructure. The European Hydrogen Strategy identified hydrogen blending as a potential interim step towards the decarbonization of natural gas. Recently, the Joint Research Centre (JRC) of the European Commission (EC) investigated the implications related to hydrogen blending into the existing gas network considering PtG as a bridge between the power system and the natural gas infrastructure [64].

Hydrogen blending in Italian natural gas grid: Scenario analysis and LCA

Building on this growing interest, our research group investigated the system-wide implication of hydrogen blending by collaborating with the Department of Industrial Engineering of Università Tor Vergata di Roma. Our study (Bellocchi et al. [65]) focused on the role of hydrogen blending in the Italian natural gas grid as a mean to facilitate higher renewable penetration and reduce greenhouse gas emissions. The study employed a detailed model of the Italian energy system using EnergyPLAN, exploring three scenarios. The first was a BASELINE reflecting 2019 conditions, then a MID-SCENARIO with i-IRES capacity increased fivefold to 158.17 GW, and an END-SCENARIO with maximum technically feasible i-RES deployment of 272.1 GW. In each scenario, surplus renewable electricity was converted into green hydrogen via PEM electrolysis and injected into the natural gas grid up to the current technical limit of 20 mol.%. The results highlighted that expanding i-RES capacity was the dominant factor driving emissions reduction, achieving up to 15% lower total energy system CO_2 emissions compared to 2019, constrained by the hydrogen blending ceiling. Within the electricity generation sector, emissions reductions reached 57% in the MID-

SCENARIO and 66% in the END-SCENARIO, supported by coal phase-out and substantial replacement of natural gas with renewables and hydrogen. The analysis further quantified the maximum feasible hydrogen contribution at approximately 38.8 TWh annually, corresponding to about 8 Mt CO_2 avoided, or 2.7% of 2019 emissions (when combining high i-RES capacity with optimized electrolyser and storage configurations). Avoidance costs were shown to decline markedly with increasing i-RES capacity and falling electrolyser costs, dropping below EUR 100 per tonne of CO_2 under favourable assumptions. Complementary Life Cycle Assessment (LCA) revealed that while fossil resource depletion decreased by up to 77%, the demand for critical minerals rose due to the material intensity of renewable and electrolyser technologies (see **LCA for the Energy System**). Overall, the study demonstrated that hydrogen blending, despite its infrastructure-imposed limitations, represents a viable transitional strategy to support renewable integration and emissions mitigation in the Italian energy system.

Table 1 Properties of Common Fuels [66].

Property	Hydrogen	Methane	Methanol	Gasoline
Lower Heating Value LHV specific energy (MJ kg^{-1})	120	48	20	43
Higher Heating Value HHV specific energy (MJ kg^{-1})	142	52	22	46
Energy density at STP (MJ Nm^{-3})	11.86	35	15,700	35,032
Maximum flame speed (m s^{-1})	2.8	0.37-0.45	0.45	0.37-0.43
Flammability limits, %vol in air	4.1-74	5.3-15	6-36.5	1.4-7.6
Explosion limits, %vol in air	18.2-58.9	5.7-14	6.7-36	1.3-3
Lean limit equivalence ratio in air	0.1	0.5	0.57	0.58
Minimum ignition energy (mJ)	0.02	0.29	0.21	0.24
Autoignition temperature (°C)	571	632	470	220
Octane (RON)	>130	120	106	92-98
Molecular diffusion coefficient (cm^2 s^{-1})	0.61	0.16	0.13	0.05
Energy density of stoichiometric mixture with air (kJ L^{-1})	3.23	3.31	3.56	3.84

As outlined above, although it is an interesting approach, blending hydrogen into the grid is an inefficient use of a valuable resource that would be better used to directly decarbonise sectors that lack alternatives, such as the industrial sector. The conversion of hydrogen into fuels (Power-to-Fuel, PtF) appears as a preferable option given the compatibility with the existing infrastructure, despite the introduction further conversion process being obviously associated with efficiency losses [38]. Nonetheless, hydrogen production is commonly the most energy-intensive process and it must also be noted that the actual objectives of energy storage solutions are to support the deployment of i-RES, enhance grid stability, and enhance the resilience and security of the energy systems. Therefore, performance parameters such the RTE should not be considered as the core of their feasibility assessment, which should be rather focused on system integration potential provided by the existence of mature infrastructure. Among the potential PtG routes, Power-to-Methane (PtM) represents one of the most effective solutions as the produced SNG is compatible with the existing NG infrastructure and the entire value chain, therefore overcoming blending limitations and boosting the interoperability of the entire energy system [18]. Moreover, as can be seen from

Figure 3, the production of SNG brings substantial advancements in terms of storage time and storage capacity, which makes it a suitable LDES to be deployed at large scale.

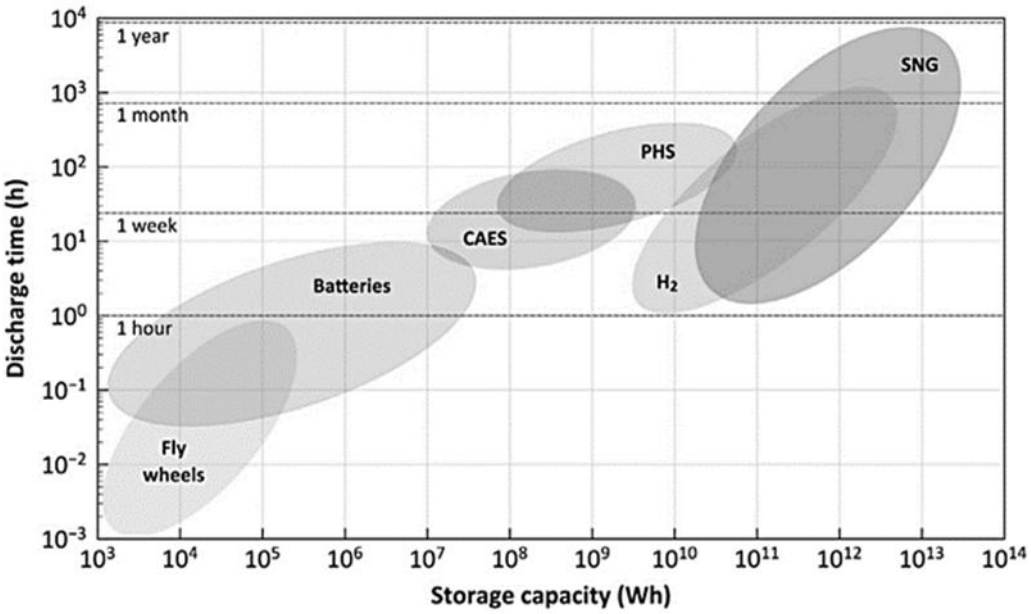

Figure 3 Storage capacity and discharge time of different technologies [22].

This storage route enables both the accelerated deployment of i-RES and the reduction of dependence on fossil-based fuels [67]. Although increasing shares of wind and solar introduce fluctuations into the electricity grid, these can be mitigated by utilizing SNG for power generation, leveraging the existing natural gas infrastructure as a flexible and sufficiently capacious storage system [68].

1.3 Thermodynamic Features

Methanation consists of a set of three reactions occurring simultaneously within the reaction system based on the operating conditions, these being CO_2 methanation (Eq. (1)), CO methanation (Eq. (2)) and Reverse Water-Gas Shift (RWGS) (Eq. (3)), which couples both Sabatier reactions:

$$CO_2 + 4H_2 \leftrightarrow CH_4 + 2H_2O \qquad \Delta H^0_{298K} = -164.7\ kJ\ mol^{-1} \qquad \text{Eq. (1)}$$

$$CO + 3H_2 \leftrightarrow CH_4 + H_2O \qquad \Delta H^0_{298K} = -206.1\ kJ\ mol^{-1} \qquad \text{Eq. (2)}$$

$$CO_2 + H_2 \leftrightarrow CO + H_2O \qquad \Delta H^0_{298K} = 41.1\ kJ\ mol^{-1} \qquad \text{Eq. (3)}$$

Overall, the methanation process is highly exothermic and is accompanied by a reduction of the total number of moles, this being stronger for CO methanation (50% volume reduction) than for CO_2 methanation (40% volume reaction) [43]. Therefore, considering the thermodynamic principles and Le Chatelier's profile, the formation of methane is thermodynamically favoured at low temperatures and high pressures. However, beside the reactions in Eq. (1)-(3), a set of side reactions (Eq. (4)-(11)) has been found to potentially occur under the same operating conditions, leading to the formation of carbon deposits and promoting deactivation phenomena (see **Section 2.1**). Among them, the Boudouard reaction (Eq. (4)), methane cracking (Eq. (5)), CO reduction (Eq. (6)) and CO_2 reduction (Eq. (7)) result in the formation of solid carbonaceous residues, whereas Eq. (8) and Eq. (9) are related to the potential formation of saturated hydrocarbons (alkanes and alkenes, respectively). Moreover, as the Boudouard reaction is thermodynamically favoured over CO methanation, it is essential to comprehensively understand the thermodynamic boundaries of the process.

$$2CO \leftrightarrow C + CO_2 \qquad \Delta H^0_{298K} = -172.4\ kJ\ mol^{-1} \qquad \text{Eq. (4)}$$

$$CH_4 \leftrightarrow 2H_2 + C \qquad \Delta H^0_{298K} = 74.6\ kJ\ mol^{-1} \qquad \text{Eq. (5)}$$

$$CO + H_2 \leftrightarrow C + H_2O \qquad \Delta H^0_{298K} = -131.3\ kJ\ mol^{-1} \qquad \text{Eq. (6)}$$

$$CO_2 + 2H_2 \leftrightarrow C + 2H_2O \qquad \Delta H^0_{298K} = -90.1\ kJ\ mol^{-1} \qquad \text{Eq. (7)}$$

$$nCO + (2n+1)H_2 \leftrightarrow C_nH_{2n+2} + nH_2O \qquad \text{Eq. (8)}$$

$$nCO + 2nH_2 \leftrightarrow C_nH_{2n} + nH_2O \qquad \text{Eq. (9)}$$

Side reactions can occur depending on the operating conditions, as each of them is featured by a different equilibrium constant. Gao et al [69]. performed a thorough thermodynamic analysis of carbon oxides methanation using the Gibbs free energy minimization method. The authors considered a set of eight reactions and evaluated the effects of temperature, pressure, H_2/CO_x ratio and feed gas composition on key parameters such as CO and CO_2 conversion, methane selectivity and yield, and carbon deposition phenomena. The main outcomes of their work with respect to CO_2 methanation are resumed in **Figure 4**,

where CO2 conversion, CH4 selectivity and CH4 yield are shown in function of operating temperature and pressure.

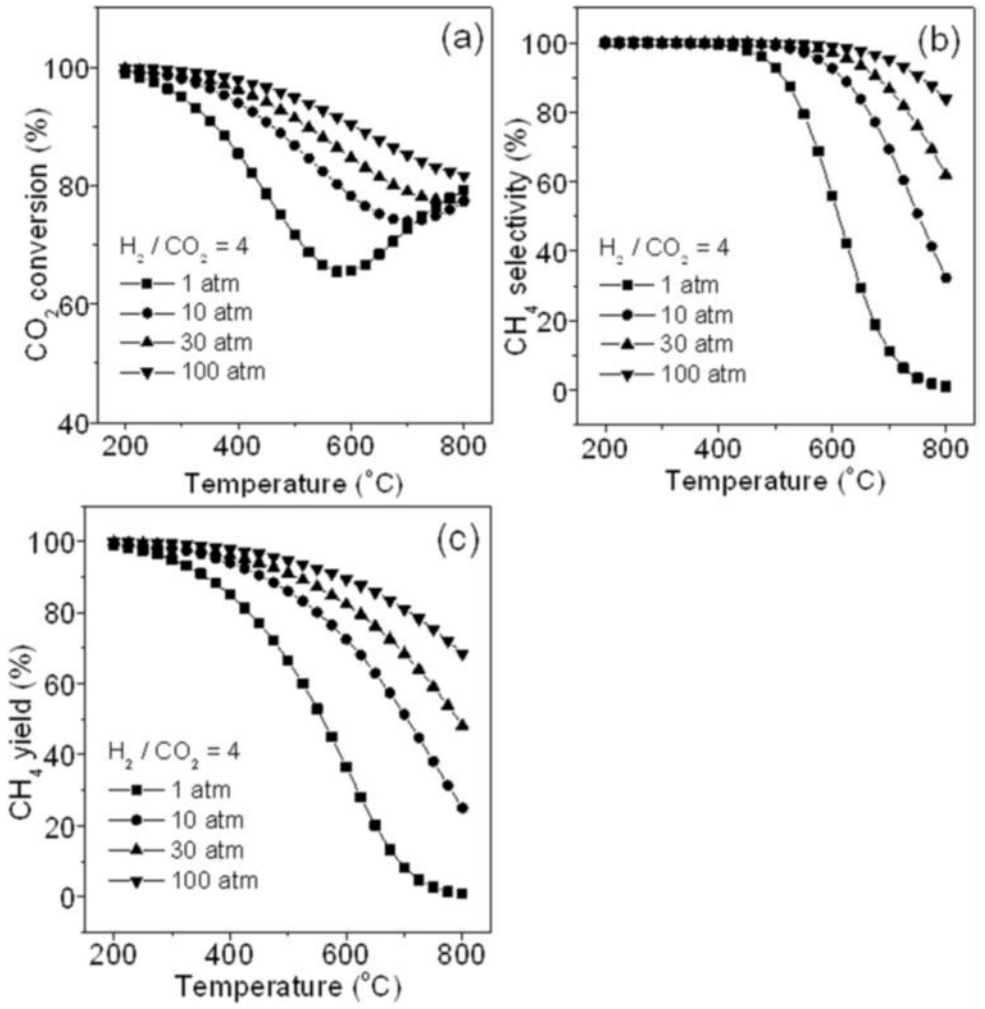

Figure 4 Effects of pressure and temperature on CO_2 methanation: (a) CO_2 conversion, (b) CH_4 selectivity, and (c) CH_4 yield [69].

The thermodynamic constraints of the methanation process mandates the development of active and selective heterogeneous catalyst to enable the occurrence of the reaction over a wide range of temperatures and guarantee high yield of methane and minimal amount of CO. Therefore, catalysts represent the first tool to address thermodynamic issues and, as discussed in **Chapter 2**, it is essential to lead advancements in the development of a proper system by selecting the appropriate active phases, promoters, support materials and synthesis techniques [70]. Currently, Ni-based catalysts represent the most cost-effective solution, but these systems suffer from severe deactivation issues prompted by the occurrence of thermal hotspot along the reaction length. As the methanation reaction proceeds, significant carbon deposition can occur at temperatures above 450 °C, fostering deactivation [25]. Therefore, beyond thermodynamic and catalyst development, one of the main challenges to face to scale up the methanation process lies in

reaction rates and in the exothermic nature of the process [71], mandating a proper design of the reactor itself. The issue of thermal management and the necessity to provide a tighter control over the emergence of temperature gradients is here treated in **Chapter 3**, where the modelling and simulation of a Multi-Tubular Heat Exchanger Reactor (MT-HER) configuration equipped with a commercial Ni-based catalyst is presented and discussed. Eventually, a further challenge lies into the compliance requirement of a SNG production plant [72]. Indeed, as discussed in **Synthetic Natural Gas (SNG) Grid Requirements**, the produced SNG must comply with certain specific and this issue is addressed as well in the chapter through the process simulation of a multi-stage production process equipped with the previously modelled MT-HER. The multi-scale approach of the present dissertation therefore addresses system-level technical and regulatory aspect to contribute in the efforts of establishing methanation as a viable alternative in the PtM and CCUS framework in the Italian context.

Chapter 2. The Catalyst

The chemical methanation reaction operates at the nexus of thermodynamic favourability and kinetic limitations [22]. The reduction of fully oxidised carbon to methane is an eight-electron process that requires a significant amount of energy to overcome the activation barrier. This is because the dissociation of a structurally stable molecule, such as CO_2, can only occur through an energy-intensive process. Moreover, the reaction is thermodynamically limited at temperatures above 300 °C, given the exothermic nature of the Sabatier reaction, and it is therefore essential to use a suitable catalyst to overcome kinetic limitations that hinder methane formation at low temperature [25,26].

The pursuit of a trade-off between thermodynamic and kinetic constraints has driven thorough research into catalysts for the Sabatier reaction through the last century, looking for systems able to reduce the activation energy and promote the reaction at moderate temperatures. Indeed, catalysts facilitate the occurrence of the reaction by altering the reaction mechanism and introducing intermediate steps featured by a lower energy level, enabling it to occur at a fast pace within the moderate temperature range dictated by the thermodynamic of the process [73]. To this end, several systems have been tested to find a proper balance between activity and selectivity and face the operating challenges that feature the process, such as the formation of thermal hotspots, phenomenon that has the potential to cause catalyst deactivation and compromise the stability of the catalytic system. Consequently, research has been directed towards the development of sophisticated catalytic systems, which integrate diverse active phases, supports, promoters, and synthesis techniques [70].

In the early stages of research, nickel (Ni) was identified as an effective active phase for the hydrogenation of CO_2 to methane. For many years, Ni-based catalysts have been utilised in industrial settings, such as the purification of syngas, as they offer an excellent compromise between activity, selectivity, cost and availability [39]. The renewed interest in CO_2 methanation within the Power-to-Methane (PtM) framework has led to the development of novel catalysts, primarily focused on enhancing low-temperature activity, stability under highly exothermic conditions, and on utilising inexpensive and abundant materials to ensure industrial scalability. Noble metals such as ruthenium (Ru) and rhodium (Rh) have been tested and often demonstrated superior performance with respect to Ni-based catalyst (e.g., higher activity at low temperatures, enhanced resistance towards deactivation, etc.) [74]. Nonetheless, despite the promising results obtained, Ni-based catalysts stand out due to their competitive edge in terms of trade-off between cost, availability and performance. Further advancements in the field include the introduction of tailored supports providing activity-boosting metal–support interaction, as well as the formulation of bimetallic catalysts to enhance kinetics and the development of novel synthesis techniques (e.g. co-precipitation of

Ni with support precursors, or deposition of Ni nanoparticles on high-surface supports) to control metal dispersion [75]. The synthesis procedure has been found to significantly influence the mechanical (e.g., strength and attrition) and physicochemical (e.g., surface area, porosity, basicity, composition, and density) properties of the catalyst, alongside its activity, selectivity and stability. Concerning the support, systems such as ceria (CeO_2), zirconia (ZrO_2) and yttria (Y_2O_3) have been demonstrated to enhance oxygen mobility, generate oxygen vacancies, and offer moderate basicity, contributing to a comprehensive performance enhancement in terms of activity and stability with respect to the conventional alumina (Al_2O_3) support. This evolution can be interpreted as a balancing act between the need to reach high activity at low temperatures and to secure catalyst durability and economic feasibility for large-scale deployment [76].

The emerging relevance of sustainability performances in process analysis prompted the affirmance of Life Cycle Assessment (LCA) methodologies to gain insights over the environmental profiles of good and services. Innovative technologies must be evaluated in a comprehensive manner to prevent the deployment of burden-shifting solutions (e.g., technologies devoted to GHGs emission abatement that leads to an increase depletion of abiotic resources). Carbon mitigation technologies such that in the framework of Carbon Capture Utilisation and Storage (CCUS) have been posed under a critical lens to holistically understand the environmental impacts associated with their development, deployment and operation. Several studies have been conducted, and guidelines have been developed to draw up a common assessment platform that could enhance and ease comparison across the different utilization routes, though there are still several gaps to address [77–79]. Nonetheless, LCA studies on CO_2 methanation are relatively scarce, and most of the performed investigations are focused on the overall process rather than on the influence of single factors such as the catalyst. Recent studies have demonstrated the pivotal role of the catalyst in ensuring optimal operational performance, also highlighting the disparities introduced by diverse synthesis methodologies with regard to activity, selectivity, and environmental impact.

The present chapter delves into the role of catalytic systems in the context of chemical methanation, undertaking a thorough investigation of the current state-of-the-art and exploring the trends in catalyst development, testing and environmental characterization. These topics are addressed in **Section 2.1**, alongside a brief overview of the contributions made by CNR-ITAE in the domain of catalyst synthesis and testing. The CNR-ITAE pioneered the use of Solution Combustion Synthesis (SCS), a one-pot method that exploits a rapid self-propagating reaction for the preparation of heterogeneous catalysts supported on oxides. **Section 2.2** therefore presents the preparation and testing procedures of their 25 wt.% Ni/20 wt.% CeO_2-55 wt.% ZrO_2 catalyst, adopted during a brief experimental campaign performed during a visiting period. These tests constitute an element of a broader ongoing collaboration, the objective of which is to ascertain the intrinsic kinetic of the developed systems. Moreover, the potential merits of expanding the characterisation of the catalyst were discussed during the visiting period, with further analysis being proposed in the form of LCA, an approach that is outlined in the methodology section and which has been endorsed by a comprehensive literature analysis. The present chapter thus seeks to contribute to the

existing body of knowledge by investigating the environmental performance of the tested Ni/CeO_2-ZrO_2 catalyst with respect to benchmark Ni/Al_2O_3 and to a similar catalyst prepared through a different synthesis technique. The outcomes of the testing and environmental assessment activities are documented in **Section 2.3**, while future perspectives and conclusions are summarized in **Section 2.4**.

2.1 Methanation Catalysts

The Sabatier reaction was originally tested over a Ni-based catalyst, which remains the commercial standard for the methanation process due to its cost-effectiveness, activity, and availability. Nonetheless, a wide range of noble and non-noble metals has been investigated as active phases for methanation catalysts, yielding promising results and in some cases surpassing the performance of Ni-based systems. Research on methanation catalysts has primarily focused on metal systems supported on metal oxides, mainly from groups VIII, IX, X, and XI[2] (**Figure 5**). Vannice et al. [80] initially classified these metals based on their activity (Ru > Fe > Ni > Co > Rh > Pd > Pt > Ir) and selectivity (Pd > Pt > Ir > Ni > Rh > Co > Fe > Ru). Later, Mills and Steffgen [81], argued that it could have been more practical to focus on the metals that are "more important for methanation catalysts", namely Ru, Ni, Co and Fe.

6	7	8	9	10	11
24 **Cr** Chromium	25 **Mn** Manganese	26 **Fe** Iron	27 **Co** Cobalt	28 **Ni** Nickel	29 **Cu** Copper
42 **Mo** Molybdenum	43 **Tc** Technetium	44 **Ru** Ruthenium	45 **Rh** Rhodium	46 **Pd** Palladium	47 **Ag** Silver
74 **W** Tungsten	75 **Re** Rhenium	76 **Os** Osmium	77 **Ir** Iridium	78 **Pt** Platinum	79 **Au** Gold

Figure 5 Group VI-XII metals from the periodic systems of elements with active catalysts for methanation marked in grey [43].

Currently, Ni-based catalysts are the sole to having reached full commercialization, as they have been widely used in industrial methanation since the first deployment in the field of syngas purification. Nonetheless, emerging demand for enhanced low-temperature performance, stability, and integration into novel applications have prompted research into alternative metal catalysts (e.g. Ru, Co, Fe) and innovative catalyst

[2] Nomenclature for relevant metals: Ruthenium (Ru), Iron (Fe), Nickel (Ni), Cobalt (Co), Rhodium (Rh), Palladium (Pd), Platinum (Pt), Iridium (Ir).

designs. Among these, Ru-based systems were first tested by Lunde and Kester in the context of a thorough investigation under NASA Contract NAS 9-9844, aimed at evaluating the Sabatier reaction in closed cycle aerospace life support systems [82]. A Ru-based catalyst was tested in this niche application along with Rh, leading to promising results in terms of selectivity and durability. However, given the prohibitive costs, noble metal-based catalysts are still regarded as feasible only for niche applications or high-constrained ones. An in-depth discussion on Ni-based catalysts is proposed in **Section 2.1.1**, while an overview of the features of catalytic systems based on other active phases is reported in **Table 2**.

Table 2 Overview of the main metals tested for the methanation process [15,74].

Active phase	Main features
Ruthenium (Ru)	Ru is a noble metal and demonstrated to offer high activity and good selectivity towards methane, standing out at low temperatures (< 300 °C, some Ru-based catalysts were found to be active also below 200 °C) and being featured by high resistance to oxidizing atmospheres and carbon deposition. The active phase of Ru-based catalyst facilitates both CO_2 dissociation and direct hydrogenation of formate and methoxy groups. Nonetheless, costs and scarcity represent the main hinderance to the widespread use of Ru-based catalysts, making it suitable only for temperature-constrained settings and other niche application where the financial viability is of marginal relevance. Besides Ni-Ru catalyst with low Ru loading have been reported as a potential compromise to achieve a trade-off between cost and activity.
Iron (Fe)	Fe-based catalysts are extensively utilized in other CO_2 hydrogenation contexts (notably Fischer-Tropsch synthesis to higher hydrocarbons) but are generally less effective for selective methane production. These catalysts have been observed to convert CO to heavier hydrocarbons via FTS pathways, rather than terminating at methane, mandating to operate at stringent temperature and pressure conditions and under over-stoichiometric H_2/CO_2 ratios to obtained high methane yield. On the other hand, Fe is both abundant and inexpensive, and it possesses high intrinsic Reverse Water-Gas Shift (RWGS) activity, which can facilitate CO_2 activation. Therefore, its use has been proposed for the preparation of Ni-Fe bimetallic catalysts, as the addition of small quantities of Fe demonstrated to enhance CO_2 dissociation and increase coke resistance).
Cobalt (Co)	Co is a transition metal and offer advantages in terms of stability and resistance to sintering. Metallic Co performs similarly to Ni in CO_2 hydrogenation reactions, which however occur at higher temperatures. Co-based catalysts are generally more thermally stable and less volatile/toxic than Ni-based ones, with operational lifetimes exceeding 500 hours without significant deactivation. Nonetheless, as for the case of Fe, Co-based catalysts suffer from low selectivity towards methane and often promote the competing Reverse Water-Gas Shift (RWGS) reaction, leading to higher CO formation

as by-product. Only a limited number of Co-based formulations (the ones supported on oxygen vacancies-rich supports) have been reported in the literature that simultaneously achieve high conversion and a selectivity above 95% >95% CH_4 selectivity. Nonetheless, Co is regarded as a suitable as a constituent of bimetallic catalysts or in circumstances where Ni is deemed unfavourable.

In summary, Ni and Ru are the most prominent metals for methanation catalysts, the former being the most appropriate choice for large-scale applications due to its cost-effectiveness and satisfactory performance and the latter being particularly effective in specialised roles due to its exceptional activity. As for Ru-based catalyst, Garbarino et al. [83] compared the effectiveness of a 3 wt.% Ru/Al_2O_3 and a 20 wt.% Ni/Al_2O_3 commercial catalyst in promoting CO_2 methanation at relatively mild operating conditions. The experimental campaign was performed by operating a FBR at atmospheric pressure and at a GHSV of 15,000 h^{-1} and, under this setting, the Ru-based catalyst outperformed the commercial Ni-based formulation. The authors reported a CO_2 conversion of 96% and the absence of carbon monoxide (CO) coproduction under favourable conditions (i.e., 300 °C and excess hydrogen). The authors stressed that the superiority of the Ru-based formulation over the Ni-based one became was mostly at temperatures below 350°C (e.g., the Ni-based formulation reached 80% methane yield only at 400 °C). Subsequent investigation on the same catalyst by Falbo et al. [84] moved towards pressurized operation and demonstrated the possibility of enhancing conversion from approximately 58% to 87% while increasing the pressure from 1 to 7 bar at 310 °C, accompanied by a methane selectivity of approximately 99.9%. Chein et al. [85] performed similar comparison at reduced throughput (i.e., they operated at a GHSV of 5,835 h^{-1}) and found that the optimal reaction temperature for all catalysts under investigation (i.e., a Ni/Al_2O_3 formulation, a $Ru\text{-}Ni/Al_2O_3$ ones) was about 400 °C (e.g., 90% conversion and 80% methane yield for Ru/Al_2O_3. Nonetheless, the Ru-based formulation outperformed the Ni-based one at mild operating conditions, with conversions of 38% and 10%, respectively, highlighting the enhanced activation of Ru under conditions where Ni is mostly inactive. On the other hand, the authors noted that, beyond the optimal temperature, both CO_2 conversion and methane yield decreased, attributing these findings to the occurrence of the RWGS reaction. However, their findings suggest that the use of bimetallic Ru-Ni catalysts can be highly effective in promoting CO_2 methanation at low temperatures. These formulations are obtained by incorporating small amounts of promoters (such as Ru, Pt, and Ce) and are considered a promising solution to enhance activity and stability. Stangeland et al. [86] demonstrated the effectiveness of combining Ru and Ni by testing a 0.5 wt.% Ru-20 wt.% Ni/Al_2O_3 catalyst which led to 82% CO_2 conversion and a 100% selectivity towards methane at 350 °Cand was found stable also when dealing with biogas mixtures.

These intrinsic differences underscore the need to select an appropriate active metal phase based on the performance requirements and economic constraints of a given application, but also to incorporate the proper support within the catalyst formulation. Indeed, the nature of the support and its interactions with

the metallic catalyst are regarded as main influencing factors in terms of catalytic performance. While supports are not featured by any level of activity and should be only considered as carriers for the active phase, their influence on the catalytic performance is significant. Support materials are designed to promote catalyst activity by increasing the available surface area, enhancing the dispersion of the active phase and providing moderate basicity to the catalytic system. Given their high surface area, different oxides have been tested as support for industrial catalysts, including alumina (Al_2O_3), zirconia (Zr_2O_3), silica (SiO_2), ceria (CeO_2), titania (TiO_2), magnesium (MgO) and yttria (Y_2O_3), each bringing different benefits in terms of performance enhancement through different mechanism (e.g., enhanced metal dispersion, enhanced reducibility, metal-support interactions, modification of electronic properties, increased thermal stability etc.). Among the ones tested for methanation, alumina is the most adopted, due to its affordability and its metal dispersion capability. Nonetheless, its tendency to sinter in the presence of water at high temperatures (above 700 °C) could lead to a reduction in surface area and catalytic efficiency Among the different crystallographic modifications of alumina, γ-Al_2O_3 is preferred for its high surface area and porosity, which promote better dispersion and catalytic performance.

Table 3 Support used for CO_2 methanation catalysts [24,74,87].

Support	Main Features
Alumina (Al_2O_3)	γ-Al_2O_3 is the most commonly adopted support material because of its relatively low price and because it promotes the catalytic activity by providing large surface areas, enhancing the thermal stability and establishing strong interactions with the active phase, leading to an optimal dispersion of metal particles and a longer stability. γ-Al_2O_3 is the most suitable crystallographic configuration due to the high surface area and porosity. Nonetheless, Al_2O_3 has a tendency to exhibit slight acidity, and has been observed to interact strongly with Ni during high-temperature calcination or reduction, resulting in the formation of nickel aluminate species ($NiAl_2O_4$). Al_2O_3 itself does not provide oxygen vacancies for CO_2 activation, therefore it is absorbed only weakly on the support surface and Al_2O_3 does not participate in any way to the reactive process, making the metal/Al_2O_3 catalyst performance completely dependent on the active phase. Despite being the benchmark support in the context of heterogeneous catalysts, the use of Al_2O_3 as a support in the methanation reaction is conditioned by its propensity to sinter in the presence of water (which is actually a product of the methanation reaction) at high temperatures.
Zirconia (ZrO_2)	ZrO_2 is an amphoteric and slightly reducible oxide, well-known for its oxygen storage capacity and surface oxygen vacancies (especially when partially stabilized in specific phases). It offers moderate basic sites that can adsorb CO_2, often forming carbonate or bicarbonate species. As a support for Ni or Ru, ZrO_2 significantly enhances CO_2 methanation at lower temperatures. The oxygen vacancies on ZrO_2 activate CO_2 by binding and polarizing the molecule. For example, Ru/ ZrO_2 catalysts benefit from a strong metal-support interaction, as interfacial oxygen vacancies transfer electron density to Ru, modifying its electronic state and enhancing CO_2 activation For Ni catalysts, ZrO_2 also provides benefits

	since it provides basic sites and vacancy-mediated CO_2 activation makes it a widely used support in advanced methanation catalysts.
Silica (SiO_2)	SiO_2 is an inert support (neither reducible nor basic) which provides a largely neutral surface. Ni/SiO_2 catalysts exhibit weaker metal–support interactions than on Al_2O_3. Nickel oxide deposits on silica are easily reduced to metallic nickel (often at ~350–400 °C), resulting in a larger fraction of active metallic Ni after reduction. However, due to the weak interaction, Ni particles on SiO_2 tend to sinter more readily at elevated temperatures, as the support does little to anchor them.
Ceria (CeO_2)	Ceria is widely recognized for its ability to promote strong metal-support interactions (SMSI) and CO_2 activation through oxygen vacancy formation. Ceria ensures a higher resistance towards metal sintering and carbon deposition by leveraging the formation of these oxygen vacances, which is commonly associated with the change of Ce valence states in redox cycling (Ce^{4+} /Ce^{3+}).

Other supports were tested as well, though are less common and effective than the ones listed in the table above. Among the available supports, CeO_2 demonstrated to be one of the most effective, as it effectively participates in the process and influences the reaction mechanisms, bringing substantial benefits in terms of obtainable selectivity. Indeed, redox cycling promotes the formation of reactive species on the surface of the catalyst, increasing the catalyst basicity and promoting the activation of CO_2 molecules [88], though these features were found to depend upon the adopted synthesis technique [89]. Cárdenas-Arenas et al. [90] also emphasized that beyond the increase in oxygen mobility, the Ni/CeO_2 surface is less subject to carbon deposition. On the other hand, non-reducible supports such as Al_2O_3 and SiO_2 do not offer these kinds of advantages but represent a cost-effectives solution and provide both stability and high metal surface area. Medina et al. reported advancements in the development of mixed oxide (e.g., CeO_2-ZrO_2, CeO_2-Al_2O_3, and ZrO_2-Al_2O_3), featured by superior activation properties and stability compared to single-component supports. For instance, doping Ce with Zr has been found to enhance oxygen storage capacity and thermal stability, leading to catalysts outperforming the benchmark Ni/Al_2O_3. Moreover, other kinds of supports based on mesoporous nanomaterials, biochar, activated carbon, and molecular organic frameworks (MOFs) were found to bring substantial benefits to the methanation process. The authors also identified the main benefits brought by the support in the methanation process, such as the increased basicity. Basicity was also found to play a major role in boosting the selectivity of Ni-based catalyst by promoting the formation of monodentate formate species, one of the principal reaction intermediates.

Deactivation Phenomena

Catalyst deactivation (i.e., the loss of activity or selectivity of the catalyst over time) is one of the major challenges in the industrial-scale deployment of methanation technologies. Deactivation severely affects the cost-effectiveness of the process, as it leads to an increase in costs and loss of performance through time. Currently, the average lifetime of industrial methanation catalysts spans from 5 to 10 years, negatively

impacting the long-term viability of the process given the increased operating costs and the progressive loss of performance. A summary of the main deactivation pathways is reported in **Table 4**.

Table 4 Deactivation phenomena and their relevance in the methanation process [22,43,91].

	Description	Relevance in methanation
Sintering	Sintering is the loss of active surface area of catalyst resulting from a prolonged exposure to high temperatures causing metals deposition and agglomeration upon the catalyst surface. This results in both a reduction of active surface area and a deterioration of the remaining active sites. A general rule of thumb prescribes to operate at temperatures of 30–40% the melting point of the active metal or less to hinder the occurrence of sintering.	Sintering frequently occur in operational settings when temperature rises over 500-550 °C (though some studies report it could initiate at temperatures as low as 245°C) and is fostered by water formation as this favours metal oxidation. Strategies to combat sintering include careful control of the reactor temperature profile and the use of sinter-resistant catalyst formulations, such as Ni alloys or perovskite-type structures that release Ni gradually.
Poisoning	Poisoning is caused by the adsorption (either chemical or physical) of chemical compounds on the active site of the catalyst leading to the reduction of available active sites. Once catalyst poisoning happens, either a chemical re-treatment of the surface or a replacement of the poisoned catalyst is required.	Sulphur poisoning is frequent in methanation processes being fed by carbon streams polluted with even small concentration of sulphur compounds. Sulphur poisoning often occurs in case of feed gases coming from steel and cement industries, as well as from biogas fermenters. To avoid the emergence of this phenomenon it is therefore mandatory to abate sulphur impurities in the carbon streams by including appropriate treatment processes (e.g., adsorption with zinc oxide).
Fouling	Fouling refers to the physical coverage of the active phase caused by the deposition of solid species from the gas phase. This is a reversible deactivation mechanism that can be overcome through catalyst regeneration. One of the forms of fouling is coking (carbon deposition), which entails the decomposition of hydrocarbons on the catalyst surface and coke formation.	During methanation, high molecular weight hydrocarbons to primarily carbons such as graphite might form, depending upon the conditions under which the coke was formed and aged. Carbon deposition is promoted by both the Boudouard reaction and methane cracking occurring at high temperatures and results in a rapid deactivation of the catalyst.

Attrition and crushing	The main mechanical deactivation mechanisms are attrition and crushing. Attrition is promoted by the collision of the catalyst particles with each other or with the reactor wall, whereby the particles lose active surface. Attrition leads to the entrainment of some abraded catalyst particles in the product gas and the consequent need to purify the stream with further mechanical treatment to avoid downstream disruptions. On the other hand, crushing is caused by both thermal stresses (due to fast catalyst heating or cooling) and mechanical stresses (due to pressure fluctuations in the reactor).	Both thermal stresses and mechanical stresses can be caused by start-up and shutdown of the methanation reactor and by load fluctuation due to flexible operations in the methanation process. Moreover, the thermal stress is increased by temperature gradients in the particles and by differences in the thermal expansion coefficients at the interface of two different materials.

Finally, it must be underlined that the overall deactivation rate is often a combination of the above-described phenomena. One of the major influencing factors is the strong exothermic nature of the reaction, which often creates localised hotspots with temperature increases of 50–150 °C, accelerating the sintering of the active metal (and its support) and encouraging the deposition of carbon, which ultimately causes the catalyst to become inactive. While the issue of thermal management can be solved by a proper design of the reactor (**Chapter 3**), recent advances in catalyst synthesis have focused on producing more robust catalytic systems that are less susceptible to deactivation.

2.1.1 Ni-based Catalysts

Ni-based catalytic systems detain a major role in most of the catalytic processes and have been a crucial enabler of the thermochemical route for carbon oxides hydrogenation to methane. As previously mentioned, Ni-based catalysts represent a trade-off between relevant performance parameters such as selectivity and activity and cost-effectiveness. Besides, Ni is abundant in the Earth's crust, and this makes Ni-based catalyst economically viable for large scale industrial applications, ensuring a stable and affordable supply. Ni/γ-Al_2O_3 is the commercial standard for chemical methanation. The presence of Ni as active phase provides a high degree of activity to the system that has been linked to the enhanced adsorption and dissociation of the reactants. Ni-based catalysts accelerate the dissociation of molecular hydrogen into its atomic form, which then promotes the hydrogenation of surface intermediates coming from the absorption and dissociation of CO_2. The dissociation of CO_2 is typically the rate-limiting step for Ni-based catalysts.

Nonetheless, despite being widely recognized as the most cost-effective solution in the field, Ni-based catalysts suffer from deactivation phenomena mostly caused by sintering and carbon deposition. These phenomena are prominent with increasing operating temperatures, and it is therefore suggested to control

both the rise of thermal hot-spot and the average reactor temperature to ensure it does not exceed 550 °C. On the other hand, several authors found that under 230 °C there is an increased chance of Ni carbonyl formation, a well-known heavily toxic compound [22,91]. While reactor temperature control could be ensured by a proper design of the reactor (see **Chapter 3**), research efforts are underway to develop synthesis procedures that lead to both a superior thermal stability and an enhanced activity also at low temperatures. Among the main factors affecting the performance of Ni-based catalyst there is the influence and the nature of the interactions of the metallic active phase with the support material, particularly when the system needs to be operated at low temperatures. As mentioned, Al_2O_3 is the benchmark support in case of Ni-based catalysts, and promotes catalytic activity as described in the previous paragraph. For Ni/Al_2O_3 systems, it was found that at high Ni loading, the metal had the tendency to tie up with the support forming $NiAl_2O_3$, a species that is not easily reducible to Ni^0 if not operating at temperatures up to 800 °C. Moreover, it was found that the formation of $NiAl_2O_3$ depends upon the catalyst synthesis procedure, highlighting how the performance of a CO_2 methanation catalyst depends not only on its composition, but also on how it is formulated. Indeed, the adopted synthesis procedure directly influences the obtainable particle size, the dispersion of the metal particles and the nature of metal-support interactions, therefore affecting catalyst reducibility and long-term stability. Ni-based catalysts supported on oxides can be synthetised through a diverse range of processes, among which impregnation (IMP), coprecipitation (CPR), deposition-precipitation (DPR), sol-gel (SG) and others[3]. The IMP method is the most widely adopted given the simplicity of the procedure.

Table 5 Catalyst synthesis techniques [75,91].

Synthesis Method	Description
Impregnation (IMP)	Synthesis through IMP is the most adopted approach given the simplicity of the procedure, which has been scaled at industrial level to produce the currently commercialized catalysts (e.g., METH 134®, Katalco). IMP entails the suspension of the oxide support in an aqueous solution containing the precursors (i.e., the metal salts) to favour the contact between the support and the active phase. In case the volume of the solution is either equal or less than the pore volume of the support, the procedure is labelled Incipient Wetness Impregnation (IW-IMP), whereas if there is an excess of the precursor solution it is called Wet Impregnation (W-IMP). IW-IMP is recommended to obtain high loading of precursors, though in the case of Ni-based catalyst it

[3] Evaluating the effects of the synthesis procedure on the performance of a Ni/Al_2O_3 catalyst, Akande et al. [215] reported that the calcined PR catalyst did not contained traces of $NiAl_2O_3$ and therefore resulted more reducible than IMP and CPR ones. Besides, the authors reported that the DPR catalyst had crystallite of smaller size with respect to the IMP one and these factors together led to enhanced performance in the production of crude ethanol, demonstrating the strong influence of the synthesis process on the catalyst performance.

	was found to promote the formation of aluminates. Finally, the IMP procedure commonly requires additional steps such as drying and calcination to promote the deposition of the metal on the support and does not generally allow to control size distribution and metal dispersion.
Coprecipitation (CPR)	CPR entails preparing an aqueous solution containing both the metal precursor and the oxide in a ratio depending on the desired metal loading for the catalyst to be formulated catalyst. The solution is than added in a drop-wise manner with constant stirring, temperature and pH to a sodium carbonate (Na_2CO_3) solution. The mixed hydroxide is then filtered, dried, and calcined. The CPR promote an intimate mixing of the metal and the support at the atomic level, as the case for the Ni-Al layered double hydroxide. CPR was also found to enhance Ni dispersion, as Ni is uniformly distributed throughout the hydroxide, and this creates stronger metal-support interactions. CPR is also used to create composite supports, such as $Ni/Ce_xZr_{1-x}O_2$ catalysts, in which the Ni atoms can substitute into the ceria-zirconia lattice enhancing dispersion and activity at low temperature by leveraging the multitude of vacancies in close proximity to the active phase. Finally, CPR requires careful control of pH and temperature to achieve consistent results, but it is an effective method of tailoring Ni-support interactions and creating robust catalysts.
Deposition-Precipitation (DPR)	The DPR procedure involves the preparation of aqueous solutions containing a predetermined amount of the precursor (i.e., the metal salts) and a second solution containing the oxide support and an appropriate quantity of sodium carbonate (Na_2CO_3) to induce complete precipitation of the metal salt. DPR combines aspect of IMP and CPR, with metal precipitation occurring by acting on the pH and causing the deposition of the metal hydroxide on the support surface. Since the precipitation occurs uniformly on the support surface, the oxide metal oxide particles are commonly smaller than the ones obtained through IMP and DPR, and this leads to enhancement in activity and higher resistance to carbon deposition, as coke tends to form on larger agglomerates. Finally, DPR allows to incorporate promoters and commonly produces catalysts that are moderately easy to reduce.
Sol-gel (SG)	SG methods involve forming a polymeric gel that contains both a support precursor (e.g., a metal alkoxide for silica or alumina) and a metal salt. Upon drying and calcination, this process yields a highly porous oxide matrix with the metal uniformly embedded throughout the network. The SG route enables excellent dispersion of the metal within the pores, often producing extremely small and well-dispersed metal oxide domains. For example, nickel incorporated via SG into a silica (SiO_2) matrix can result in very fine NiO particles that, after reduction, produce metallic Ni confined within the pores—thereby suppressing sintering and enhancing stability. However, at higher metal loadings, agglomeration of Ni particles during reduction becomes unavoidable.

Concerning Ni-based catalyst, different studies have been performed to understand the implications of the synthesis process and the support. Abate et al. [92] prepared two Ni-Al hydrotalcite samples (HTLCs) by CPR and tested the preparation procedure at different pH to then investigate the ability of the two systems to

promote CO_2 hydrogenation. The authors benchmarked the obtained results with commercial Ni/Al_2O_3 catalysts with equal Ni loading by testing them under the same reaction conditions. The synthetized samples demonstrated superior performance with respect to the commercial formulation, leading to a CO_2 conversion of 86% at 300 °C, a result that was ascribed to the higher reducibility, surface areas and metal dispersion. Song et al. [93] tested a microwave-assisted (MA-IMP) method to synthetize a 20 wt.% Ni/Al_2O_3 catalyst aiming at enhancing Ni dispersion onto the support. The authors compared the activity results of the catalyst obtained through MA-IMP with an equivalent catalyst prepared by IMP, outlining substantially higher dispersion of the active phase alongside an increase in active sites under low temperature and a strengthening of basicity. These improvements led to a better catalytic activity at low temperatures while keeping a good level of selectivity. Thought the last years, Ni/CeO_2 catalytic systems has emerged as a promising solution given the favourable cost-to-activity ratio and the enhanced performance of these systems deriving from the above-mentioned formation of the oxygen vacancies on the ceria support. Pan et al. [94] investigated the catalytic activity of $Ni/Ce_{0.5}Ze_{0.5}O_2$ catalyst prepared through different synthesis methods, those being IMP, PR, and urea combustion (UC). The authors outlined a strong influence of the preparation method on the catalyst performance, with IMP identified as the one leading to the highest surface area, oxygen vacancies, Ce(III) and basic sites, and therefore to the highest activity. Ashok et al. [95] synthetised a series of Ni-based catalysts supported on $Ce_xZr_{1-x}O_2$ prepared by AE, IMP, and PR methods. The authors reported that the 10 wt.% Ni/ $Ce_xZr_{1-x}O_2$ catalyst prepared via AE method demonstrated superior catalytic performance at similar operating conditions and attained the maximum CO_2 conversion (55%) and methane selectivity (99.8%) at a relatively low reaction temperature (275 °C). The enhancements in catalytic activity were attributed to a higher incorporation of Ni species into the CeO_2 lattice, which likely resulted in an imbalance of electric charge and lattice distortion, favouring the generation of oxygen vacancies.

Ni-based catalyst deactivation

A closing note is related to the main deactivation phenomena that occur when using Ni-based catalysts. Starting from sintering, Ni has a Tammann temperature of nearly 590 °C, which means that above this temperature Ni atoms become significantly mobile on the surface [24]. Nonetheless, even below that temperature, the prolonged exposure to moderate-high temperatures (400-500 °C) and the presence of steam were found to induce sintering, further stressing the need for a proper thermal management of the reactor [25].

Ni-based catalysts were also found to be subject to chemical deactivation phenomena rising form vapour-solid reactions and leading to the formation of inactive species such as nickel carbonyl ($Ni(CO)_4$) at low-to-moderate temperatures (~230 °C) and, therefore, during start-up and shut-down phases. Moreover, Ni-based catalyst used in biogas methanation suffered from sulphur poisoning in presence of hydrogen sulphide (H_2S), which caused the nickel sulphide (NiS) and led to a drastic decrease in activity. Therefore, the

presence of sulphur compounds in the feed gas stream must be avoided by properly managing the downstream of biomass gasification units to reduce H_2S content to 10-100 ppb [15].

Reaction Mechanisms

The achievement of the performance requirements in terms of activity, selectivity, and stability critically relies on a thorough understanding of the fundamental mechanisms underlying the conversion of CO_2 and hydrogen into methane [22,24]. Consequently, the preparation of an efficient catalyst for chemical methanation demands an in-depth knowledge of the reaction pathways and the roles of the reaction intermediates involved. Although significant progress has been made in elucidating these mechanisms, the field remains open to debate regarding the key elementary steps and the identity of the most relevant intermediates, which are strongly dependent on the nature of the catalytic system employed. A comprehensive review by Miao et al. [96]provided a detailed overview of the main mechanistic hypotheses for CO_2 methanation as well as the undesired phenomena leading to catalyst deactivation. They emphasized that two principal reaction schemes are generally invoked to explain the observed catalytic behaviour, these being the associative and the dissociative pathways (**Table 6**). The associative scheme predicts the associative adsorption of CO_2 and the subsequent participation of adsorbed hydrogen atoms in braking C-O bonds and forming the oxygenates that will be hydrogenated to methane. On the other hand, the dissociative scheme entails the preliminary cleavage of the C-O bond leading to the formation of an oxygen atom and a carbonyl, which is then hydrogenated.

Table 6 Reaction mechanisms behind CO_2 methanation [96].

	Associative Scheme	**Dissociative Scheme**
General Description	Gaseous CO_2 is adsorbed as carbonate ($CO_{3,ads}$) onto the carrier and the presence of hydroxyls prompts the breakage of C-O bonds reducing the splitting energy barrier. $CO_{3,ads}$ is then hydrogenated into oxygenates such as bicarbonate ($HCO_{3,ads}$), formate ($HCOO_{ads}$), and formyl (CHO_{ads}). The latter intermediates are then progressively hydrogenated into methane. The associative scheme does not foresee the formation of CO intermediate	Gaseous CO_2 is adsorbed ($CO_{2,ads}$) onto the carrier and undergoes splitting into carbonyl (CO_{ads}) and an oxygen atom. Alongside surface carbon (C_{ads}), CO_{ads} represents the main intermediate of this reaction mechanism, that involves the hydrogenation of CO. CO methanation can proceed either by following an associative/hydrogen-assisted route or a dissociative/direct CO splitting one. While the first pathway involves formyl (CHO_{ads}), carbon hydroxyl (COH_{ads}), and formyl (CHO_{ads}) as main intermediates along with the direct hydrogenation of C_{ads}, the dissociative route is majorly driven by the successive hydrogenation of C_{ads}.

Active phase and support roles	The metal–support interface provides active sites, with hydrogen adsorbed and dissociated on the metallic phase, then transferred to the support. Given the competition between C-O bond scission and H_xCO species hydrogenation, the metal/oxide interfaces is supposed to play a prominent role in strengthening the binding of these species to facilitate bond splitting. The support stabilizes oxygenate intermediates, and the interface facilitates C–O bond cleavage and enhances selectivity to methane.	The metal surface, particularly low-coordination sites like steps and kinks, lowers the barrier for direct CO_2 dissociation. C–O bond scission occurs on the metal, forming C_{ads} and O_{ads}, which are subsequently hydrogenated. Surface carbon can also form via the Boudouard reaction (disproportionation of two CO molecules to C and CO_2).

The formate route has been indicated as the most prominent one by many researchers. The so-called formate route includes the simultaneous adsorption of CO_2 onto the carrier and H_2 onto the metal sites. The interaction of adsorbed CO_2 with hydroxyl groups leads to the formation of bicarbonate species, which are hydrogenated to formate species, these being the key intermediate for the conversion into methane. The formation of methane is supposed to occur through the hydrogenation of CHO_{ads} via the formation of formaldehyde and methoxy species. Catalysts assume a major role in determining the reaction mechanism, mostly conditioning it with reference to the temperature operational ranges and the basicity of the system. The latter was also found to play a major role in boosting the selectivity of Ni-based catalyst by promoting the formation of monodentate formate species, as demonstrated by the investigation of He et al. [97]. The authors tested a Ni-Al hydrotalcite derived catalyst and obtained a 82.5% CO_2 conversion and a 99.5% methane selectivity at 350 °C, ascribing the improvement in performance with respect to a conventional Ni/Al_2O_3 prepared through IMP to the presence of basic sites and the facilitated activation of CO_2. Cárdenas-Arenas et al. [90] performed a series of *in situ* DRIFTS analysis to understand the reaction mechanisms featuring Ni/Al_2O_3 and Ni/CeO_2 catalysts and the reason behind the superiority of the latter system. The authors attributed the superior performance of Ni/CeO_2 systems to the availability of two active sites, one at the NiO-Ce interface and another on Ni^0 particles, with the former enhancing the dissociation of CO_2 and the latter available for hydrogen dissociation (**Figure 6**)

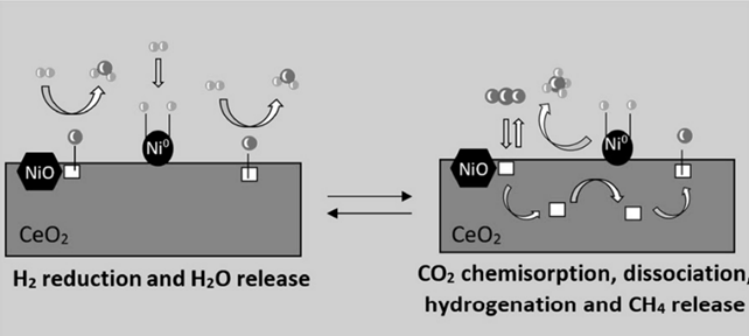

Figure 6 Schematic representation of the reaction mechanisms on Ni/CeO_2 proposed by Cardenas-Arenas et al. [90].

On the other hand, the authors outlined that on Ni/Al_2O_3 catalyst the reactions take place on the same active sites, slowing the release of water and accumulating formate on the surface, therefore delaying CO_2 chemisorption and decreasing the turnover rate of the catalyst. Moreover, the authors stressed that the formation of formate as reaction intermediate resulted in an increase production of CO.

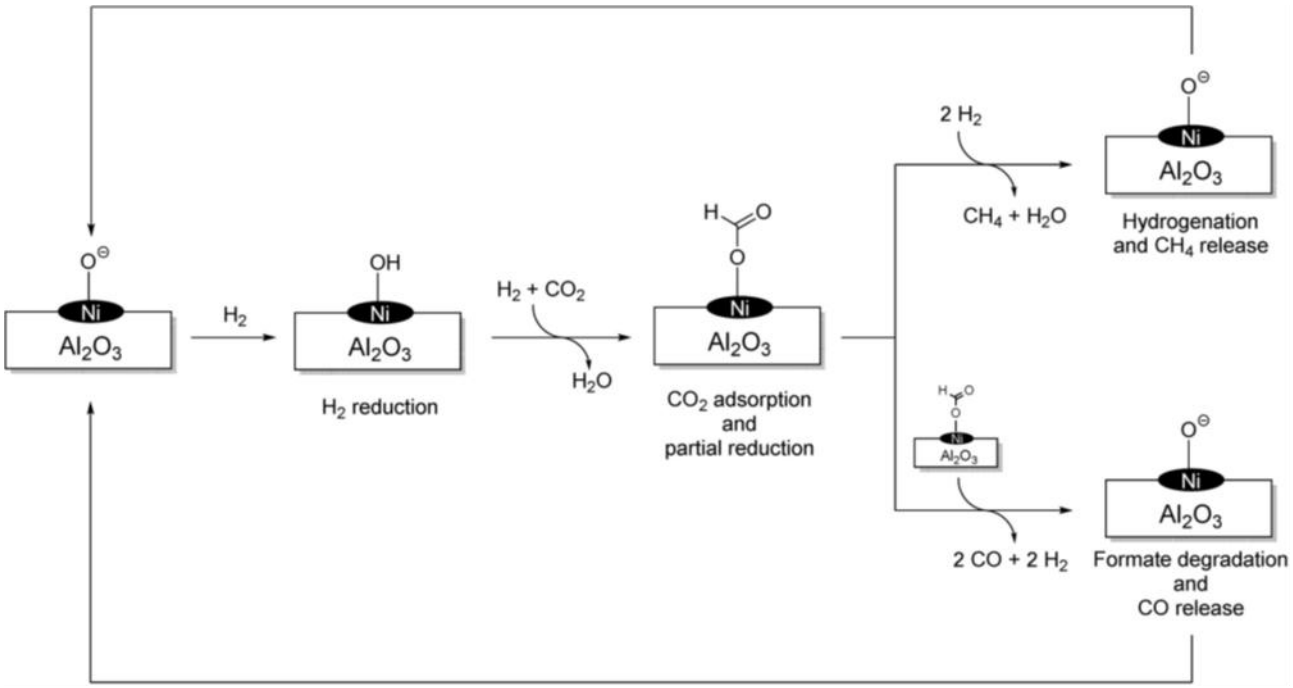

Figure 7 Schematic representation of the reaction mechanisms on Ni/Al_2O_3 proposed by Cardenas-Arenas et al. [90].

2.1.2 The Ni/Ce-Zr Catalyst

The Institute for Advanced Energy Technologies (ITAE) "Nicola Giordano" of the Italian National Research Council (CNR) has a key role in the European research landscape devoted to energy transition technologies, being a reference point for electrochemical, catalytic, and thermochemical energy conversion processes. Under the guidance of Dr. Antonio Vita and Dr. Cristina Italiano, the research group of Hydrogen Production Technologies and Catalytic Materials (FPMAT) has developed and tested a range of catalytic systems and

reactor configurations to operate the methanation process at low temperatures. The research efforts have been largely focused on the synthesis and characterization of advanced Ni-based catalysts, supported on doped oxides such as CeO_2, zirconia ZrO_2 and Y_2O_3. The objective of their research was to demonstrate the enhanced effectiveness of these kinds of support in enhancing activity and stability under operational conditions, leveraging features such as metal dispersion and oxygen mobility. FPMAT has pioneered the application of Solution Combustion Synthesis (SCS) for the synthesis of these catalytic systems (see **Section 2.2.1**), testing their effectiveness in different forms and reactor configurations. Indeed, the developed Ni-based catalysts have been tested both as powders and as coating for open-cell ceramic foams, operating at both lab-scale and pilot-scale. Investigations on structured catalyst have led to promising results, given the higher conversion efficiency and enhanced reaction control provided by the higher surface area, enhanced mass and heat transfer, and lower pressure drops.

Italiano et al. [76] started investigation the methanation of carbon oxides (both CO and CO_2) using 15 wt. % Ni-based catalysts supported on CeO_2, Al_2O_3 and Y_2O_3 oxides, then investigating the effects of different Ni loading (7-35 wt. %) on the catalytic system supported on Y_2O_3. The obtained results highlighted a higher susceptibility of Ni/CeO_2 to coke deposition driven deactivation, while the loss of activity for the Ni/Al_2O_3 was linked to the formation of $NiAl_2O_4$. On the other hand, Ni/Y_2O_3 catalyst demonstrated a substantial activity degree (majorly linked to an enhanced Ni dispersion within the support and to the medium-strength basicity) and high resistance towards both coking and sintering during the stability tests. Vita et al. [98] investigated the bench-scale performance of 25 wt. % Ni/GDC catalyst supported on ceramic monolith (MO) and open-cell foam (FO) prepared by the In Situ Solution Combustion Deposition (IS-SCD) method to coat the support with a thin, uniform and high-resistance catalytic layer. The authors conducted different experimental runs in *quasi-adiabatic conditions* and found that the geometry of the support exerted a significant effect on the thermal profile of the catalytic bed, being therefore regarded as a determining factor for the superiority of the MO configuration over the FO one. Later, Italiano et al. [99] performed a similar investigation by comparing (bench-scale) the viability of two structured catalysts based on high thermal conductivity silicon carbide (SiC) based and alumina (Al_2O_3) based structured catalysts coated (loading of 0.5 g cm^{-3}) through IS-SDC with an active phase of 25 wt. % Ni, 20 wt. % CeO_2 and 55 wt. % ZrO_2. The tests, performed in a Heat Exchanger Reactor (HER) using air as cooling medium, revealed that a proper thermal management enhanced the performance of both investigated configurations. Besides, the authors reported that SiC foam provided a more favourable and uniform temperature profile, as SiC foam was featured by a higher thermal conductivity of SiC than alumina. Moreover, the latter favoured the rise of thermal hot spots, and the consequent equilibrium shift towards CO (via RWGS) under identical operating conditions. The group also contributed to the development of bimetallic Ni-noble metal catalyst at low noble metal loading. The work of Tsiotsias et al. [100] was aimed at investigating the catalytic performance of Ni-based catalyst doped with 1 wt. % of different noble metals (Ru, Pt, Rh, Pd, and Ir) supported on Pr-doped CeO_2. The authors reported that Ru was the only loading that effectively enhanced the catalytic

activity of the corresponding monometallic system (80% conversion, 99.5% selectivity towards methane with respect to 80% conversion, 99.5% selectivity towards methane in the base case at 325 °C). The improvements obtained were attributed to the homogeneous dispersion on Ru along the support (as single atoms or small clusters) and also atop the medium-sized Ni nanoparticles (DFT analysis evidenced a more favourable setting for CO_2 and H_2 adsorption and dissociation). On the other hand, the authors reported a worsening of the catalytic performance consequent to the use of Rh and Pd and no noticeable effects for Pt and Ir. Other authors also found that the use of Ru and Pt as promoter is effective in enhancing the dispersion of Ni particles improving reducibility, stability and resistance to sintering and carbon deposition. Medina et al. [24] identified Ru as the most influential promoter, highlighting the enhanced hydrogenation activity and the higher resistance to deactivation phenomena are essential as the main features leading to higher methane yields.

A focus on Solution Combustion Synthesis (SCS)

Solution Combustion Synthesis (SCS) is a self-propagating high-temperature synthesis (SHS) technique that has been recently introduced and adopted for the preparation of a variety of inorganic nanomaterials. SCS was first described in 1967 by Russian scientists Merzhanov, Skhiro, and Borovinskaya, who prepared ceramic and intermetallic compounds via solid flame combustion [101].

SCS relies on a self-propagating exothermic redox reaction that occurs starting from an aqueous solution generally comprising one or more oxidizers (i.e., the precursors in catalyst synthesis, therefore the metal nitrates) and an organic fuel. The latter is often a high-nitrogen organic such as glycine (NH_2CH_2COOH) or urea ($CO(NH_2)_2$), which serves as a reducing agent and combustion fuel. The synthesis procedure generally entails the following steps [102,103]: (1) preparation of a homogeneous aqueous solution to enhance the intimate mixing, at molecular level, of the oxidizer and the organic fuel; (2) sample concentration to increase the viscosity; and (3) ignition and combustion.

The ignition phase is the sole energy demanding stage of this procedure, though given the high amount of heat released by the combustion reaction itself (temperatures can reach up to 1500 °C) the reaction occurs rapidly and does not necessitate further external energy. Only a small amount of heat (e.g., a hotplate or furnace preheated to 250-350 °C) is required to initiate the combustion. Given the rapid completion of the combustion reaction, the process is commonly assumed to be adiabatic. Internal chemical energy, originating from fuel combustion and nitrate decomposition, substitutes for the external fuel or electricity that would otherwise be needed for high-temperature processing. After combustion, additional heating may be required (e.g. holding at 500–600 °C for 0.5–1 hours) to ensure complete conversion, but this is minimal compared to conventional multi-hour calcination. The main features of the synthetized powders, such as crystalline size, surface area, and extent of agglomeration are commonly assumed to depend on the enthalpy of combustion and the flame temperature, emphasising the major role of the nature of the oxidizers and the fuel [102]. Some authors report that given the high temperatures attained, the

crystallization process occurring during combustion is sufficient to ensure that the synthetized materials have reached the desired specifications in terms of degree of crystallization and purity (therefore, it is possible to avoid calcinations treatments).

The main advantages of SCS lies are related to the significant reduction in synthesis time and the use of simple equipment, beside the inherent versatility of a procedure that can be used to produce high purity and stable products of different sizes and shapes with a precise control over morphology, surface area and metal dispersion. Moreover, the process is scalable and versatile in terms of application, making SCS a cost-competitive and economically attractive solution [103]. From the techno-economic and environmental perspective, it is important to note that the energy demand in SCS is concentrated in the production of the precursors and the inherent fuel energy, rather than in long-term heating processes. A broader review of SCS in catalyst preparation reinforced these findings by describing the versatility of the method across a range of catalytic systems. The authors emphasized that SCS enables fast, energy-efficient production of porous, nanostructured oxides, where properties such as phase composition, morphology, and surface chemistry can be controlled by tuning synthesis parameters like the choice of fuel, metal precursors, and reaction atmosphere. This positions SCS as a hybrid approach that combines the benefits of combustion synthesis and precipitation techniques, resulting in materials with desirable textural and catalytic properties.

The FPMAT research group first adopted SCS to prepare Ni/CeO_2 nano powders for biogas Oxy Steam Reforming (OSR) [104,105]. The authors investigated the influence of both Ce-precursor and fuel (oxalyldihydrazide, urea, carbohydrazide and glycerol) on the morphological and structural properties of the synthetized catalyst, founding that the use of urea was effective in guaranteeing an enhanced dispersion of the active phase (Ni) alongside an increase in surface areas, particle size and reducibility. Besides the catalytic systems described above and formulated by the FPMAT research group, recent studies demonstrated that SCS is highly effective in preparing Ni-based catalyst for methanation. Zhao et al. [106] prepared Ni/Al_2O_3 at different Ni loadings, spanning from 10 to 50 wt.%. The authors found that a complete conversion of CO could be obtained above 20 w.t% Ni, with the formulations based on SCS outperforming with respect to the ones prepared by impregnation method. Summa et al. [107] tested the preparation of Ni-Mg-Al mixed-oxide catalysts through SCS to overcome the challenges of the conventional approaches used in synthetising hydrotalcite-derived catalysts. The authors compared the catalytic performance of a series of Ni-Mg-Al systems with a Ni loading of 20 wt.%, assessing the feasibility of proceeding with both a stoichiometric and an above-stoichiometric SCS performed with urea as fuel. The catalysts formulated via SCS outperformed the reference hydrotalcite-based one, achieving CO_2 conversion of up to 89% at 300 °C, driven by a small specific surface area and an increased basicity of the catalyst surface. Moreover, the authors suggested that an increase in urea content was likely to lead to the formation of a spinel phase. Later, Summa et al. [108] also investigated the chance of promoting the obtained catalyst with Co to enhance reducibility, basicity, and textural properties. Among the investigated synthesis routes, the authors reported

that while the simultaneous combustion of all the precursors would have led to a substantial decrease in activity, the addition of Co in a second step effectively enhanced the catalytic performance with respect to the first synthetised formula. Collectively, these studies confirm that SCS is an effective alternative to conventional thermal decomposition routes for preparing high-performance Ni-based catalyst. On the other hand, given the high impregnation effectiveness recorded for Ru-based formulations through conventional preparation methods, this synthesis technique has been scarcely applied. Based on the extensive reviews of Tommasi et al. [15] and Zhang et al.[74], none of the high-performing Ru-based catalyst has been prepared via SCS, whereas other techniques such as solvent-free SG routes and metal-organic frameworks (MOFs) templated supports have been tested to further enhance Ru dispersion [109]. A notable exception is represented by the work of Sharma et al. [110], who tested and compared SCS and co-precipitation methods to directly incorporate Ru into the ceria lattice and produce Ru-doped ceria supports (i.e., $Ce_{0.95}Ru_{0.05}O_2$). The authors confirmed that the substitution of Ru in ceria could lead to the creation of abundant vacancies and distinctive carbonate intermediates, further demonstrating the potential application of SCS to Ru-based applications.

2.1.3 Environmental Implications

Despite being the core of each chemical process, the role of catalysts has been only marginally addressed in recent literature on the economic and environmental implications of CO_2 utilization. From the chemical perspective, catalysts are essential to enable the reaction advancement as they function as a reduction lever of the activation energy and foster reaction selectivity towards desired products [75]. The need to advance CCUS technologies and come closer to commercialisation has prompted the development and investigation of both novel catalyst for heterogeneous catalyst hydrogenation and conversion approaches based on photocatalysis and electrocatalysis. Focusing on the first route, metal-based catalyst such as copper (Cu), nickel (Ni), and cobalt (Co) have been extensively employed in CO_2 hydrogenation, more often combined with supports or zeolites (i.e., microporous aluminosilicate mineral) to foster effectiveness are mostly far from the commercial scale, and there is therefore the need and the opportunity to screen and select the proper catalytic system in the early-stage phase also based on their environmental footprint.

Agarski et al. [111] developed a multi-criteria analysis to assess the competitiveness of their synthesis procedure for a Ni-based catalyst supported on reticulated ceramic foam (Ni-Pd/Al_2O_3) with respect to conventional synthesis procedures. The authors prepared a monolithic Ni-Pd/Al_2O_3 by impregnating α-Al_2O_3 with an ultrasonically generated aerosols of dissolved metal chloride (i.e., palladium chloride, $PdCl_2$ and nickel chloride, $NiCl_2$) at 200 °C. The performed LCA allowed to demonstrate the superior environmental performance of their synthesis approach with respect to other Ni-based catalyst and synthesis processes, all featured by a significantly higher energy consumption leading the resulting environmental footprint. More recently, Kar and Veluswamy [112] developed and applied an LCA-based screening criteria to aid the selection of the most sustainable Cu-based catalyst for the catalytic conversion of CO_2 to ethanol. The authors compared Cu/C-0.4 (0.4 wt.% of Cu supported over carbon) and Cu@Na-Beta (2 to 5 nm Cu

nanoparticles embedded in Na-Beta zeolite) considering electricity purchase from either the local grid or a stand-alone solar photovoltaic system, for a total of four different product systems. Performing the environmental assessment over 17 different impact categories, the Cu@Na-Beta resulted to be most suitable system under the environmental perspective in each considered category. Concerning with the Fischer-Tropsch Synthesis (FTS) process, Aromaa-Stubb et al. [113] investigated the environmental impacts resulting from the use of Co-based catalysts, focusing on their manufacturing and recycling potential (recycling of spent catalyst as cobalt hydroxide, cobalt sulfate, or cobalt carbonate). The authors adopted a gate-to-gate approach to investigate the impacts of Co-based catalyst in FTS and a cradle-to-gate perspective while looking at catalyst manufacturing. The assessment was referred to the pro 1 MT of 20 wt. % Co-based catalyst.

Several studies have been conducted to understand the environmental implications of certain process configurations in the framework of CO_2 methanation. Nonetheless, most of these studies focused on the whole process rather than on the catalyst lifecycle, majorly looking at other stages of the methanation process (e.g. hydrogen production and carbon sequestration) [24,75]. This underscores a research gap in the assessment of the holistic performance of the methanation process, with a focus on the catalyst role. Recent advancements in the field of methanation have been accompanied by comprehensive LCA studies focused on pilot-scale implementation and on the impacts associated with industrial-scale deployment of this technology. Dealing with the biological route, a recent work by Heber et al. [114] investigated different scale-up scenarios of a pilot-scale trickle-bed reactor for biological methanation projected up to 2050. The authors found that scaling up the plant could lead to a reduction in the overall environmental footprint of the process with significant ecological benefits (potential emissions reduction ranging from 23 to 780 compared to the current pilot set-up). The performed hot-spot analysis revealed that the largest impacts were attributable to hydrogen production, given the high energy-intensive nature of the electrolysis process. Navajas et al. [115] investigated a Power-to-Methane (PtM) configuration fed with CO_2 supplied by the chemical looping combustion (CLC) of biomass (PtM-bioCLC) to understand the actual environmental impacts associated with different configurations. As for the chemical route, most of the performed investigations are focused on the impacts of the operational stage under different feedstock procurement scenarios or methanation concepts. Gerloff [116]analysed different scenarios of SNG production by varying carbon sources, hydrogen production technologies and background settings related to the current (2019) and perspective (2030 and 2050) energy system structures in Germany as well as to the case of stand-alone renewable energy plants. The author found that producing hydrogen through Solid Oxide Electrolysis Cell (SOEC) led to the lowest GHG emissions in all the investigated scenarios except that of stand-alone power generation, in which the best choice resulted to be Alkaline Electrolysis (ALK). Nonetheless, the author revealed that except for renewable energy driven SNG production, all the considered routes had a higher environmental footprint than conventional natural gas extraction. Their outcomes underscore the crucial role of electricity supply in enabling an effective enhancement of environmental performance and suggest

that a more sustainable production of SNG will be possible once the share of renewable energies will reach higher values. Similarly, Vega Puga et al. [117]performed an LCA focusing on global warming potential (GWP) in order to determine the actual emission factor the electricity mix should have to deliver a meaningful environmental benefit with respect to the fossil counterpart. The authors outlined that only a decrease in the grid emission factor down to 121 g $CO_{2,eq}$ per kWh_{el} would have led to an environmentally sounding process. Federici et al. [118] investigated the environmental implications of a methanation pilot plant (1 mol h^{-1} of methane) consisting of a 1 kW prototype of a patented alkaline water electrolysis unit equipped with graphite electrodes aimed at syngas production and a catalytic reactor equipped with a Ni/CaO-Al_2O_3 catalyst. The developed prototype reached a methane yield of 25.5%, a CO_2 conversion of 44.2% and a methane selectivity of 96.5% while operating a 1 bar. The performed environmental assessment accounted for on-field gathered data to model the foreground process and outlined a major relevance of energy inputs and construction materials to the obtained environmental profile, the latter likely resulting from the considered scale of the plant.

Shifting the focus on the catalyst, Wang et al. [119] investigated the environmental performance of methanation carried out employing a Ni/CeO_2 catalyst supported over activated biochar (Ni/Ce-ABC) obtained through pyrolysis, *in situ* activation with $NaHCO_3$ and Ce doping. The authors found that biochar-based catalyst could contribute to mitigate the environmental burden related to the catalytic system, as this guaranteed similar performance with respect to conventional catalyst while reducing the impacts connected to metal oxides. Nonetheless, the synthesis phase was the one linked to the highest share of environmental impacts and the obtained reduction in the other impact categories was ascribed to the use of biomass as raw material, as well as on the co-production of syngas. Sayyah et al. [120] performed a thorough LCA on CO_2 methanation considering five different catalytic systems under similar operating conditions, either supported over metal oxides (Ni/Al_2O_3 and Ni/TiO_2) or zeolites (Ni/Na-ZSM-5, Rh@HZSM-5, and Rh@KZSM-5). Based on the higher conversion and methane selectivity, the authors reported that Ni/Al_2O_3 was highly effective in mitigating the environmental burdens of the methanation process by lowering the generation of toxic wastes and the release of GHGs emissions (for instance, the GWP resulted 20% and 25% lower than the cases of Ni/TiO_2 and Ni/Na-ZSM-5, respectively). Moreover, the authors identified the use of Rh@HZSM-5 as critical in terms of environmental toxicity given the high level of harmful emissions associated to the production of Rh (0.0044 kg CFCs and 2,229 kg of SO_2 per kg of Rh). Eventually, to describe the relation between the catalyst features and the investigated environmental impact indicators, the authors stated that conversion and selectivity were the most influencing parameters to determine the *greenness* of a catalytic system. Sayyah et al. [121] developed a machine learning-based multi-objective optimization algorithm to identify the proper lifecycle structure of CO_2 methanation processes able to minimize the environmental externalities while delivering the best possible technical performance. Considering a Ni/Al_2O_3 catalyst obtained through a impregnation technique, the authors

found that the synthesis phase contributed the most to the whole process environmental impacts, with the production of nickel nitrate outstanding in terms of significance on the contribution tree.

2.2 Methods

2.2.1 Catalyst Synthesis

25 wt. % Ni/20 wt. % CeO_2-55 wt. % ZrO_2 catalyst powder was obtained through Solution Combustion Synthesis (SCS). The synthesis procedure entailed the preparation of an aqueous solution containing high-purity reagent-grade nickel nitrate ($Ni(NO_3)_3{\cdot}6H_2O$, Sigma Aldrich), cerium nitrate (($Ce(NO_3)_3){\cdot}6H_2O$), Sigma Aldrich), and zirconium oxynitrate hydrate ($ZrO(NO_3)_2){\cdot}6H_2O$, Sigma Aldrich) as oxidizing precursors and urea ($CH_4(N_2O)$, Sigma Aldrich) as the organic fuels (i.e., the reducing agent). The amounts of nitrates and urea were computed to obtain a fuel-to-oxidizer ratio (φ) equal to 1, meaning that the total oxidizing powers of the nitrate ions (O) exactly balances the reductant (F) and complete combustion occurs without residual oxidizers or fuel. This condition guarantees that the reaction evolves according to stoichiometric conditions and there is no participation of atmospheric oxygen in the reaction, which however proceeds up to the complete oxidation of fuel, releasing the maximum amount of energy. Besides, the amounts of metal precursors were therefore computed to yield the desired catalyst composition upon forming nickel oxide (NiO), ceria (CeO_2) and zirconia (ZrO_2).

The metal precursors and the fuel were dissolved in 500 mL of distilled water under vigorous magnetic stirring (1500 rpm) and a slight degree of heating (35 °C) to enhance the dissolution of zirconium oxynitrate. Once obtained a homogeneous solution, this was placed in a muffle furnace preheated at around 350 °C and the solution was left there for around 2 hours. In the furnace, the solvent gradually evaporates until the mixture reaches the self-ignition condition and, once dry-out is reached, the combustion process is trigger and there is a rapid temperature rise that sustain the reaction. The intense exotherm decomposition of the nitrates yields to a voluminous fluffy solid product that contains the metal oxide phases (largely amorphous or nanocrystalline at this stage) and residual char, alongside small amounts of encapsulated gaseous bubbles made of CO_2, N_2, and water vapor. These gases (alongside possible traces of carbon monoxide and nitrogen oxides) are generated due to the high temperatures and short reaction times and are essential to inhibit crystallites growth, limit the formation of agglomerates, and favour the formation of a porous structure. The combustion reaction is generally described using propellant chemistry and, for the investigated case, it is described by Eq. (10), representing a stoichiometric redox reaction between the fuel and the oxidizers with the net oxidizing valency of the metal nitrates equalled to the net reducing valency of the fuel.

$$0.45Ni(NO_3)_2 + 0.43ZrO(NO_3)_2 + 0.11Ce(NO_3)_3 + 1.76CO(NH_2)_2 \rightarrow 0.45NiO + 0.43ZrO_2 + 0.11CeO_2 + 9.52H_2O + 1.76CO_2 + 2.82N_2 \quad \text{Eq. (10)}$$

The final refinement of the catalyst powder was conducted via a calcination treatment, designed to eliminate any residual organic compounds and thereby ensure the completion of the crystallisation of the oxide support. The calcination process was conducted in air at 600 °C for a duration of 2 hours (heating ramp of 5 °C per minute) and, following its completion, the resultant powder was cooled to room temperature, was collected in a laboratory jar and subjected to classification. The friable powder obtained from the calcination was not suitable for the catalytic testing, and it was therefore pelletised through a uniaxial hydraulic pressure (application of static pressure of 100 MPa over a period of 12 hours) and sieved to obtain a uniform particle size and avoid dust that could have interfered to mass transfer phenomena within the reactor. The dense pellet was crushed and gentle grinded using a mortar and pestle and the resulting fragments were then sieved to 50–70 mesh, collecting only particles in the 212–300 µm size range (approximately 250 µm average). The sieved catalyst (50–70 mesh granules) was stored for subsequent reactor testing.

2.2.2 Catalyst Testing

Catalytic performance of the 25 wt. % Ni/20 wt. % CeO_2-55 wt. % ZrO_2 catalyst (Ni/Ce-Zr formulation in following sections) powder was evaluated in an independently controlled fixed-bed tubular reactor (FR-100, micrometrics®) whose specifications are resumed in **Table 7**.

Table 7 Technical specifications of the FR-100 reactor.

Reactor	Material	Design Param	ID (mm)	OD (mm)	Length (mm)
R01	SS316	650 °C@100bar 800 °C @1bar	9.1	14.3	304.8

The catalyst granules (50–70 mesh) were diluted with inert quartz (inert SiO_2 grains of similar size) to mitigate hot spots and axial temperature gradients in the bed. A total of 200 mg of catalyst was thoroughly mixed with 1,800 mg of quartz, corresponding to a 1:9 catalyst-to-quartz mass ratio. The diluted catalyst bed was loaded into R1 and the resulting bed (approximately 25 mm of length) was confined between two quartz wool plugs and a porous plate made of Hastelloy (20 µm pore size) to ensure the physical containment of the catalytic material within the heated zone Additionally, 15 µm metal filters (F-04 and F-05) were installed at both the inlet and outlet of the reactor to protect the upstream and downstream instrumentation from fine particulates. A type-K thermocouple (TT-02) with an Inconel sheath and high-temperature connector was used to closely monitor the reaction temperature. The thermocouple was inserted coaxially into the reactor and positioned 5 mm above the porous plate, thereby residing in the central region of the catalyst bed. Once assembled, the reactor was inserted into the tubular furnace, and temperature regulation was

achieved via a PID controller. The latter ensured stable ramping and holding phases with minimal overshoot and high thermal reproducibility.

Prior to introducing reactive gases in the reaction system, the catalyst was activated *in situ* by reducing NiO to metallic Ni (Ni^0). To this end, the reactor was firstly purged with an inert stream of pure nitrogen and then treated with a 50% H_2/N_2 gaseous stream (80 mL min^{-1}) at 600 °C for 1 hour (heating ramp of 20 °C per minute to avoid thermal degradation). The H_2 flow rate and the treatment time were selected consistently with previous studies on a similar catalyst system to secure the full reduction of NiO to metallic Ni. Once the reduction phase ended, a N_2 stream was flushed to fasten reactor cooling and bring it back to initial reaction temperature (N_2 flow rate of 40 mL min^{-1}).

The methanation tests were carried out at atmospheric pressure using a feed gas mixture with a H_2:CO_2:N_2 volume relation of 4:1:5 (i.e., stoichiometric reactant ratio for the Sabatier reaction and nitrogen used as internal diluent. The total flow rate was set to 400 mL min^{-1}, equivalent to a weight-specific velocity (WSV) of around 12,000 mL $(g_{cat}\ h)^{-1}$ for the 0.2 g catalyst loading and to a gas hourly space velocity (GHSV) on the order of 15,000 h^{-1} referred to the diluted bed volume. The gas flowrate was precisely regulated using a mass flow controller (Bronkhorst Mass Flow), and once steady-state conditions were established, the catalytic activity was evaluated over a temperature range of 150 °C to 450 °C, in steps of 25 °C, and at pressure of 1, 5 and 10 bar. The PID-controlled furnace enabled a programmed temperature ramp with minimal overshoot, with the inert dilution mitigating hot spot formation and providing an adequate assurance that the measured temperature was close to the true bed temperature. The outlet gas composition was automatically evaluated at each temperature set-point after an equilibration period via an on-line gas chromatograph (Agilent 7890, Agilent) equipped with thermal conductivity detector (TCD) and flame ionization detector (FID). At the end of each experimental run, the reactor was cooled and flushed under nitrogen environment (40 mL min^{-1}). For each test, at least three sets of data were recorded for each reaction condition. Catalytic performances were evaluated in terms of CO_2 conversion (Eq. (11)) and CH_4 yield (Eq. (12)).

$$\chi_{CO_2}(\%) = \frac{F_{CO_{2,in}} - F_{CO_{2,out}}}{F_{CO_{2,in}}} \cdot 100 \qquad \text{Eq. (11)}$$

$$Y_{CH_4}(\%) = \frac{F_{CH_{4,out}}}{F_{CO_{2,in}}} \cdot 100 \qquad \text{Eq. (12)}$$

where *in* and *out* notation refers to the inlet and outlet molar flow rate of the reagent mixture and the product stream, respectively.

2.2.3 Catalyst Environmental Impacts

Life Cycle Assessment (LCA) is an internationally standardized and institutionally recognized methodology aimed at computing the environmental impacts associated to the lifecycle of goods, processes, and services

[122,123] (see **Life Cycle Assessment (LCA)**). The present investigation has been performed with the software openLCA 2.0.0. and was aimed at investigating and comparing the environmental impacts of different synthesis techniques and methanation concepts considering activity tests performed at similar operating conditions. The synthesis process represents the initial phase of the lifecycle of catalyst, and it is the main object of the present investigation. The reference catalyst (CAT-01) is a Ni/Al_2O_3 prepared through WI and tested by Song et al. [93], while CAT-02 refers to CNR-ITAE Ni/Ce-Zr formulation and CAT-03 is a Ni/Ce-Zr formulation prepared through WI and tested by Ashok et al. [95].

Table 8 Synthesis procedure for CAT-01 [93] and CAT-03 [95]

Catalyst	Synthesis Procedure
CAT-01	A 20 wt.% Ni/Al_2O_3 catalyst prepared through WI. The synthesis procedure consisted in preparing the solution containing the metal precursors, adding γ-Al_2O_3 and then let the solution under controlled mixing at room temperature for 6 hours. The solution was than dried at 120 °C for 6 hours and calcined at 400 °C for 4 hours. Prior to operation, the catalyst was reduced with H_2:N_2 of 4:5 at 450 °C
CAT-03	A 10 wt. % Ni/50 wt. %CeO_2-40 wt.% ZrO_2 catalyst prepared through WI. The synthesis procedure consisted in preparing the solution containing the metal precursors, adding CeO_2/ZrO_2 in a 1.35 ratio, and then let the solution under controlled mixing at 80 °C for 3 hours. The solution was than dried at 120 °C for 24 hours and calcined at 500 °C for 5 hours. Prior to operation, the catalyst was reduced with H_2 at 450 °C

The three catalysts were compared with respect to two different functional units, the first being referred to the production of 1 kg of catalyst and the second to the production of 1 Nm^3 of methane. The system boundaries, depicted in **Figure 8**, includes extraction and processing of raw materials, manufacturing of laboratory-grade chemicals, catalyst synthesis, catalyst post-treatment, catalyst reduction and reactor operation. End-of-life of the catalysts is not included in the system boundaries.

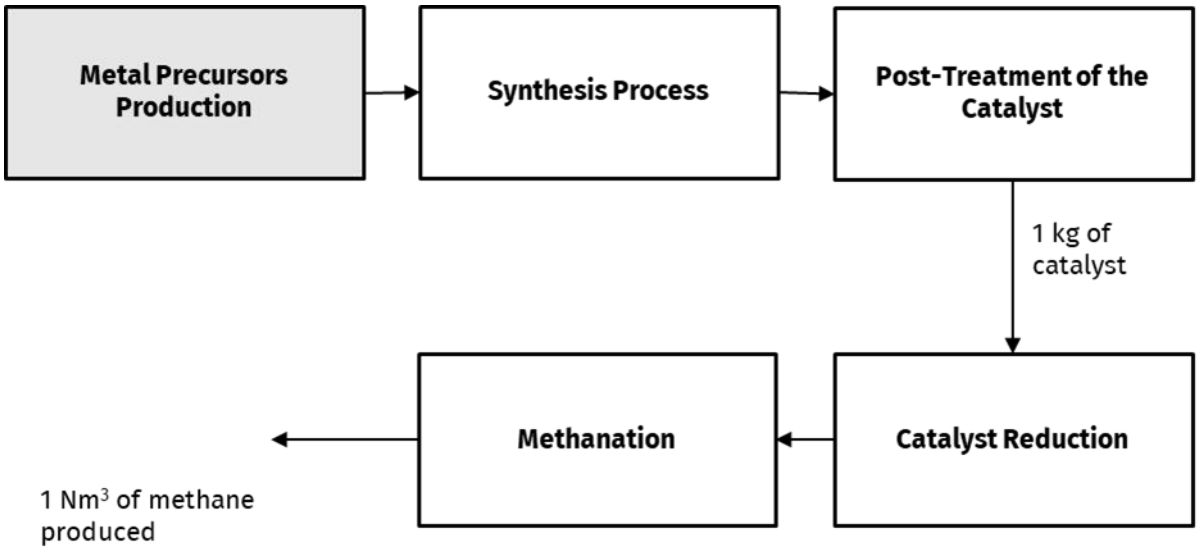

Figure 8 Cradle-to-gate system boundaries to produce 1 kg of catalyst and 1 Nm^3 of methane through CO_2 methanation.

For all the three investigated cases, the system boundaries include:

- **Catalyst Manufacturing**. This product system includes the synthesis processes (i.e., WI and SCS) modelled with foreground data and the extraction, production, and transportation of precursors and supports (i.e., metal nitrates, alumina, ceria-zirconia) modelled by retrieving data from literature.
- **Reactor Operation**. This product system is modelled using foreground data taken from literature and on-field testing campaign. Reactor operation phase includes both material inputs (e.g., the catalyst, possible inert, and the feed gas) and energy inputs (e.g., electricity, heat, cooling medium). Methane is considered as the unique output (and functional unit) of the process.

The testing conditions and the results obtained three catalytic systems under investigation are reported in **Table 9**.

Table 9 Steps of the synthesis procedures adopted to formulate the catalysts under investigation

Parameter	CAT-01	CAT-02	CAT-03
WSV [mL ($h\ g_{cat}$)$^{-1}$]	4,200	12,000	20,000
H_2:CO_2:N_2	4:1:4	4:1:4	4:1:7.5
Temperature [°C]	325	325	300
CO_2 Conversion [%]	84.3	89.6	45

CH_4 Selectivity [%]	97.9	91.0	99.8
CH_4 [mol $(g_{cat}\ h)^{-1}$]	0.02	0.44	0.03

Life Cycle Inventory

The quantitative comparison of the environmental impacts related to CAT-01, CAT-02 and CAT-03 relies upon a detailed Life Cycle Inventory (LCI) that was compiled for each investigated system. The LCI covers the most significant energy and material inputs and outputs related to the synthesis and utilization of each catalyst, first considering the production of 1 kg of catalyst in the pre-reduced form and then reactor operation.

The data used for the LCI phase are categorized as follow:

- **Foreground Data**. These data are directly related to catalyst synthesis and experimental testing and were gathered during controlled laboratory campaigns conducted at CNR-ITAE as far as concern CAT-02. These data include material and energy inputs, process conditions, and emissions and are further classified with reference to their quality
    - Data related to material inputs for catalyst synthesis, catalyst and inert dosages, and reactor performance are actual values coming from multiple test replicates. Therefore, those reflect real system behaviour under representative operating conditions and are considered high-quality primary data, with complete technological and geographical representativeness, and high temporal relevance.
    - Energy consumption data were estimated based on process duration, equipment nameplate power ratings, and energy balances around individual steps (e.g., furnace calcination, thermal reduction). Given their estimated nature and the absence of real-time monitoring, these data are associated with a lower degree of precision. Their temporal and technological representativeness is consistent with lab-scale conditions, but improvements in data quality could be achieved via integrated power metering and explicit modelling of equipment efficiency.
- **Background Data**. Data for upstream processes (e.g., precursor synthesis, electricity generation, rare earth separation) were sourced from the ecoinvent v3.9 database and refer to the Italian context. In case of lack of available data for Italy, Europe averaged (Rest of Europe, RER) or global (GLO) data were used. These are considered secondary data, with good completeness and geographical representativeness, though specific sub-processes (e.g., metals extraction) may still carry uncertainties due to variation in industrial practices.

Starting from the precursors, the LCI incorporates the upstream impacts related to the production of the nitrates used as precursors for all the three catalysts under investigation. The inventories for the metal nitrates precursors were not included in the selected database and were therefore modelled based on

literature data and considering the most common synthesis procedures. The synthesis of $Ni(NO_3)_2)\cdot 6H_2O$ was supposed to be performed through direct oxidation of NiO by nitric acid (HNO_3), according to Eq. (13).

$$NiO + 2HNO_3 + 5H_2O \rightarrow Ni(NO_3)_2 \cdot 6H_2O \quad \text{Eq. (13)}$$

Similarly, $ZrO(NO_3)_3)\cdot 6H_2O$ was supposed to be synthetised in accordance to Eq. (14).

$$ZCl_4 + 2HNO_3 + 7H_2O \rightarrow ZrO(NO_3)_2 \cdot 6H_2O + 4HCl \quad \text{Eq. (14)}$$

Concerning cerium nitrate, this compound is one of the most adopted sources of cerium in the synthesis of micro- and nano-structured CeO_2, though it also frequently used as reagent for several synthesis processes such as sol-gel and coprecipitation. Cerium nitrate could be obtained through different routes, as it can derive from the dissolution of CeO_2 or cerium carbonate ($Ce_2(CO_3)_3$) in HNO_3 or be directly separated as a by-production of the extraction of bastnäsite or monazite ores. The process is known to be both resource- and energy-intensive, as demonstrate by a recent investigation performed by Ratthanapraa and Suwanmanee, [124] who conducted a thorough LCA to evaluate the environmental burdens related to the production of CeO_2, leveraging the data gathered from a field study performed by the Thailand Institute of Nuclear Technology. The authors considered two different production routes for CeO_2 production from monazite ore, the main source of domestic rare earth in Thailand. The two routes differ for a final liquid-liquid extraction step, which was found to contribute for nearly 35-85% of the total environmental impacts and 79% of the total damage scores to human health and resource. Nonetheless, the authors did not report a detailed inventory for $Ce(NO_3)_3)\cdot 6H_2O$, which appeared as a by-product of the post-treatment of the cerium hydroxide ($Ce(OH)_3$) cake. On the other hand, a comprehensive LCI of the synthesis of cerium nitrate as catalyst precursor was proposed by Sanchez et al. [125], who considered it as a by-product deriving for bastnäsite ore mining in China. The proposed inventory was replicated using the available providers within ecoinvent.

Asides from the nitrates, urea, and third-party purchased supports (as for the case of Al_2O_3 and CeO_2-ZrO_2 used in CAT-01 and CAT-02, respectively), the synthesis processes used deionised water as solvent and minor electricity inputs for stirring (**Table 10**)

Table 10 Energy consumption for mixing. Values are referred to 1 kg of catalyst.

Mixing	CAT-01	CAT-02	CAT-03
Temperature [°C]	25	45	80
Duration [h]	6	2	6
Power [kWh]	3	1.4	4.8

The detailed inventory for the synthesis process is reported in **Table 11**. The generation of wastewater containing nitrates is entailed as well.

Table 11 LCI of the synthesis process. 1kg of catalyst as functional unit.

	CAT-01	CAT-02	CAT-03
Nickel Nitrate [kg]	1	1.2	0.5
Cerium Nitrate [kg]	-	0.5	-
Zirconium oxynitrate hydrate [kg]	-	1.5	-
Urea [kg]	-	1.1	-
Deionized Water [kg]	0.5	0.5	0.5
Alumina [kg]	0.8	-	-
Ceria [kg]	-	-	0.5
Zirconia [kg]	-	-	0.4
Nitrates in water [g]	0.3	-	0.1

Concerning the post-treatment, the inventory accounted for both drying and calcination stages (**Table 12**). The heat demand for drying was estimated upon considering a 5% residual moisture and accounting for the heat of vaporization at the operating conditions, while the input powers for calcination were scaled based on the ones reported by Sayyah et al. [126,127]. Synthesis processes lead to liquid and solid waste generation and flue gas emissions. Previous literature works underline that the environmental impacts are mostly dependent on the synthesis process and the starting material, with wastes and emissions increasing with the scale of production. It must be noted that SCS does not generate neither gaseous contaminants nor liquid effluents, as deionized water evaporates during combustion and nitrogen is form under stoichiometric conditions. On the other hand, as calcination is an oxidative process, this procedure for catalyst supports impregnated with metal salts is known to release nitrogen dioxide (NO_2) from the nitrates in solution.

Table 12 LCI of the synthesis process. 1kg of catalyst as functional unit.

	CAT-01	CAT-02	CAT-03
	Drying		
Temperature [°C]	120	-	100

Moisture	5%	-	5%
Thermal Energy [kJ]	211.19	-	165.90
Calcination			
Temperature [°C]	400	600	500
Duration [h]	4	2	4
Power [kWh]	5	3.75	6.25
Nitrogen Oxide Emitted [g]	0.1	-	0.1

Operational inputs for the catalyst during use include the hydrogen reduction step and heat removal (to bring the reactor back to the initial inlet temperature). All catalysts were *in situ* reduced to Ni^0 by using different amounts of hydrogen and operating at different temperatures. The reduction step is referred to the catalyst loadings required to generate 1 Nm^3 of methane, which were determined by considering the testing conditions, with a particular reference to the WSV and the estimated productivities. The heat demands were computed by accounting for the overall energy expenditure required to attain the reduction conditions. The LCI of the reduction stage can be found in **Table 13**, whereas that of the operational phase is reported in **Table 14**.

Table 13 LCI of the catalyst reduction stage. Data are referred to 1 Nm^3 of methane as functional unit.

	CAT-01	**CAT-02**	**CAT-03**
Catalyst [kg]	2.60	0.10	1.39
Temperature [°C]	450	600	450
Duration [h]	4	1	1.25
Hydrogen [Nm^3]	12.5	0.5	25.1

Heat [MJ]	84.39	4.35	152.47

Table 14 LCI of the methanation stage. Data are referred to 1 Nm^3 of methane as functional unit

	CAT-01	**CAT-02**	**CAT-03**
Temperature [°C]	325	325	300
Nitrogen [Nm^3]	4.85	6.13	16.70
Hydrogen [Nm^3]	4.85	4.90	8.91
Heat [MJ]	23.37	23.31	40.61

Hydrogen is assumed to be produced through a renewable energy (50% solar photovoltaic, 50% wind) fed Proton Exchange Membrane (PEM) electrolysis with specific consumption of 55 kWh per kg of hydrogen [128].

Life Cycle Impact Assessment (LCIA)

The selection of the impact assessment categories has been made to secure alignment with the technological focus of the investigated systems and established practices in the field of LCA (see **LCIA Method**). Considering methanation as a carbon utilization technology, Global Warming Potential (GWP) is naturally the most prominent impact category to be considered, reflecting the need to control and reduce greenhouse gases (GHGs) emissions, and it is therefore essential to include Global Warming Potential (GWP) as a category of interest. Nonetheless, the inclusion of further categories is of paramount importance to avoid burden-shift and overlook environmental trade-off, such as increased toxicity or resource use associated with the investigated systems. Moreover, the European Joint Research Centre (JRC) released an impact assessment guideline providing a set of recommendations about the impact categories and related methods to be included in studies performed in the European context. Therefore, in accordance to existing guidelines and similar literature works, and given the substantial relevance of the method in the European context, the ReCiPe 2016 v1.03, midpoint (H) impact assessment method was selected and the following impact categories were included: Climate Change (GWP100), Terrestrial Acidification Potential (TAP), Ecotoxicity Potential (ETP), Fossil Fuel Potential (FFP), Freshwater Eutrophication Potential (FEP), Marine Eutrophication Potential (MEP), Surplus Ore Potential (SOP), Ozone Depletion Potential (ODP), Particulate Matter Formation Potential (PMFP), Photochemical Oxidant Formation Potential (OFP), Water Consumption

Potential (WCP) [129]. By broadening the impact scope, the present investigation provides a robust and multi-dimensional environmental assessment of the investigated systems, increasing the reliability for decision-makers and enhancing the relevance of the findings for academic, industrial, and policy stakeholders.

2.3 Results and Discussion

2.3.1 Catalytic Tests

The catalytic performance of the Ni/Ce-Zr formulation (25 wt.% Ni/20 wt.% CeO_2-55 wt.% ZrO_2) were first evaluated over the temperature range 150-450 °C under atmospheric pressure (**Table 15**). The catalyst was found to be scarcely active at temperatures lower than 200 °C, where both CO_2 conversion and CH_4 yield were negligible and stayed below 1%. Above 200 °C, the reaction initiated with CO_2 conversion reaching 0.33% and sharply increasing thereafter, reaching 29.4% at 250 °C while yield closely tracked it and established at 26.4% at the same temperature. Within the temperature range between 275-300 °C, the catalyst demonstrated to be highly active, whit conversion reaching a maximum value of 89.6% at 325 °C and yield establishing at 80.7% (corresponding to a CH_4 productivity of 0.43 mol $(g_{cat}\ h)^{-1}$). A further increase in temperature did not appreciably improve conversion, which plateaued near 89% to then slightly decrease beyond 375 °C and reaching 79.6% at 450 °C. Accordingly, CH_4 yield decreased to 69.9% at the same temperature, indicative of approaching thermodynamic limitations and possible reverse water–gas shift (RWGS) contributions.

Table 15 Ni/Ce-Zr formulation activity results at WSV 12,000 cm^3 $(g_{cat}\ h)^{-1}$ and atmospheric pressure.

Temperature [°C]	CH_4 [mol. %]	C_2H_6 [mol. %]	CO_2 [mol. %]	H_2O [mol. %]	H_2 [mol. %]	N_2 [mol. %]	CO [mol. %]	χ_{CO_2}	Y_{CH_4}	CH_4 rate [mol $(g_{cat}\ h)^{-1}$]
150	0.02	0.00	10.22	0.04	39.83	49.91	0.00	0.11	0.18	0.00
175	0.10	0.00	10.21	0.20	39.52	49.96	0.00	0.13	0.99	0.01
200	0.33	0.00	9.95	0.66	38.87	50.19	0.00	3.15	3.19	0.02
225	0.99	0.01	9.40	1.98	36.63	51.00	0.00	10.01	9.46	0.05
250	2.87	0.01	7.68	5.95	30.15	53.12	0.21	29.40	26.40	0.14
300	6.79	0.02	4.28	14.39	16.41	57.30	0.82	64.19	56.86	0.30
325	9.68	0.01	1.63	20.38	6.38	60.90	1.02	86.89	77.65	0.42
350	10.14	0.00	1.30	21.25	5.02	61.30	0.98	89.64	80.74	0.43
375	10.07	0.00	1.32	21.17	5.09	61.32	1.04	89.50	80.16	0.43

400	9.97	0.00	1.49	20.83	5.79	61.02	1.04	88.04	78.41	0.42
425	9.63	0.00	1.77	20.13	6.99	60.60	0.88	85.74	77.57	0.42
450	9.00	0.00	2.12	19.09	8.43	60.28	1.09	82.81	72.90	0.39

Under mild pressurization at 5 bar (**Table 16**), the activity of the Ni/Ce-Zr formulation slightly enhanced over the entire temperature range compared to atmospheric pressure. The reaction initiated at the same temperature (225 °C) and maintained comparable conversions and yields up to 300 °C, beyond which the activity resulted to be slightly higher than the atmospheric case. Indeed, a conversion of 89.6% was reached at 300 °C, while the plateau at 325-350 °C was of about 92.2% (vs. 89% of the atmospheric case). Similarly, CH_4 yield resulted to be 80.1% at 350 °C, corresponding to roughly the same CH_4 productivity of 0.43 mol $(g_{cat}\ h)^{-1}$. The reaction showed minor thermodynamic constraints at temperatures higher than 400 °C, with conversion dropping to 83.6% and yield to 72.1%, outlining potential beneficial effects of a slight pressurization while operating at high temperatures and underscoring the robustness of the Ni/Ce-Zr formulation in that temperature range.

Table 16 Ni/Ce-Zr formulation activity results at WSV 12,000 cm3 $(gcat\ h)^{-1}$ and 5 bar.

Temperature [°C]	**CH_4 [mol. %]**	**C_2H_6 [mol. %]**	**CO_2 [mol. %]**	**H_2O [mol. %]**	**H_2 [mol. %]**	**N_2 [mol. %]**	**CO [mol. %]**	χ_{CO_2}	Y_{CH_4}	**CH_4 rate [mol $(g_{cat}\ h)^{-1}$]**
150	0.02	0.00	10.26	0.04	39.85	49.83	0.00	1.17	0.20	0.00
175	0.09	0.00	10.23	0.18	39.58	49.91	0.00	1.68	0.89	0.00
200	0.34	0.00	10.04	0.68	38.75	50.19	0.00	4.02	3.24	0.02
225	1.04	0.00	9.44	2.09	36.38	51.04	0.00	11.28	9.82	0.05
250	2.86	0.01	7..56	6.27	29.88	52.88	0.54	31.39	25.98	0.14
300	7.46	0.03	3.63	15.86	14.12	57.97	0.93	69.98	61.76	0.33
325	10.35	0.01	0.99	22.08	3.87	61.33	1.37	92.22	81.02	0.43
350	10.46	0.00	0.81	22.43	3.14	61.64	1.51	93.69	81.46	0.44
375	10.50	0.00	0.75	22.55	2.86	61.90	1.81	94.06	81.60	0.44
400	10.13	0.00	1.13	21.67	4.48	61.22	1.51	91.16	79.45	0.43
425	10.06	0.00	1.14	21.62	4.47	61.17	1.41	91.04	78.82	0.42
450	9.92	0.00	1.36	21.18	5.36	60.85	1.33	89.27	78.25	0.42

Finally, at the highest tested pressure of 10 bar (**Table 17**), the catalyst continued to demonstrate slightly superior performance to the previous cases. At intermediate temperatures (225–275 °C), conversion was slightly higher than at 5 bar, reaching 31.4% at 250°C, with a similar yield (25.9%). As for the 5 bar case, conversions in the 300-350 °C temperature region increased, hitting values up to 94.1%, selectivity of 81.6% and a productivity of CH_4 productivity of 0.43 mol $(g_{cat}\ h)^{-1}$. Beyond 375 °C, conversion declined slightly due to equilibrium constraints and dropped to 87.2% at 450 °C, still higher than the corresponding values at lower pressures. Similarly, yield remained above 76% at 450 °C, maintaining a productivity of 0.41 mol $(g_{cat}\ h)^{-1}$.

Table 17 Ni/Ce-Zr formulation activity results at WSV 12,000 cm3 $(gcat\ h)^{-1}$ and 10 bar.

Temperature [°C]	CH_4 [mol. %]	C_2H_6 [mol. %]	CO_2 [mol. %]	H_2O [mol. %]	H_2 [mol. %]	N_2 [mol. %]	CO [mol. %]	χ_{CO_2}	Y_{CH_4}	CH_4 rate [mol $(g_{cat}\ h)^{-1}$]
150	0.02	0.00	10.37	0.04	39.78	49.78	0.00	0.04	0.20	0.00
175	0.10	0.00	10.33	0.20	39.49	49.89	0.00	0.59	0.92	0.00
200	0.34	0.00	10.10	0.68	38.73	50.15	0.00	3.41	3.25	0.02
225	1.04	0.01	9.51	2.08	36.60	51.05	0.00	10.56	9.81	0.05
250	2.86	0.01	7.85	5.99	30.06	52.96	0.26	28.83	25.94	0.14
300	7.43	0.02	3.67	15.55	14.42	58.22	0.70	69.24	62.30	0.33
325	10.00	0.01	1.31	21.34	5.00	61.00	1.34	89.73	78.68	0.42
350	10.22	0.00	1.00	21.95	3.87	61.43	1.52	92.17	79.80	0.43
375	10.25	0.00	1.00	21.99	3.83	61.44	1.49	92.22	80.05	0.43
400	10.21	0.00	1.13	21.76	4.38	61.17	1.34	91.10	80.09	0.43
425	9.99	0.00	1.34	21.28	5.16	60.93	1.31	89.46	78.65	0.42
450	9.74	0.00	1.58	20.71	6.23	60.51	1.23	87.49	77.25	0.41

Across all three pressure regimes, CNR-ITAE Ni/Ce-Zr formulation exhibited the characteristic sigmoidal temperature–conversion profile typical of CO_2 methanation over Ni-based catalyst, already identified in a previous preliminary study. The onset of significant activity occurred at ~225 °C in all cases, while the maximum observed CO_2 conversion and CH_4 yield improved with increasing pressure, coherently with thermodynamic predictions. The optimal operating temperature for maximum CH_4 productivity shifted upward with pressure, rising from 325 °C at atmospheric pressure (0.43 mol $(g_{cat}\ h)^{-1}$) to 325°C at 10 bar (0.44 mol $(g_{cat}\ h)^{-1}$). The moderate gain in conversion from 5 bar to 10 bar suggests that above 5 bar, the reaction

approaches equilibrium limitations despite the kinetic benefits of higher partial pressures. In all cases, at temperature > 350 °C conversion and yield declined slightly, potentially reflecting the shift of equilibrium back toward CO via RWGS and the entropic penalty of the exothermic reaction. This observation underscores the necessity of operating within the identified optimal temperature–pressure window to maximize performance while minimizing energy penalties and avoiding catalyst deactivation.

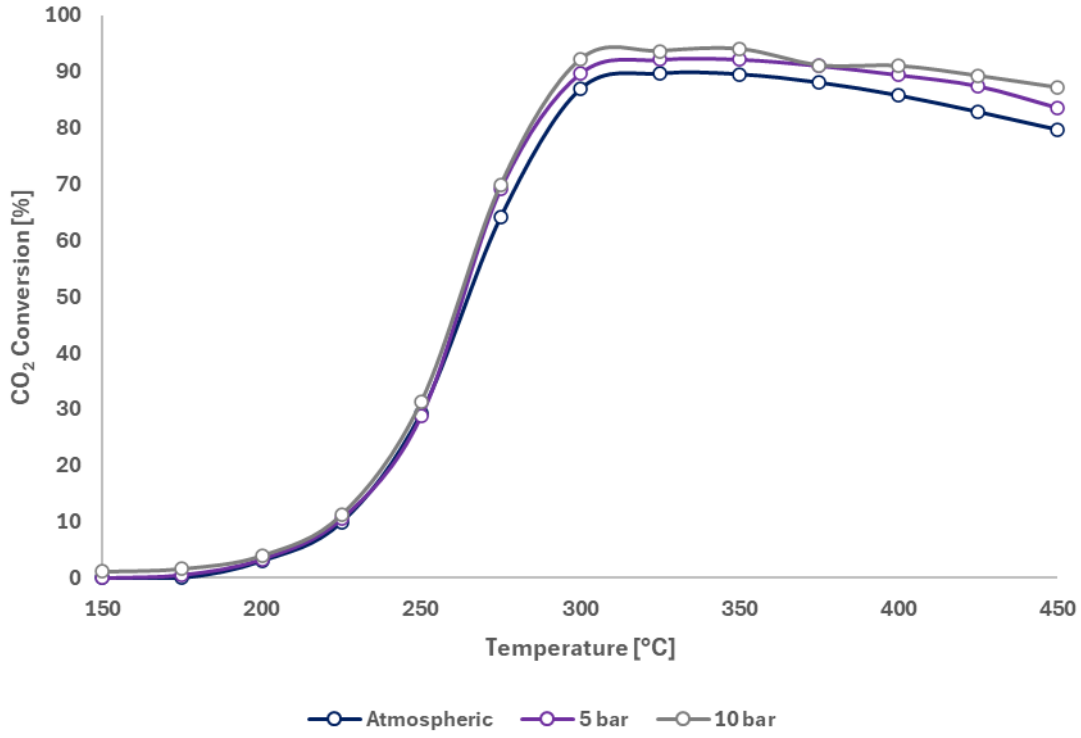

Figure 9 Ni/Ce-Zr formulation conversions results at WSV 12,000 cm3 $(gcat\ h)^{-1}$ and different pressure.

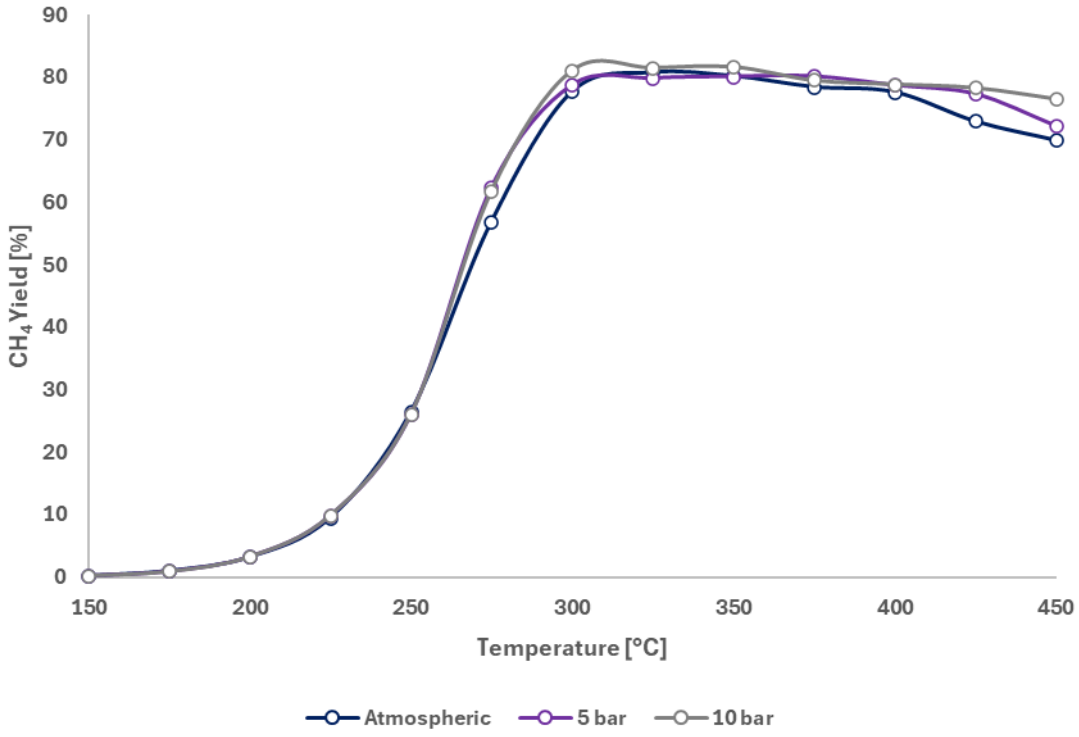

Figure 10 Ni/Ce-Zr formulation yield results at WSV 12,000 cm3 (gcat h)$^{-1}$ and different pressure.

Insights on the reaction mechanism

The performed experimental campaign is part of a long-term collaboration with CNR-ITAE aimed at determining the intrinsic kinetics of the Ni/Ce-Zr catalyst. While at the current status there are not enough data gathered under diverse conditions to properly develop and identify a certain kinetic model a preliminary investigation on the reaction mechanism promoted by the system suggest the possible mechanism underlying the catalyst activity. CNR-ITAE team have indeed performed some test to identify the rate-determining step by using spectroscopic techniques such as in situ Diffuse Reflectance Infrared Fourier Transform Spectroscopy (DRIFTS) to characterise the absorbed intermediates that formed on the catalyst surface throughout the reaction. The findings outlined the temperature-dependant variation of the bands corresponding to the C-H stretching vibration methane, reaching a maximum value at around 300 °C, in agreement with the temperature-dependent CO_2 conversion rate trend obtained during the performed catalytic tests. Moreover, the presence of a strong HCOO signal at temperatures close to 200 °C has been ascribed to high methane formation event at low temperature. Overall, based on the DRIFT evidence, the supposed mechanism should involve CO_2 absorption and subsequent reaction with oxygen vacancies and hydroxyl groups to form carbonate and bicarbonate species that are then hydrogenated to methane on the catalyst surface. Moreover, as the bands of carbonate species have been shown to exhibit significantly greater stability during the hydrogenation reaction at 250 °C, this suggest that carbonate species might represent the main intermediates, with their hydrogenation being the rate-determining step during the CO_2 methanation process. These findings suggest that the formate route might represent the underlying mechanism of the tested Ni/Ce-Zr formulation and are consistent with a recent investigation performed by Onrubia-Calvo et al. [130]. The authors indeed provided the first kinetic model of a Ni/CeO_2 formulation investigating the catalyst behaviour under differential and integral conditions. Previous tests on their catalyst confirmed that the presence of oxygen vacancies at the metal-support interface prompts the binding and activation of CO_2 while Ni^0 promotes hydrogen dissociation [90,131]. As a results, the most abundant reaction intermediates included bicarbonate and formate on vacancy-rich ceria, while hydroxyl species from water have been found to inhibit activity at moderate temperate by saturating those interfacial sites [90]. Based on these findings and a dedicated testing campaign, Onrubia-Calvo et al. [130] derived mechanistically informed LHHV model for three different routes (i.e., carbon route, formyl route and formate route). The performed DRIFTS studies, alongside the validation of different rate equations based on either the dissociative formyl mechanism or the associative formate mechanism made it possible to discriminate both the actual reaction mechanism and the proper kinetic model. The authors concluded that the mechanistic model assuming the hydrogenation of bicarbonates to formate as the rate-determining step was the one that best fitted the obtained experimental data. The authors further outlined that the formate mechanistic model assuming an active site for CO_2 adsorption (locate at the Ni/CeO_2 interface) and one for hydrogen dissociation (Ni^0) led to more realistic parameters, outlining the unique promotional effect of ceria in CO_2 methanation. Their experience represents a starting point for further investigation on the intrinsic kinetic of the Ni/Ce-Zr formulation developed and tested at CNR-ITAE.

2.3.2 Environmental Assessment

The environmental assessment was conducted by considering catalysts having the same active phase but different supports. As mentioned in **Section 2.1**, the widespread use of alumina in commercial catalyst is majorly due to the established trade-off between performance and costs. Nonetheless, Ni/Al_2O_3 catalysts have to operate at high temperatures to reach satisfactory conversion, since alumina is mostly inert and its interaction with Ni generally leads to the formation of inactive (and sometimes damaging) phases. Therefore, while investigating the performance of different methanation concepts to produce the same quantity of methane, the use of Ni/Al_2O_3 (CAT-01) is expected to require either higher reaction temperature, larger catalyst volumes or the implementation of process intensification strategies (these being out of the scope of the present investigation), all bringing to an increase in operational energy use.

However, considering the manufacturing of 1 kg of catalyst, results in **Figure 11** demonstrates that the synthesis CAT-02 has a higher environmental footprint in most of the investigated categories, majorly ascribable to the background process related to the precursors. Indeed, considering GWP100, 46.62% of the 21.8 kg of CO_2 was ascribed to zirconium oxynitrate production, while the 29.28% rose from nickel nitrate production. The latter was also the driver of GWP100 for CAT-01, contributing for 54.88% to the GWP100, whereas the procurement of ceria dominated the category (50.27%) in case of CAT-03, followed by nickel nitrate production. On the other hand, CAT-03 is featured by the highest impacts in SOP (driven completely by the purchase of ceria) and CAT-01 was found to have the highest impact in terms of OFP, due for the 83.07% to the release of NO_2 during calcination (also contributing for the 55% of the impacts in case of CAT-03).

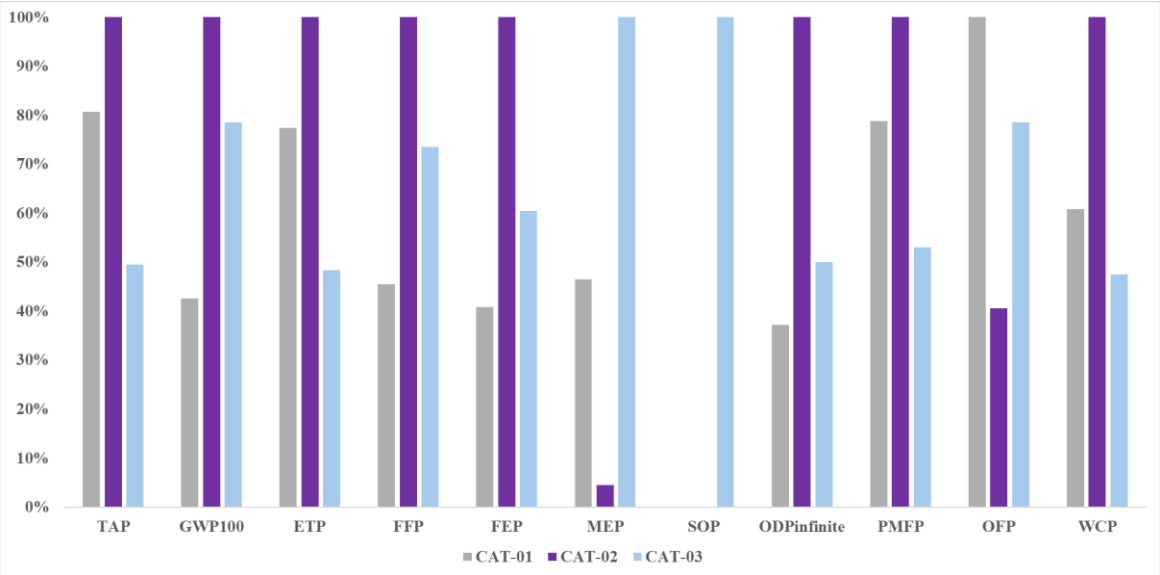

Figure 11 LCA results for the manufacturing of 1 kg of catalyst.

On the other hand, considering the production of 1 Nm^3, both the manufacturing phase and the use of hydrogen dominates the impacts. Indeed, while in case of CAT-02 the production of this amount of methane

requires small amounts of catalyst, in case of CAT-01 and CAT-03 the impacts of the manufacturing phase are more reflected in the LCA outcomes. Moreover, the higher reducibility of CAT-02 resulted in a significantly lower demand of hydrogen (and, therefore, water). Looking at GWP100, the reduction phase account for the 78.37% of the 149.13 kg of CO_2, with hydrogen and heat contributing for 52.12% and 13.12%, respectively. Similarly, hydrogen and heat contribute for the 53.82% and 15.06% of the 163.92 kg CO_2 of CAT-01. Similar shares were found for CAT-02, though the score was drastically lower (19.37 kg CO_2).

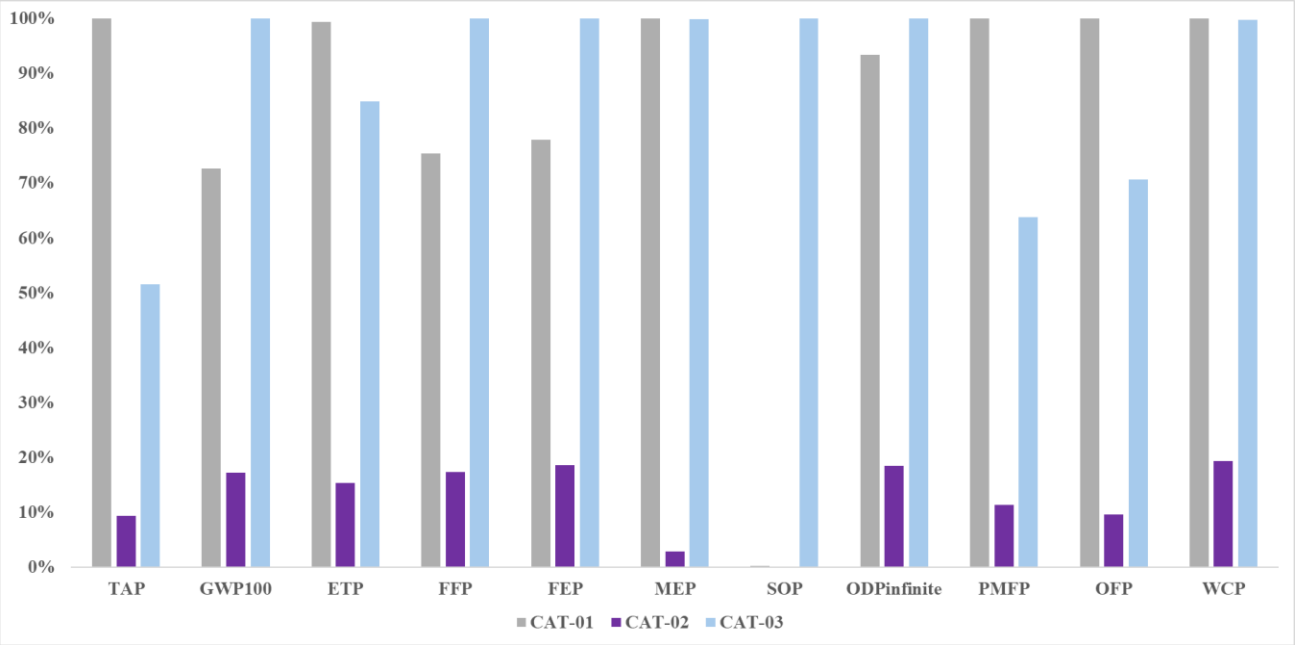

Figure 12 LCA results for the production of 1 Nm^3 of methane.

2.4 Conclusions

The present chapter addresses key aspects of developing an efficient catalyst for CO_2 methanation. It provides an overview of the current state of the art, focusing on nickel (Ni)-based catalysts and the role of ceria (CeO_2) and zirconia (ZrO_2) as supports. The choice to focus on Ni as the active phase and CeO_2 and ZrO_2 as the support was motivated by two factors. Firstly, Ni-based catalysts currently represent the industrial benchmark for CO_2 methanation and secondly, the work herein discussed was performed during a visiting period at CNR-ITAE, a leading research institute which recently proposed a highly active Ni/Ce-Zr formulation. Ceria-zirconia mixed oxides (CeO_2- ZrO_2) enhance Ni-based catalyst performance by providing oxygen vacancies and improving Ni reducibility at lower temperatures. Ni/Ce-Zr have demonstrated excellent CO_2 methanation activity even at temperatures up to 350 °C, whereas simpler supports such as ZrO_2 alone exhibit negligible activity at such temperatures. These performance enhancements motivate the use of advanced synthesis techniques, such as solution combustion synthesis (SCS), for Ni/Ce-Zr catalysts, as SCS is known to produce highly dispersed, nanostructured catalysts with superior properties compared to those prepared by conventional methods.

The performed investigation built on previous works by Italiano et al. [76,99] on structured catalysts by testing the 25 wt.% Ni/20 wt.% CeO_2-55 wt.% ZrO_2 in powder form. The Ni/Ce-Zr formulation demonstrated excellent performance under a wide range of conditions, providing: (1) a maximum CO_2 conversion of 89.6% and a CH_4 yield of 80.7% obtained at 325 °C and atmospheric pressure; (2) a maximum CO_2 conversion of 92.2% and a CH_4 yield of 80.1% obtained at 350 °C and 5 bar; and (3) a maximum CO_2 conversion of 94.1% and a CH_4 yield of 81.6% obtained at 350 °C and 10 bar. These results highlight responsiveness and robustness of the Ni/Ce-Zr formulation, demonstrating that moderate pressurisation can increase both activity and yield, while further increases in pressure yielded diminishing returns, suggesting that 5 bar might represent an optimal compromise between performance and energy cost. The Ni/Ce-Zr formulation also exhibited a broad operational window, maintaining a conversion above 985% across a wide temperature range at elevated pressures. The high methane selectivity (>75%) across all conditions might reflect the ability of the Ni/Ce-Zr formulation to suppress the Reverse Water Gas-Shift (RWGS) reaction even at high temperatures and pressures. Overall, the effectiveness of the Ni/Ce-Zr formulation at relatively low temperatures suggest it might represent an attractive solution for industrial applications, as it could enable reductions in investment and operating costs. Nonetheless, further investigation is needed to assess the long-term thermal stability and tolerance to impurities commonly found in biogenic and fossil carbon sources. In particular, the presence of hydrogen sulphide (H_2S) could result in the formation of cerium oxide sulphides (CeO_2S), which could compromise the stability of the catalyst [132].

Beyond activity testing, the present chapter deals with an expanded characterisation of the Ni/Ce-Zr formulation aimed at evaluating its environmental implications. The environmental impacts of producing both 1 kg of catalyst and 1 Nm^3 of methane were assessed and compared with catalysts that had the same active phase (Ni) but were supported on different oxides (Al_2O_3) or were prepared using conventional methods. The findings emphasised the importance of such assessments in understanding the life cycle implications of catalyst synthesis. Although SCS was associated with higher environmental impacts per kg of catalyst produced, the superior activity and productivity of the Ni/Ce-Zr formulation during operation effectively reduced the environmental burden per Nm^3 of methane produced, and this was attributed to the higher conversion rates, productivity and improved reducibility. However, the analysis also revealed that major environmental hotspots are connected to the production of nickel nitrate and rare-earth oxides (Ce and Zr), which contribute significantly to the categories of human toxicity, ecotoxicity, and resource scarcity. These findings emphasise the importance of balancing performance gains with environmental costs when developing catalysts for industrial applications and highlight the need to expand characterisation frameworks beyond activity, selectivity, and stability. The introduction of rare-earth elements and the choice of synthesis route inevitably impact environmental performance in comparison to more conventional Ni/Al_2O_3 catalysts. However, it must be noted that although the Ni/Ce-Zr formulation was tested under the most industrially relevant conditions at significantly higher space velocities (and therefore under more stringent conditions), the activity tests of the other catalysts were conducted under different

operating conditions. Therefore, future assessments should harmonise data gathering and include further metric such as stability. Indeed, while the influence of manufacturing is expected to diminish with scale, the performed investigation demonstrated that synthesis techniques significantly impact both activation hydrogen demand and operational performance. This makes it essential to consider the entire value chain when designing a methanation process. Finally, beyond environmental assessment, the preliminary evaluation of financial implications and analysis of value chain risks are critical for guiding research and commercialisation strategies. On the one hand, the production costs vary significantly between laboratory and industrial scales due to the small batch sizes and complex procedures used in laboratories compared to the economies of scale achievable in industry. On the other hand, value chain considerations must account for the sourcing of chemicals based on rare-earth elements or other critical raw materials, as these carry supply and price risks.

In conclusion, the present investigation demonstrates that CNR-ITEA Ni/Ce-Zr formulation, synthesised via SCS, can overcome the kinetic and thermodynamic limitations of the Sabatier reaction and represents a more sustainable and scalable solution than benchmark systems when impacts are normalised to methane output. Besides, this work marks the beginning of two complementary initiatives aimed at facilitating the scaling up of the Ni/Ce–Zr catalyst developed at CNR-ITAE. The first initiative involves conducting a detailed investigation of the kinetic mechanisms promoted by the catalyst, while the second is aimed at implementing a holistic assessment framework that recognises industrial catalysts must be highly active and selective, as well as environmentally and economically viable throughout their lifecycle.

Chapter 3. The Reactor and The Plant

The practical requirements of industrial scale up mandates the development of proper reactor design, known as *methanation concepts*, capable of guaranteeing an optimal thermal management and an adequate purity of the product stream (SNG stream). Going beyond the role of the catalyst and the necessary improvements in that field, one of the main priorities and methanation-related research lines addresses the modelling and design of optimized methanation concepts capable of ensuring improved process performance under realistic operating conditions [71]. In the broad architecture of methanation, the reactor constitutes the core unit wherein the methanation reaction is carried out, and its design must reconcile multiple, conflicting requirements such as attaining high conversion rates, securing precise thermal control, and providing robustness under transient regimes and scalability.

Multiple design strategies have been pursued to overcome the issue of exothermicity in methanation reactors. Traditional industrial schemes employ staged adiabatic fixed-bed reactors (FBR) with intercooling, an approach used in processes like the Lurgi methanation systems which allows to achieve high overall conversion but at the cost of increased complexity and volume (multiple reactors and heat exchangers in series) [44]. Looking at a trade-off, the concept of Multi Tubular Heat Exchange Reactors (MT-HER) emerged as a viable solution offers precise temperature control through the tube walls, mitigate hotspot formation and maintain the catalyst in the desired temperature window even under high conversion conditions or variable feed rates. The design of these kinds of reactors can be obtained by performing a thorough modelling and simulation to identify the optimal conditions and ensure a balance between performance and equipment complexity [133]. These activities are crucial to scale-up the technology and understand the influence of key design parameters and operating conditions.

Therefore, the present chapter first deals with the development a comprehensive one-dimensional pseudo homogeneous model of the reactor was developed and implemented in MATLAB environment. The model encompasses a kinetic model of CO_2 methanation, alongside heat, mass and momentum balance equations to investigate and gain insights on the heat and mass transfer phenomena occurring throughout the reactor. Then, leveraging the outcomes of the developed reactor model, a detailed process simulation for a multi-stage methanation plant is investigated, consisting of a series of MT-HERs with interstage cooling and condensation. The purpose of this approach is to eliminate the water produced as a by-product and to shift the thermodynamic equilibrium towards enhanced CO_2 (and hydrogen) conversions and elevated methane concentrations in the produced SNG. The adopted approach is in line with established best practices of the Research Group, including those proposed by De Falco et al. [134,135] and D'Ambrosio et al. [44,136]. Before delving into the details of the performed investigation, **Section 3.1** first provides an in-depth overview of

the various reactor configurations that have been proposed, investigated and validated to provide an overview of the current framework based on technological maturity and integration potential. Analogously, the section outlines the current literature landscape related to modelling, simulation and assessment of different plant layouts for SNG production via CO_2 methanation. Building upon this framework, the subsequent section provide a detailed account of the mathematical modelling and process simulation activities undertaken to define and streamline first a MT-HER configuration suitable for the production of 100 $Nm^3\ h^{-1}$ of SNG and then the entire plant (**Section 3.2**). The reactor has been modelled through a one-dimensional pseudo homogeneous model integrating the intrinsic kinetic expression of a commercial Ni/Al_2O_3 catalyst taken from literature. The core outcomes are presented in **Section 3.3** where a discussion is provided with reference to the influence of pressure and space velocities on temperature control and conversion efficiency. The technical performances of the investigated process configuration are then discussed with a focus on the regulatory compliance of the obtained SNG stream. In conclusion, **Section 3.4** provides a discussion of the entire modeling and assessment framework, alongside the most relevant conclusions that should drive future efforts in the field to advance the technology.

3.1 Reactor Modeling and Plant Simulation

The Sabatier reaction has been investigated over a wide range of operating conditions, catalytic systems and reactor configurations [44,137]. Several authors have attempted to streamline the reactor design to attain optimal yield and conversion to methane and ensure a high degree of compatibility of the SNG stream with the end-user specification to avoid the need for complex downstream processes [38]. Throughout the last decades, substantial progress has been made in the design of methanation reactors, which evolved from conventional designed based on adiabatic Fixed-Bed Reactor (FBR) arrangements to modern configurations based on either packed or structured Multi-Tubular Heat Exchanger Reactor (MT-HER) settings to enhance the thermal management of the reaction. More advanced reactor concepts were subsequently developed to address remaining limitations in heat and mass transfer. Microchannel reactors (MRs) leverage a very high surface-to-volume ratio to achieve superior heat removal and temperature control. Modelling and pilot studies demonstrated their effectiveness in avoiding hot spots and enhancing reaction rates. In parallel, process intensification strategies led to the development of sorption-enhanced methanation (SEM) and sorption-enhanced reactors (SERs), aimed at boosting conversion while mitigating water-induced sintering and catalyst deactivation. Fluidized-bed reactors (FRs) have also been investigated for methanation, offering excellent gas-solid contact, nearly isothermal operation, and high conversion rates per pass. Finally, three-phase reactors (TPRs) or slurry bubble reactors (SBRs) have gained attention for their exceptional thermal management capabilities. **Table 18** provides a more detailed overview on these concepts.

Table 18 Methanation concepts [15,43,137,138].

Concept	Description
Fixed Bed Reactor (FBR)	FBR represent the most widely adopted configuration for the large-scale synthesis of chemicals. In a FBR, a heterogeneously catalysed gas-phase reaction takes place on the surface of a stationary catalyst. Most FBR systems incorporate direct or indirect heat removal to maintain an optimal temperature profile along the flow path. The catalyst must also minimise pressure drop, which is especially important when conversion per pass is low, and a high gas circulation rate is required. Concerning methanation, different FBR configurations have been tested by integrating diverse thermal management approaches, these being featured by a specific temperature profile along and across the reactor. Despite challenges such as hotspot formation and process complexity arising from multiple reactors, FBRs remain a mature, cost-effective and high-TRL technology.
Structured Reactor	Structured reactors, such as open-cell foam systems and microchannel arrays, are poised to become central in next-generation methanation concepts. Investigations on structured catalyst led to promising results, given the higher conversion efficiency and enhanced reaction control provided by the high surface area, enhanced mass and heat transfer, and lower pressure drops. Structured reactors equipped with open-cell ceramic foams or monoliths secure low pressure drops and superior heat and mass transfer characteristics. These features have been demonstrated by both modelling studies and on-field deployment tests and are mostly linked to the enhanced radial heat dispersion provided by the structured catalyst. Moreover, structured reactors are able to handle fast ramping and load changes. These peculiarities are essential to proceed with the scaling of methanation reactors to the industrial scale and integrate them with renewable energies.
Fluidized-Bed Reactor (FR)	In FR, the catalyst is suspended in the gaseous stream, and the thermal management is performed by monitoring the fluidization of the solid catalyst. The excellent mixing within the reactor secure high mass and heat transfer rates and ensures that the temperature within the reactor can be kept uniform to minimize the thermal stress on the catalyst. Early studies showed fluidized beds can avoid hot spots and achieve high conversion per pass if equipped with internal cooling coils, resulting in the possibility of using a single reactor rather than a reactor cascade. Fluidized beds operate at lower pressures (a few bar) and have low pressure drop, similar to foams. However, catalyst attrition and more complex engineering (cyclone separators, etc.) are challenges. To date, no large commercial CO_2-methanation uses fluidized beds, but they remain an option for scale-up due to inherent isothermal behaviour. Other drawbacks include catalyst blowout in case of uncontrolled gas velocities, a significant catalyst consumption because of attrition (which also causes shorter reactor life) and the scarce degree of flexibility given by the necessity to operate at certain fluidization velocities.
Three-Phase Reactor (TPR)	TPR are slurry systems characterized by a non-reactive circulating liquid phase, such as dibenzyl toluene, in which fine catalyst particles (< 100 µm) are kept suspended by the gas flow. In other words, the catalyst is in a suspended state and liquid and gas enter through a distributor at the

bottom of the reactor, so the process is also known as Liquid Phase Methanation (LPM) [24]. The liquid phase is characterized by a high heat capacity which allows for effective and accurate reactor temperature control, implying low thermal stress on the catalysts. The main disadvantages of the slurry reactors are the decomposition and the evaporation of the heat transfer fluid and the fact that, in comparison to other reactors, there are more mass-transfer resistances, since the gaseous reagents and products have to travel through the liquid phase in order to reach and leave the catalyst surface. Therefore, its adoption at industrial scale is still constrained by challenges such as mass transfer resistances, heat transfer fluid degradation, and catalyst recovery requirements. Continued research into improved slurry media, advanced catalyst designs, and efficient catalyst separation technologies is key to unlocking its full potential in commercial applications.

Sorption Enhanced Reactor (SER)

SER results from the process intensification of FBR and are commonly equipped with blended packing made up of a catalyst and an absorbent or an hybrid/bi-functional catalyst. This methanation concept is aimed at enabling the *in-situ* removal of water, which is the main by-product of the reaction, to shift thermodynamic equilibria and mitigate deactivation issues such as sintering (promoted by water formation). The sorbent regeneration commonly occurs by applying either temperature or pressure swing methods, though these methods have been found to potentially damage the reactor and limit reactor lifetime due to cycling operation. Laboratory and pilot-scale studies have demonstrated its potential for enhancing conversion and selectivity beyond what can be achieved in FBRs, but the technology remains at a relatively early stage compared to them, and industrial implementation is limited by the above discussed challenge and scalability issues.

The above listed methanation concepts have been tested by integrating diverse thermal management approaches, these being featured by a specific temperature profile along and across the reactor. To classify and distinguish these different approached, Kiewidt and Thöming [139] used the Seminov number (Eq. (15)), which represents the ratio between the heat production rate and the cooling rate. The authors developed a Seminov number optimization (SNO) to perform a thorough comparison of the optimal axial temperature profiles in a single-stage reactor and maximize the obtainable methane yield for a given reactor length. Based on *Se*, methanation reactors are classified as described in **Table 19**.

$$Se = \frac{Da \cdot B}{St} \qquad \text{Eq. (15)}$$

Where Da is the Damkohler number, B is the heat production potential and St is the Stanton number.

Table 19 Methanation concepts classification based on thermal management approach [138,139].

	Seminov Number	Description
Adiabatic	$Se \to \infty$	The adiabatic approach has been largely adopted in the design of FBR and represents one of the most common routes for scale-up. The lack of an integrating cooling system leads to the formation of distinct thermal hot spot throughout the reactor bed, with spikes which can overcome 650 °C and mid-to-high temperatures at the reactor outlet. The adiabatic FBR is therefore featured by substantial drawbacks concerning catalyst deactivation and CO formation, which bring to an increased complexity (and cost) of complementary equipment part of the Balance of Plant (BoP), such as coolers, recycling compressors, and downstream treatment units. Thermal mitigation strategies include inert dilution, gas recirculation and reactor segmentations
Isothermal	$Se \to 0$	Although this represents the most thermodynamically favoured pathway (given that the process would take place at temperatures that maximise the conversion of carbon oxides), it is all but impossible to operate a FBR in an isothermal manner. Conversely, FR and TPR can be operated isothermally, a chance that is accompanied by minimal thermal stress on the catalysts and a straightforward process configuration. Nonetheless, the capacity of these reactors to operate at elevated temperatures is improbable, and this in turn limits reaction rates. The endeavours to operate a FBR in an isothermal manner have resulted in the development of costly and intricate designs, which failed in avoiding the formation of hot spots and the associated issues.
Polytropic	$0 < Se < \to \infty$	This behaviour is typical of cooled FBR and SR in a HER arrangement and, as stated above, it implies a shift of the hot spot rise closer to the reactor inlet an a reduction of its intensity. Besides, the cooled FBR/SR delivers a product gas at significantly lower temperatures (< 300 °C) and still allow to achieve high conversion rates, though both the investment and operational costs increase.

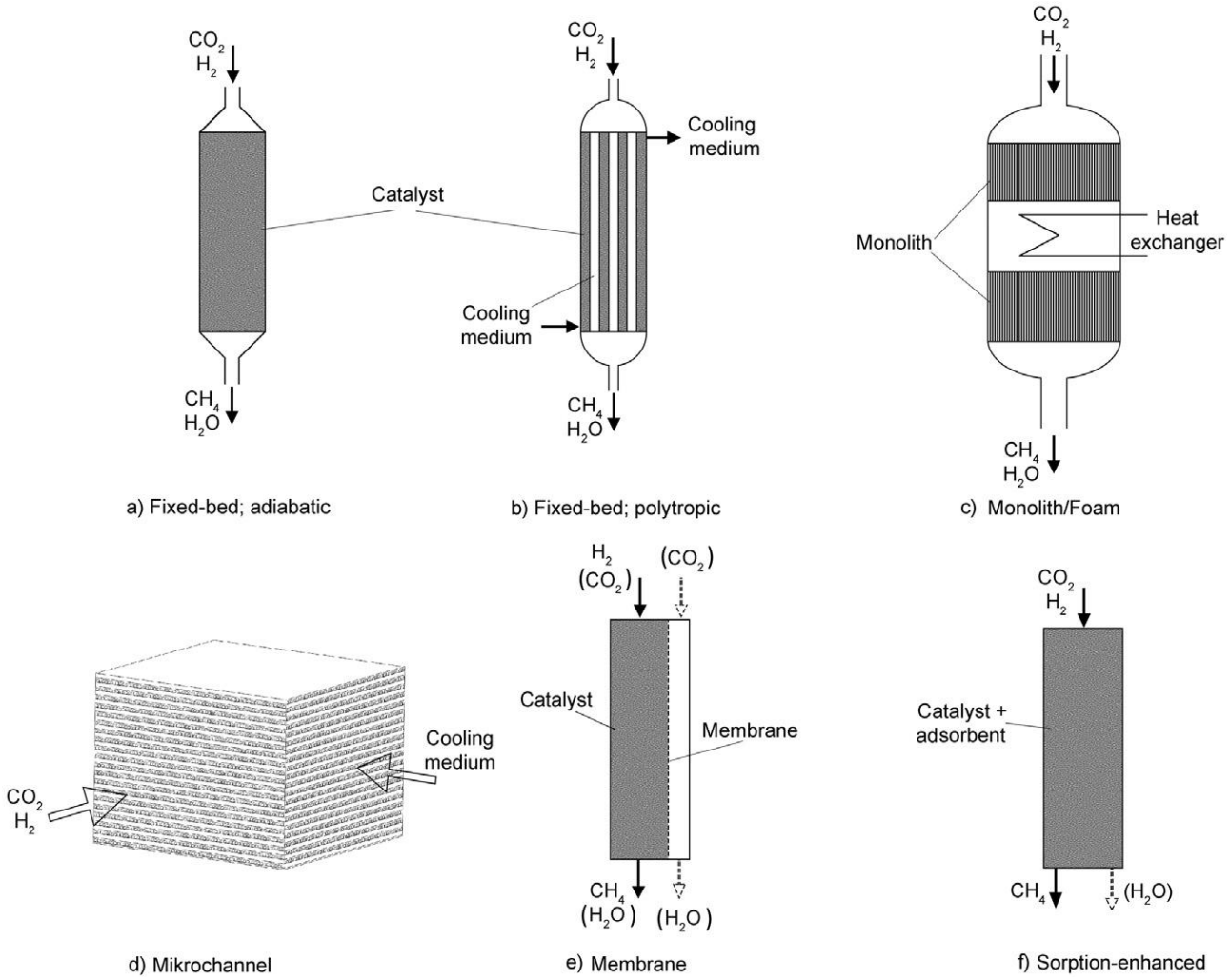

Figure 13 Methanation concepts [138].

3.1.1 Pilot Projects

The production of SNG through catalytic CO_2 methanation has been widely investigated and demonstrated in the context of different pilot projects. Several authors attempted to track the advancements in this field and gather data related to the development pathway of methanation technologies. Rönsch et al. [43]reported that in the first decades of CO_2 methanation development, most of the industrial players focused on process configurations integrating FBR. Indeed, several companies such as Outotec, EtoGas GmH and MAN proposed their methanation concept in the form of staged FBR with intermediate cooling, FBR with steam cooling, and isothermal FBR with molten salt cooling. Moreover, a recent review by Tommasi et al. [15] also emphasized the role of these companies and of the Centre for Solar Energy and Hydrogen Research (ZSW) located in Stuttgart (Germany) in the advancement of CO_2 methanation reactors. The EtoGas methanation plant in Wertle (Germany) is currently one the largest at a worldwide scale (15 GWh of annual production capacity) and is fed by a 6.3 MW_{el} Alkaline Electrolyser (ALK) and biogenic CO_2 coming from

anaerobic digestion. The EtoGas unit consists of a bundle reactor cooled with molten salts to ensure temperature control, and the plant is also equipped with a hydrogen storage unit as buffer.

One of the first and most significant *proof of concept* of CO_2 methanation was provided by the EU-funded Integrated High-Temperature Electrolysis and Methanation for Effective Power to Gas Conversion (HELMETH) project. The project demonstrated, for the first time at pilot scale, the technical feasibility of integrating a pressurized high-temperature steam (@15 bar, 800 °C) Solid Oxide Electrolysis Cell (SOEC) with a methanation unit made of three MT-HER in series, a condensation unit, and a drying unit. The demonstrator operated in Dresden (Germany) and successfully injected a pipeline-grade SNG stream produced with an electricity-to-SNG efficiency higher than 76% (which, at the time of results publication, was the highest efficiency ever reported for a PtM system [140]). The most relevant PtM initiatives across Europe were comprehensively reviewed by Bailera et al. [44] who analysed over 40 initiatives covering both thermo-catalytic and biological methanation pathways. The review confirmed the predominance of FBRs in deployed projects, particularly in the German and French contexts, while also noting the emergence of biological methanation as a competitive alternative which gained interest due to the opportunity to operate under milder conditions and with greater resilience to impurities. Among the numerous initiatives identified outside Italy, the Jupiter 1000 project in France and the BioPower2Gas in Germany had a pioneering role in the advancements of CO_2 methanation. The former, besides being the first French PtM initiative, constituted the first industrial-scale demonstrator to hybridise electrolysis configuration, integrating both ALK and PEM electrolyser with a catalytic methanation reactor. This configuration enabled the project to simultaneously assess the ramifications of disparate hydrogen production technologies on methanation performance, thereby functioning as a bridge between the electricity and gas grids. On the other hand, the BioPower2Gas project in Germany marked the first PtM demonstration based on biological methanation and implemented within an existing biomethane production facility with the explicit objective of evaluating the long-term stability of integrating electrolysis-derived hydrogen with anaerobic digestors. BioPower2Gas sought to enhance biomethane output and generate a bio-SNG stream that met grid specifications, thereby demonstrating the potential of biological methanation to complement existing biogas upgrading pathways by utilising residual CO_2 in the biogas stream. As said, Germany led the advancements in this field by promoting one of the major research and development projects, such as the EU-funded *Store&Go* project, aimed at evaluating the techno-economic feasibility of PtM as a large-scale, high-density energy storage solution. The project involved 27 European partners from both the academic and industrial environment entailed the deployment of three distinct pilot plants based on different methanation concepts and with different objectives to gain insights on the integration potential of methanation pathways within the existing infrastructure.

Table 20 Store&GO demonstration plants [141,142].

Location	Objective	Methanation Concept	Carbon Source	Hydrogen Source	Outcomes
Falkenhagen, Germany	Production of SNG intended to grid injection	Monolith Reactor (Isothermal)	Bioethanol Plant	2 MW Alkaline Electrolyser	192 MWh SNG System Efficiency 53% 85% Conversion
Solothurn, Switzerland	Production of biomethane to be injected into the local distribution grid	Biological Methanation	Anaerobic Digestion of Sewage Sludge	350 kW PEM Electrolyser	173 MWh SNG System Efficiency 76% n.a.
Troia, Italy	Production of Liquefied Natural Gas (LNG) to be regionally distributed in cryogenic vessels	Structured Reactor	Direct Air Capture (DAC)	1 MW Alkaline Electrolyser	33 MWh LNG System Efficiency 29% 95% Conversion

At the Italian level, both CNR and Enea provided relevant contributions. The FPMAT group of CNR-ITAE investigated a MT-HER configuration in a testing facility comprising a gas mixing and pre-heating section, the HER, and a post-processing section with a condenser and the on-line analyser of the dried gas. As discussed in **Chapter 2**, the group employed this laboratory bench-scale setup to investigated the performance of an MT-HER and of silicon carbide (SiC) and alumina (Al_2O_3) foams activated by Ni/CeO_2-ZrO_2 catalyst. On the other hand, within the context of the *Ricerca di Sistema* Research Program on Electrical Grid funded by the Italian Ministry of Sustainable Economic Development, Enea Casaccia Research Centre provided a significant contribution to the advancements of CO_2 methanation reactor. Bassano et al. [143] tested a moveable and modular MT-HER consisting of seven tubes equipped with a Ru-based catalyst bed

diluted with inert material to gain insights on the methanation process in different phase of operation, from start-up to shut-down. The authors investigated the behaviour of the reactor at different space velocities, gas inlet composition, and operating conditions, confirming the significant influence of operating pressure and residence time within the reactor. Subsequently, Deiana et al. [144] focused on the design and testing of a FBR equipped with Ni-based catalyst to produce 1 $Nm^3\ h^{-1}$, assessing its performance over a 10 h period to assess the dynamic behaviour of the system. A stable CO_2 conversion of approximately 70% was obtained and the system demonstrated to handle fluctuations in renewable energy supply.

More recently, Pintér [145] analysed 44 projects executed between 2000 and 2020 and compared them based on a set of screening criteria. Most of the surveyed projects were related to chemical methanation technologies (72.7%), whereas biogas resulted as the main source of CO_2 in the deployed plants. The authors also stressed a substantial heterogeneity in electrolysis technologies. The findings of Pintér [145] are quite aligned with the ones of the European Biogas Association (EBA) which underscores the crucial role of the EU in the development of this technology. Indeed, only the 6.8% of the projects analysed by Pintér were located outside Europe (i.e., 2 projects in the United States and 1 in Thailand), while the 50% of the considered initiatives were realized in Germany and Denmark [145]. Up to date, Germany has the largest share of realised demonstrations in Europe and, in the domain of methanation technology, Audi e-gas plant still holds particular significance.

In late 2024, the European Biogas Association (EBA) launched the first assessment about the rollout of e-methane in the European region [146]. The EBA devoted substantial efforts in mapping existing *e*-methane plants, their constituent technologies and functioning principles, identifying 35 methanation plants in operation in 2023 and 20 further deployment projects under development. The authors found that more than 91% of the currently operational facilities fell between the *fully renewable* classifications, while the prospective share of *fully renewable* plants is of 80%[4]. In 2023, there were 10 European countries which had either operational or planned *e*-methane plants, with Germany, France, and Finland leading the development of the technology with. Projections indicate that by 2027, this capacity will nearly reach 3,000 GWh per year, equivalent to 0.27 billion cubic meters (bcm).

3.1.2 Modelling Strategies

Reactor modelling is a valuable tool for simulating and understanding the complex physicochemical phenomena occurring within the reactor. Modelling represents a way to predict the behaviour of a reactor and streamline its performance by exploring different operating conditions or reactor configurations, thus

[4] The surveyed plants were categorised based on both the source of electricity (i.e., non-renewable electricity and renewable electricity) and the source of CO_2 (i.e., biogenic or fossil), considering *e*-methane plants fed with biogenic CO_2 and renewable electricity as *fully renewable e-methane plants*.

easing the scale up from laboratory to pilot-scale equipment. A heterogeneously catalysed gas phase reaction can be described by means of mass, energy and momentum balance equations alongside proper transport and kinetic equations leading to a set of either Ordinary Differential Equations (ODEs) or Partial Differential Equations (PDEs). Based on the approach used to describe heat and mass transfer phenomena and to handle the gas-solid interface, mathematical models are distinguished and classified into homogeneous, pseudo-homogeneous, and heterogeneous models (**Table 21**).

Table 21 Fixed-bed reactor modelling strategies. Adapted from Froment and Bischoff [147]and Stegehake et al. [148] .

	Homogeneous	**Pseudo-Homogeneous**	**Heterogeneous**
Description	This is the simplest approach, frequently used in early scoping, in which the catalyst bed is treated as one bulk phase and the reaction occurs in a well-mixed volume without any distinction between the gaseous and solid phase	The solid and gaseous phases are treated as a single interpenetrating continuum with the catalyst surface being at the fluid bulk conditions, including a factor that deliver an effective rate constant and heat of reaction by accounting for internal transfer phenomena	The model uses separate balances for the gaseous and solid phases and accounts for both temperature and concentration profiles within the catalyst pellet by considering intra-particle diffusion, enabling a more effective prediction of heat and mass transfer phenomena
Pros and Cons	Simplest approach but quite unrealistic	Sufficiently accurate if mass and heat transfer resistances are small	Highly accurate but computationally intensive
Gas-solid transfer phenomena	Neglected	Effectiveness factor	Film coefficients and effective diffusivities
One Dimensional	n.a.	Plug Flow Reactor (PFR) and possibly axial mixing	Interfacial gradients and intraparticle gradients
Bidimensional	n.a.	Radial mixing	Radial mixing

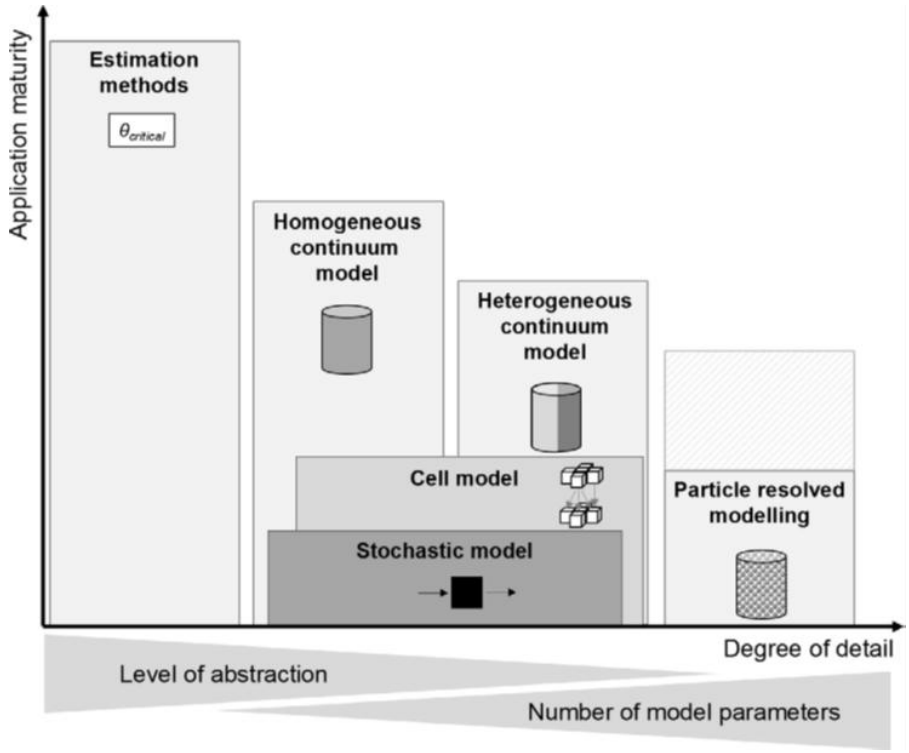

Figure 14 Fixed-bed reactor modelling strategies as a function of application maturity and degree of detail [148].

The simplest pseudo-homogeneous model is the plug flow reactor (PFR) model, a one-dimensional model which neglects both concentration and temperature gradients across the reactor section. Adopting a PFR model, the mass, energy and momentum balances are derived with respect to a differential cylindrical volume element which comprises the whole cross section. The PFR model can be slightly complicated to account for the axial mixing phenomena occurring throughout the reactor length, which assumes of the plug-flow rate fall and the need to account for diffusive contributions to mass and heat transport, generally leading to smoother axial gradients than that obtained with the PFR model. The *axial dispersion* model therefore accounts for effective mass dispersion coefficients and heat transport conductivities.

Table 22 One-dimensional models.

	Phase	Mass Balance	Energy Balance	Momentum Balance
Pseudo-Homogenesous	Unique	$\frac{\partial(u_g c_i)}{\partial z} = \rho_{bed} \sum_{j=i}^{n} \nu_{i,j} \eta_j r_j$	$(u_g c_{tot}) \bar{c_p} \frac{\partial T}{\partial z} = \rho_{bed} \sum_{j=i}^{n} (-\Delta H_j) \eta_j r_j - \frac{4}{d_t} U(T - T_c)$	$\frac{\partial P}{\partial z} = -\frac{150(1-\varepsilon)^2 \mu_g u_g}{\varepsilon^2 d_p^2} - \frac{1.75(1-\varepsilon)\rho_g u_g^2}{\varepsilon^2 d_p}$
Heterogeneous	Gas Phase	$\varepsilon \frac{\partial c_i}{\partial t} = -\frac{\partial(u_g c_i)}{\partial z} - k_{m,i} a_v (c_i - c_{i,cat})$	$\varepsilon \frac{\partial \left(\rho_g c_{p_g} T_g\right)}{\partial t} = -u_g \frac{\partial \left(\rho_g c_{p_g} T_g\right)}{\partial z} - \frac{4}{d_t} U(T_g - T_c) + h_f a_v (T_{cat} - T_g)$	$\frac{\partial P}{\partial z} = -\frac{150(1-\varepsilon)^2 \mu_g u_g}{\varepsilon^2 d_p^2} - \frac{1.75(1-\varepsilon)\rho_g u_g^2}{\varepsilon^2 d_p}$
	Solid Phase	$\rho_{bed} \sum_{j=i}^{n} \nu_{i,j} \eta_j r_j - k_{m,i} a_v (c_i - c_{i,cat}) = 0$	$\rho_{bed} c_{p_{cat}} \frac{\partial (T_{cat})}{\partial t} = -\frac{h_f a_v}{(1-\varepsilon)} (T_{cat} - T_g) + \rho_{bed} \int_j^n (-\Delta H_j) \eta_j r_j$	

Concerning heat transport phenomena, it must be noted that in case of a one-dimensional model it is still possible to account for all the entire heat transport resistances exerted by the element which takes part to the heat transport process. To this end, the formula for the overall heat transfer coefficient proposed by Dixon [149] can be used. Indeed, though it was derived from a two-dimensional pseudo-homogeneous model of a FBR based on a single radial collocation point and accounting for the wall Biot (Bi) number (Eq. (16)-(17)). The coefficient obtained presented an error of 3.8% in the exact asymptotic value over the entire range of Bi. Furthermore, its validation was conducted for a one-dimensional model with reference to conversion and bed centre temperature values. It is a sequential combination of the wall heat transfer resistance because of the increasing bed porosity close to the wall, and the radial heat transfer resistances within the catalyst bed.

$$\frac{1}{U} = \frac{1}{\alpha_{eff}} + \frac{1R_{ext}}{3\lambda_{er}} \frac{Bi + 3}{Bi + 4} \qquad \text{Eq. (16)}$$

$$Bi = \frac{a_w R_{ext}}{\lambda_{er}} \qquad \text{Eq. (17)}$$

The appropriateness of the Dixon formula to describe the heat transfer phenomena in a one-dimensional, pseudo-homogeneous model was confirmed by the investigation performed by De Falco et al. [150] on a FBMR for the industrial production of hydrogen by steam methane reforming (SMR). The authors tested and validated its use in predicting the influence of heat transfer on the reactor performance.

3.1.3 Methanation Modelling

To support the design and deployment of methanation reactors, several authors made use of modelling and simulation approaches to predict their performance and streamline the project phases. Kiewidt and Thöming [139] based their SNO approach on a one-dimensional pseudo-homogenous model developed to simulate the performance of an externally cooled FBR and compare them with the isothermal and adiabatic cases. The authors outlined that the polytropic FBR was the one associated with the highest methane yield given the chance of optimising the temperature profile within the reactor, emphasising the role of catalyst supports in enhancing and tailoring the heat transport properties. Gruber et al. [151] developed multiple numerical models to describe the behaviour of the MT-HER tested during the HELMETH project (**Section 3.1.1**), equipped with a bi-disperse catalyst-silicon carbide (SiC) bed and operated under different operating conditions. The FBR used boiling water as cooling medium and the authors we able to validate their model comparing the obtained results with the actual reactant conversions and the actual temperature profile along the reactor length.

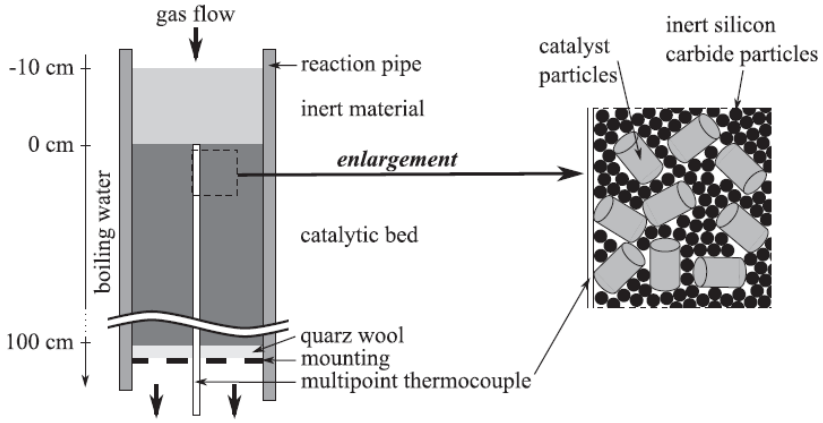

Figure 15 Schematic representation of the boiling water-cooled FBR configuration investigated by Gruber et al. [151].

Sun et al. [26,152] focused their efforts on the challenge of heat removal within the methanation reactor and modelled a HE-FBR configuration with the catalyst placed in the shell and the cooling molten salt flowing in the tubes. Being the ultimate objective of their investigation the maximization of methane production over extended periods of operation, the authors' endeavours were directed towards avoid catalyst deactivation caused by methane cracking occurring at elevated temperatures. Using a transient pseudo-homogeneous mathematical model, the authors indicated that despite the decline in performance caused by catalyst deactivation, the designed reactor could have last more than 10,000 hours in operation maintaining methane yields and conversion above 80%. Bremer et al. [25] proposed a dynamic optimization approach based on a bi-dimensional model of a FBR to understand the proper control strategies to be integrated to control hot spot formation and streamline the start-up of the reactor. The authors adopted a finite volume method (FVM) and solved the set of Partial Differential Equations (PDEs)

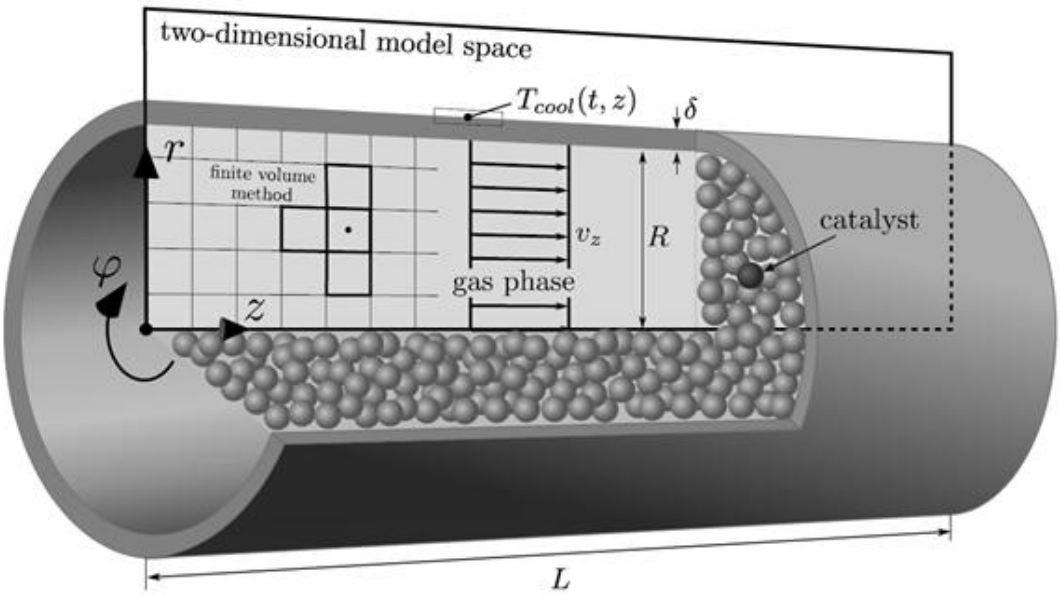

Figure 16 Schematic illustration of the FBR modelled by Bremer et al. [25].

Tsuboi et al. [153] developed a mathematical model to predict the behaviour of a FBR equipped with a novel Ni/ZrO_2 catalyst and estimate the kinetic parameters of the reaction rate model based on the gathered experimental data. Krammer et al. [154] performed a thorough modelling and validation study on an externally cooled FBR aiming at designing a high-capacity CO/CO_2 methanation reactor for industrial scale. The authors considered both the instance of oil cooling and ambient air cooling and validated their model in the range of 4,000 h^{-1} to 29,000 h^{-1} and from 1 to 6 bar. The authors stressed that the design of an effective methanation reactor should consider the reduction of tubes diameters alongside an increase in space velocities, with carbon oxides conversion rising from 61% to 93% while passing from 8,000 h^{-1} and 80 mm diameter to 29,000 h^{-1} and a diameter of 14 mm. All of the above reported studies adopted either a homogeneous or a pseudo-homogeneous modelling approach. Among the performed studies considering a heterogeneous model, there are some worth-mentioning approaches such as that of Zimmermann et al. [155], who modelled a FBR through a heterogeneous model aimed at investigating the influence of particle activity, permeability and heat conductivity on the overall reactor performance. The authors considered three different designs of the catalytic bed, distinguished based on particle properties description. The outcomes of the investigation outlined that, beside the need to operate below the deactivation temperature (~500 °C for the considered catalyst), the particle design could exert a substantial influence on the process performance, with egg-shell type particles being regarded as the best possible solution.

3.1.4 Proposed Plant-Scale Designs

Leading players such as Lurgi and Johnson Matthey have developed and are currently delivering cascaded adiabatic Fixed Bed Reactor (FBR) arrangements, which integrate different process intensification strategies to enhance the overall process performance [43]. These arrangements guarantee to obtain up to 96-98 vol.% of methane in the produced SNG if a proper heat management strategy is implemented to control the adiabatic operation [156]. Nonetheless, although these configurations are well suited for large-scale commercial settings, the Balance of Plant (BoP) comprises interstage coolers and recycling compressors, leading to a substantial increase in both investment and operational costs. Szima and Cormos [157] investigated a simple process design entailing a methanation reactor operating at high pressure and moderate temperature (@50 bar, 300 °C) considering an FBR cooled by means of boiling water. The simulated plant was intended to handle the CO_2 captured from a 450 MW_{el} Integrated Gasification Combined Cycle (IGCC), equal to nearly 82 tons of CO_2 per hour. The author proposed the use pinch analysis to optimize process heat integration and obtain technical and economic gains by integrating a steam turbine to recover the energy released by the reaction. The outcomes of the simulation demonstrated the chance of producing nearly 350 million Nm^3 of SNG (94.7 vol.% of methane) while simultaneously producing ~228 GWh of electricity. Moreover, a separator was integrated into the process simulation, and the collected water was used to partially fed the electrolysis unit. Salomone et al. [158] investigated the techno-economic performance of off-grid i-RES based PtM system integrating a SOEC unit to produce hydrogen. Plant operation was simulated by means of a model built on MATLAB environment and including an intermittent electric profile. The authors reported an overall efficiency of around 77% (based on the Lower Heating Value, LHV), though outlining a significant number of necessary shutdowns of the plant (up to 356 on annual basis). Vega Puga et al. [117] investigated a SNG plant fed by electrolytic hydrogen and CO_2 obtained from biogas upgrading. The simulated plant consisted of two FBR in series (operating @7bar and ~270 °C as inlet temperature) cooled with thermal oil and with a partial inter-stage removal of water, while a separator (dehydration unit) and a compressor were included to ensure the compliance with the German DVGW G 260 standard. Concerning the Italian context, Perna et al. [156] presented a detailed design and annual performance assessment of a PtM plant at different electrical input scales (ranging from 1 to 6 MW) and fed with renewable electricity produced by a 12 MW_{el} wind farm. The authors simulated a process scheme resembling the Topsøe Recycle Energy-efficient Methanation (TREMP) configuration, considering a series of four FBR with interstage cooling and achieving a CO_2 conversion of 99.2%. However, given the low methane content in the produced SNG (~ 32.1%), the authors included both a water separation unit and a commercial Pebax®-based membrane system to comply with gas grid specifications (methane >95 vol.%). The authors performed both steady-state and dynamic analyses to investigate the response of the system to different load factors and demonstrated that the plant performance heavily depended upon the size and operation of the intermediate hydrogen storage unit. Tripodi et al. [159]designed a full-scale integrated process consisting of a MT-HER and a purification unit to separate unreacted CO_2 and remove water by means of

amine scrubbing and Pressure-Swing Adsorption (PSA), respectively. The authors pointed out that the purification unit and the recycling reactants were both essential elements to achieve a conversion higher than 75%, resulting from the interconnection of four reactive stages operating at atmospheric pressure and temperatures < 400 °C. Moreover, the authors reported that the production of 10^5 Nm^3 per day required an overall heat demand of 9.2 MW_{th}, outlining the need for implementing proper heat management and integration strategies.

3.1.5 Process Intensification Strategies

The development of a full-scale PtM/CCUS process mandates the implementation of proper process intensification strategies to enhance the process performance in terms of CO_2 conversion, cost-effectiveness, and reactor stability over time [159,160]. Among the different issues encountered in the streamline of these processes, that of water formation is a common hinderance to their profitable, safe, and secure operation. Therefore, steam separation is regarded as one of the most crucial process intensification routes to obtain enhancements in conversion in case of equilibrium limited reactions, and this can be performed by both in-situ removal of water of through the implementation of a multi-staged process with intermediate condensation. Concerning the former pathway, the attempts to shift reaction equilibria of the Sabatier reaction firstly led to the development and testing of Sorption Enhanced Reactor (SER), a concept which is widely discussed in recent literature [161,162]. SER are commonly equipped with sorption materials such as zeolite and silica to locally remove steam from the gaseous stream, and several research efforts are undergoing to optimize both the overall reactor performance and the hybrid catalytic systems to be used.

The benefits of SER and of Selective Membrane Reactors (SMR) have been discussed by van Kampen et al. [163] with reference to the production of Dimethyl Ether (DME) and Methanol (MeOH), with the authors outlining the need to consider also practical aspects such as heat management and membrane characterization apart from the thermodynamic aspects. Crucial issues include the hydrothermal stability and selectivity of membranes and the heat management of the exothermic reaction when using adsorptive reactors, as these factors can affect long-term performance, so they need to be addressed alongside the thermodynamics when designing intensified reactors. The idea of Fixed-Bed Membrane Reactor (FBMR) for methanation was proposed by Ohya [164] in 1997 and was intended to remove water to shift reaction equilibria and obtain higher methane yield. Ohya's pioneering investigation showed that integrating a water-permselective membrane could increase CO_2 conversion by up to ~18% under certain conditions compared to an equivalent reactor without a membrane. Building on this, Schlereth and Hinrichsen [71] explored a FBMR with the aim to exploit the advantage of separate feeding in terms of heat management and obtainable conversion. In their study, hydrogen was fed gradually along the reactor (through a membrane or multiple inlets) while CO_2 was fed at the inlet. This distributed feeding allowed a more uniform reaction rate and temperature profile, and the authors outlined that such an arrangement could achieve a

high initial conversion (up to 92%) in the first section while enabling to separate the duties of conversion and equilibrium shifting.

From the process perspective, an alternative to in-situ water removal is represented by the chance of operating the reactors in series and performing an intermediate condensation, a common practice adopted both in established commercial processes and in the reviewed literature. Faria et al. [165] investigated in-situ water removal in an methanation reactor using an equilibrium model that also accounted for carbon oxide (CO) and coke formation, illustrating how steam separation enhanced CO_2 conversion independently of the operating temperature and pressure. The authors also identified the optimal temperature and pressures to maximise methane yield and minimize coke formation. A worth-mentioning approach was adopted by Hashemi et al. [166], who modelled an isothermal FBR for CO_2 methanation to identify the optimal water removal point that maximise conversion while minimizing thermodynamic penalties, the latter identified by analysing the exergy losses. The author found that, as the length of the reactor increased, the water removal point with the highest conversion was shifted towards the end of the reactor, accompanied by a smaller thermodynamic penalty. On the other end, shorter reactors presented an optimal water removal point at middle lengths. Finally, the authors noted a scarce dependence of the optimal removal point from the operating conditions, whereas the presence of methane in the feed stream resulted in this point moving upstream. A thorough thermodynamic analysis encompassing the exergy losses was also performed by Uebbing et al. [167], who investigated four different process configurations for methanation, concluding that feeding biogenic CO_2 and methane directly into the reactor (direct biogas methanation) resulted in the highest exergy efficiency. Nonetheless, it must be noted that the overall energy efficiency (electricity-to-electricity) was of only 23.4% (excluding heat recovery) and the irreversibility accompanying the conversion from electricity to methane were enormous, highlighting substantial thermodynamic limits and the need to work on heat integration. Their research also demonstrates that excess heat recovery can enhance exegetic efficiency, though the fundamental trade-offs between additional chemical conversion steps and energy losses persist. A thorough assessment of multi-stage process intensification strategies encompassing the energy and exergy analysis was proposed by our research group in a recent work which outcomes are summarised below.

A thorough assessment of multi-stage process intensification strategies was carried out by our research group in a recent work, focusing on direct CO_2-to-DME synthesis. In D'Ambrosio et al. [136] a novel multi-stage Condensation-Enhanced Carbon Utilization (multi-CECU) process for DME production was proposed. This approach applies the principles discussed above (staging and intermediate removal) to the synthesis of DME, an equilibrium-limited reaction where removing water by-product is particularly beneficial. In our work, six distinct reactor configurations were modelled (including a conventional single-stage process and five multi-stage arrangements) to quantify improvements in performance due to staged operation with inter-stage condensation. The simulations, incorporating both thermodynamic and kinetic analyses, indicated that a four-stage configuration offers the optimal performance gains. Specifically, the 4-stage multi-CECU design (**Figure 17**) achieved a CO_2 conversion of approximately 97.2%, a single-pass conversion efficiency to DME of ~64.4%, and an exergy efficiency of ~79.0%. These figures represent a significant improvement over the single-stage baseline, demonstrating how intermediate removal of water (and methanol, the intermediate in DME synthesis) drives the reaction further toward completion. Furthermore, the implementation of heat-recovery strategies between stages enabled the multi-CECU process to reduce external heating requirements by nearly 60% and decrease the cooling duty by approximately 40% in comparison with the single-stage case. This substantial reduction in utility demands highlights the energy-efficiency benefits of the intensified process. In summary, the multi-CECU methodology proved to be a viable and highly effective process intensification strategy for CO_2 conversion to fuels/chemicals (in this case, DME).

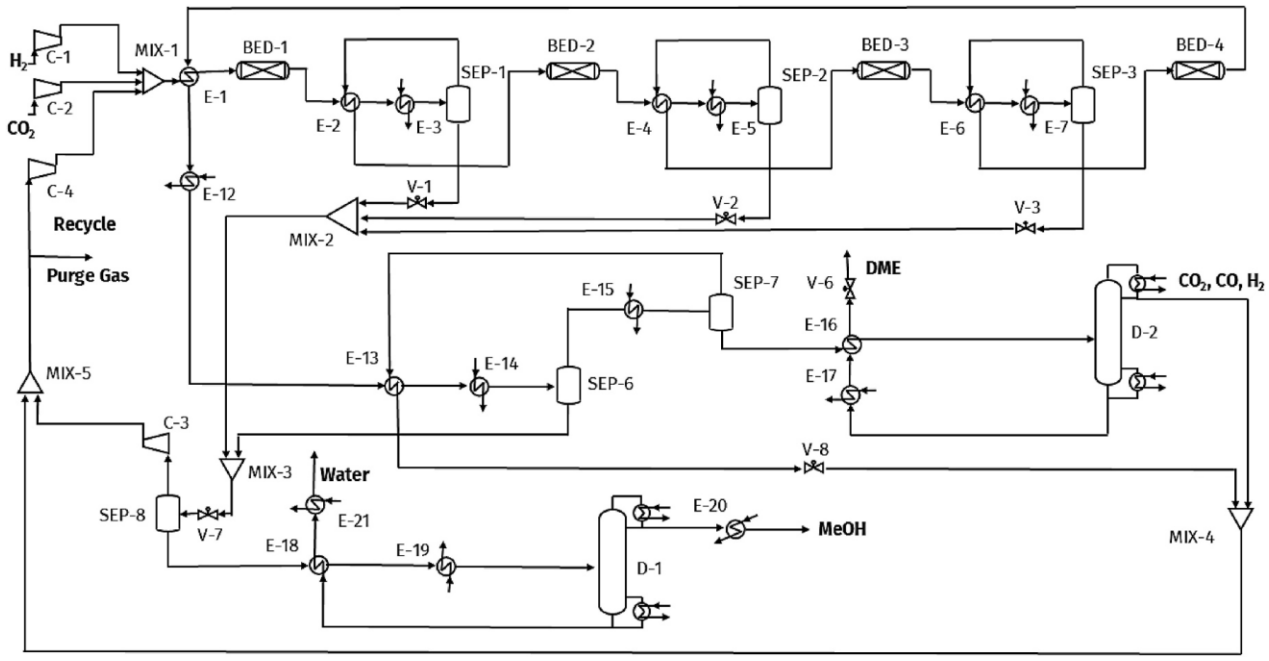

Figure 17 Process scheme of the 4-stages arrangement of the multi-CECU process.

3.2 Methods

3.2.1 Reactor Configuration

Building on the previous discussion, FBR has been selected as basic concept to design the methanation reactor. Nonetheless, considering the substantial heat released by the methanation rection and the temperature-sensitive nature of the selected Ni/Al_2O_3, a Multi Tubular Heat Exchange Reactor (MT-HER) configuration was developed to ensure a proper control of the temperature profile, mitigate the occurrence of thermal hot spots, and generate mid-pressure steam. As pointed out in **Section 3.1**, the MT-HER methanation concept has been widely applied in both modelling studies and on-field pilot projects and could therefore be considered as standard concept given the chance of effectively manage the thermal behaviour of the reactor [168]. Bench and pilot scale projects adopted different cooling strategies, spanning from air cooling [99] to diathermal oils [169] and considering both co-current and counter-current designs, with the former approach being regarded as the most suitable to curb thermal hotspot in the entry regions of the reactor. According to Sun and Simakov [26], the common practice of using mineral oils as cooling medium is likely to lead to uncontrolled operation as these fluids are not capable of handling high temperature flows. Therefore, the authors suggested to incorporate molten salts as cooling medium, providing evidence of their effectiveness in this field. Though agreeing with the assumption that diathermal oils and similia are more suitable for laboratory and pilot scale testing than for industrial-scale deployments, the present investigation is built upon the need to favour system integration. Industry trends favour modularity and compactness, particularly in the context of a branched and renewable energy-based system as pointed out in the previous sections. Therefore, while molten salts are a widely recognized intermediate vector in thermal energy storage, the MT-HER design of the present study consider a boiling-water cooling approach to exploit the production of mid-pressure steam and secure a more controllable design [134]. Gruber et al. [151] demonstrate the effectiveness of using pressurized boiling water as transfer medium, pointing out that the increased in vessel wall thickness was the main disadvantage of this approach.

Design of the Heated Exchanger Reactor

The design of the HER relies on the Kern's method used to design shell and tube heat exchangers [170,171]. The method proved to satisfactory predict the heat-transfer coefficient for standard designs of commercial heat exchanger, thought its effectiveness in estimating pressure drops is slightly minor given the inherent inefficiencies of the process and issues such as leakage and bypass. The first step of this design approach is to define the tentative geometry of the exchanger, starting from the selection of the tube diameter (d_t) and of the tube layout, this being either based on a square pitch or a triangular pitch. The latter selection directly affects the heat transfer rate, as it determines the cross-sectional area for shell-side flow and, therefore, the fluid dynamic behaviour of the shell-side fluid (i.e., the cooling fluid as concern the investigated case).

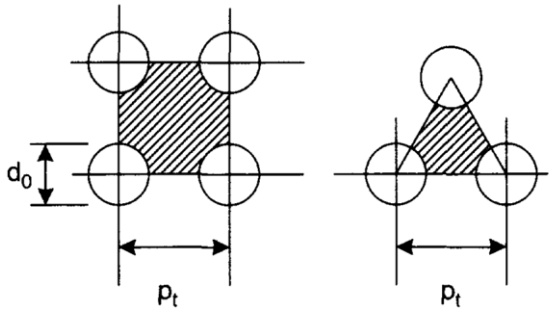

The selection of the triangular pitch is regarded as the optimal choice in the design of MT-HER as it allows for a tighter packing of the bundles of tubes and reduces the rise of preferential pathways and by-passes [133,170]. Considering this layout, the shortest centre-to-centre distance between adjacent tubes (i.e., the so-called tube pitch, p_t) being coherent with Eq. (18)

$$p_t \geq 1.25 \cdot d_t \qquad \text{Eq. (18)}$$

On the other hand, the choice of the single tube diameter (d_t) has been guided by the need of balancing mechanical integrity and thermal performance. Considering a MT-HER equipped with 2-inch (50.8 mm) standard tubes cooled by means of saturated boiling water (@ 220 °C and ~23 bar) and an internal pressure ranging from 1 to 10 bar, a Birmingham Wire Gauge (BWG) 14 has been applied (i.e., a 1.83 mm of wall thickness) to secure the possibility to operate at higher critical pressures (i.e., up to ~ 45 bar) and guarantee a conservative 75% safety margin and avoid to incur in an excessive thermal resistance or in substantial manufacturing costs. Upon considering the exothermic nature of the Sabatier reaction, which can give rise to localized temperature hotspots, the selection of the pipe material has been made in consideration of the need to provide long-term mechanical stability and resistance to potential hydrogen infiltration phenomena across a wide temperature range. SS316 is frequently employed in conventional methanation units and offers an adequate resistance towards hydrogen embrittlement phenomena [61,172]. The stainless-steel wall introduces a moderate conductive resistance, assuming that the thermal conductivity of the wall (k_{steel}) is of nearly 20 W (m K)$^{-1}$, likely negligible if compared to convective resistances on the bed and shell sides (see **Section 3.2.4**). The design of methanation reactor intended for industrial use must comply with the actual industrial needs, therefore ensuring a streamlined operation featured by low pressure drops at high gas input capacities and high conversion rates, as reported by Krammer et al. [154]. The authors stressed the importance of evaluating the actual capacity of the system under development with reference to the Gas Hourly Space Velocity (GHSV). Therefore, the solution procedure begins by defining the operating conditions of the system (inlet temperature of 230 °C and variable pressure) and computing the reactor geometry in terms of number of tubes (Eq. (19)) and shell diameters (Eq. (20)), considering a commercial 2” tube size.

$$N_t = \frac{F_{in}}{V_r.GHSV} \quad \text{Eq. (19)}$$

$$D_b = OD_t \left(\frac{N_t}{K_1}\right)^{(1/n_1)} \quad \text{Eq. (20)}$$

3.2.2 Kinetic Model Selection

Since Sabatier first investigated the role of heterogeneous catalysts for the methanation of carbon oxides, several kinetic models have been proposed to describe the reactive process considering different catalytic systems, operating conditions and modelling approaches [15]. In the early stages of research into the kinetics of CO_2 methanation, the focus was predominantly on the measurement of initial reaction rates and the application of rudimentary rate equations based on Power-Law Models (PLM) and mostly developed by estimating the apparent activation energies, such as that of Lunde and Kester [82], who developed a PLM for a Ru-based catalyst which is still considered as foundational for CO_2 methanation promoted by Ru. A step forward was brought by the work of Weatherbee and Bartholomew [173], who conducted the first systematic and detailed kinetic analysis of CO_2 methanation, employing a 3 wt.% Ni/SiO_2 catalyst under differential reactor conditions with highly diluted gas streams to minimise mass and heat transfer artefacts. After these first investigations, the field has advanced considerably, with a plethora of rigorous kinetic studies being carried out over both Ni- and Ru-based catalysts [15]. These studies have increasingly adopted Mechanistic Models (MM) based on the Langmuir-Hinshelwood-Hougen-Watson (LHHV) rate model to describe the direct CO_2 methanation reaction, fitted against experimental data. A comparison between these approaches is provided in **Table 23**.

Table 23 Kinetic models for carbon oxides methanation [73].

Model	Power Law Models	Mechanistic Models
Description	In PLMs, the rate las is given by the product of concentrations of reacting species. These models offer simplicity and analytical tractability though they lack physical meaning and are generally limited in their predictive capabilities, particularly in conditions that diverge from those employed in the estimation of parameters. Indeed, PLM are straightforward and involve a low number of estimation parameters. Moreover, PLM does not generally account for the influence of product inhibition or competitive adsorption phenomena, and this hinders their reliability at	Mostly based on the Langmuir-Hinshelwood-Hougen-Watson (LHHV) rate model, MM are highly effective in capturing the complexity of surface reactions and provide deeper insights into both the underlying reaction mechanisms and the rate-determining steps. These mechanistic formulations are grounded in catalytic surface reaction theory, where the overall rate expression is derived from assumed elementary steps, including adsorption, surface reaction and desorption. Thes models require a more extensive amount of experimental data for accurate parameter estimation and are more

	high conversions, elevated pressures and in case of both water and methane accumulation.	computationally demanding, particularly when integrated into reactor simulations.

In summary, while PLM could be used for macro-scale models over tight operating conditions, LHHV models are best suited for reactor design and scale-up studies spanning differential to integral regimes and including dynamic simulations where inhibition and reversibility play a major role [73]. Nonetheless, a significant constraint pertains to the identifiability of parameters in multi-parameter mechanistic models, particularly in non-ideal conditions. Furthermore, the integration of kinetic expressions with catalyst deactivation mechanisms (e.g. sintering or sulfur poisoning) is of paramount importance in the industrial context and this area remains underdeveloped and is the focus of ongoing research [174]. Among the most widely cited and applied kinetic expressions for modelling and simulation studies of CO_2 methanation processes are those developed by Xu and Froment [175], Lunde and Kester [82], Koschany et al. [176], and Champon et al. [176] Xu and Froment [175] developed one of the earliest and most cited LHHW model describing the methanation of CO_2 over a 15 wt. % $Ni/MgAl_2O_4$ catalyst, incorporating the three reactions generally occurring during methanation, namely CO_2 and CO methanation and RWGS. The authors considered competitive adsorption of species (i.e., CO_2, CO, hydrogen, methane and water) and leveraged steam reforming data to validate the model under the given operating conditions range. The model provides an optimal fit under moderate to high pressure (up to 30 bar) and temperatures between 280 and 400°C, and it is therefore a reference model for high-pressure methanation reactors used in Power-to-Methane (PtM) applications. Nonetheless, the authors did not investigate the influence of the support and assumed relatively simple competitive adsorption mechanisms without delving into the actual reaction schemes and the formations of the main intermediates. Subsequently, Koschany et al. [176] further developed a comprehensive kinetic model based on intrinsic measurements over coprecipitated Ni/Al_2O_3 catalyst. Their model includes contributions from both the direct CO_2 methanation and both RWGS and CO methanation, proposing elementary step-based expressions. Their mechanistic formulation captures adsorption, surface reaction and desorption steps, and has been validated across a wide range of partial pressure. The model exhibits excellent predictive capabilities under industrially relevant conditions (i.e., GHSV up to 50,000 h^{-1} and up to 340°C and 14 bar). Nonetheless, given its complex form, their model has been mostly used for detailed reactor design and computational fluid dynamics (CFD) modelling. Eventually, Champon et al. [177] conducted a rigorous kinetic investigation on a commercial Ni/Al_2O_3 catalyst using both differential and integral reactor experiments. Their study evaluated and modified existing kinetic expressions to describe both the direct methanation route and the indirect rout via RWGS and CO methanation. Three kinetic equations corresponding to these reactions were derived within the LHHV framework and simultaneously fitter to experimental conversion and selectivity data across different temperatures (i.e., in the range between 350 °C and 450 °C) and conversions (i.e., from 5 to 75%). Their model demonstrated an accuracy of nearly 20% in predicting methane formation rates under varying operational regimes thought their work

stands out for the comprehensive model discrimination strategy and systematic treatment of inhibition by water, methane and CO.

For the present investigation, an industrial Ni/Al_2O_3-Ca[5] which is commercialised under the name of METH 134®, and its intrinsic kinetic expression derived by Miguel et al.[6] [178] was considered (Eq. (21)).

$$r_{CH_4} = \frac{k p_{CO_2}^{0.5} p_{H_2}^{0.5}}{\left(1 + K_{OH} \frac{p_{H_2O}}{p_{H_2}^{0.5}}\right)^2} \left(1 - \frac{p_{CH_4} p_{H_2O}^2}{p_{CO_2} p_{H_2}^4 K_{eq}}\right) \quad \text{Eq. (21)}$$

The authors investigate five different mechanistic-based models, each considering a different reaction mechanism. The proposed kinetic assumed a formyl intermediate mechanism and the hydroxyl group being the most abundant species and was selected after discriminating the investigated models based on thermodynamic consistency and statistical significance of rate constant and adsorption constant parameters (95% confidence level). The rate constant (k) and the adsorption constant (K_j) were calculated using the Arrhenius (Eq. (22)) and Van't Hoff (Eq. (23)) equations.

$$k = k_0 exp\left[\frac{E_A}{R}\left(\frac{1}{T_{ref}} - \frac{1}{T}\right)\right] \quad \text{Eq. (22)}$$

$$K_j = K_{0,j} exp\left[\frac{-\Delta H_j}{R}\left(\frac{1}{T_{rif}} - \frac{1}{T}\right)\right] \quad \text{Eq. (23)}$$

Concerning the equilibrium constant, Miguel et al. [178] considered the empirical expression derived by Lunde and Kester [82] and describing the dependence of with the absolute temperature (Eq. (24)).

$$K_{eq}(T) = exp\left[\left(\frac{1}{1.987}\right) \cdot \left(\frac{56000}{T^2} + \frac{34633}{T} - 16.4 \cdot ln\, T + 0.00557 \cdot T\right) + 33.165\right] \quad \text{Eq. (23)}$$

3.2.3 Model Development

The design of the methanation reaction was based on the implementation of a comprehensive mathematical model in MATLAB environment. Schlereth and Hinrichsen [71] stressed that although bi-dimensional models (the $\Lambda(r)$ model) provide a precise and quantitative evaluation of the empirical evidence, one-dimensional pseudo-homogenous model (i.e., a PFR model) are still capable of reliably and

[5] The Al_2O_3 support is modified by adding calcium (Ca) as promoter to enhance both catalytic activity and stability, thus overcoming the early emergence of deactivation phenomena.

[6] The paper also reports a brief overview of some industrial methanation catalysts, classifying them in terms of active phase (mostly Ni-based catalyst), nominal operating conditions, shape and size. Among them, the PK-7R (23 wt.% Ni available in ring shape with size of 5.0x2.5 mm) is the common catalyst of the TREMP process, whereas the Katalco series (Ni-based catalyst in pellet shape with sizes ranging from 3.1x3.6 mm to 5.4x3.6 mm) is supplied by Johnson Matthey and was used for the experimental campaign performed by Enea Casaccia Research Centre.

effectively describing the behaviour trends of the reactor. Moreover, the authors stated that the use of heterogeneous model does not brings substantial enhancement excepts for cases of large catalyst equivalent diameters, small pore radii and small Reynolds numbers, as in those instances the heat and mass transfer limitations are severe and need to be considered. Fischer et al. [179] indicated that a one-dimensional pseudo-homogenous model (i.e., a PFR model) can provide a sufficient accuracy in predicting CO_2 conversion and the other performance trends within an FBR while significantly reducing computational burdens. The effectiveness of this approach was also validated by other authors in case of small reactor diameters. Therefore, a PFR model was integrated with an effectiveness factor to accommodate the intraparticle mass and heat transport limitations between the catalyst and the gaseous stream. Furthermore, regarding the spatial dimension, Tommasi et al. [15] recently emphasised the advantages offered by bi- and three-dimensional models. However, these advantages do not justify the significant expense in terms of computational effort. Moreover, as industrial FBR operates under constant operating conditions (i.e., in stationary mode) and it is important to look at the maximising the stationary operation, the model has been developed in steady state conditions.

Therefore, the stationary behaviour of the HER considered in the present investigation was modelled under the following assumptions, leading to a set of steady-state mass, energy, and momentum balance equations:

- The system is treated as one-dimensional, with negligible radial gradients of temperature and concentration; the only independent spatial variable is the axial coordinate z, aligned with the reactor axis.
- The gas and solid phases are treated collectively as a single, pseudo-homogeneous phase. The reaction rate is corrected by an effectiveness factor to account for intraparticle diffusion resistance, whereas interparticle diffusion is assumed negligible given the selection of small pellet size and operating conditions that serve to minimise internal gradients.
- Mass and heat transfer coefficients are derived from semi-empirical correlations, which are calibrated against experimental data.
- The physicochemical properties of the reacting mixture (e.g. viscosity, heat capacity, thermal conductivity) are modelled as functions of local temperature and composition and thus vary along the reactor length.
- The model explicitly accounts for the pressure drop along the reactor axis, rather than assuming it to be negligible, thus ensuring a more accurate description of momentum transport.

Material Balance

As for the mass balance equations, these are reported in (Eq.(25)-(28) for the four components

$$\frac{dF_{CO_2}}{dz} = -\eta r_{CH_4} \rho_{cat} (1-\varepsilon) \pi {r_t}^2 \quad \text{Eq. (25)}$$

$$\frac{dF_{H_2}}{dz} = -4\eta r_{CH_4} \rho_{cat} (1-\varepsilon) \pi {r_t}^2 \quad \text{Eq. (26)}$$

$$\frac{dF_{CH_4}}{dz} = \eta r_{CH_4} \rho_{cat} (1-\varepsilon) \pi {r_t}^2 \quad \text{Eq. (27)}$$

$$\frac{dF_{H_2O}}{dz} = 2\eta r_{CH_4} \rho_{cat} (1-\varepsilon) \pi {r_t}^2 \quad \text{Eq. (28)}$$

$$F_{CO_2}(0) = F_{CO_2 in} \quad \text{Eq. (29)}$$

$$F_{H_2}(0) = F_{H_2 in} \quad \text{Eq. (30)}$$

$$F_{CH_4}(0) = F_{CH_4 in} \quad \text{Eq. (31)}$$

$$F_{H_2O}(0) = F_{H_2O in} \quad \text{Eq. (32)}$$

The energy balance inside the tube was expressed as reported in Eq. (33), valid for the whole reactor at any given reactor section, alongside its boundary condition (Eq. (34)).

$$\frac{dT_g}{dz} = \frac{\rho_{cat}(-\Delta H_r)\eta r_{CH_4}}{\rho_g c_{p_g} u_g} - U_t \frac{4}{d_t} \frac{(T_g - T_o)}{\rho_g c_{p_g} u_g} \quad \text{Eq. (33)}$$

$$T_{gas}(0) = T_{gas\ in} \quad \text{Eq. (34)}$$

In Eq. (32), U_t is the tube-side overall heat transfer coefficient, which accounts for the radial heat transfer resistance of the catalyst bed and the wall heat transfer resistance as described by Dixon [149]. The model of the MT-HER was completed with the integration of the momentum balance to assess the pressure profile along the axial reactor coordinate according to the Ergun equation (Eq. (35))

$$\frac{dP}{dz} = -\frac{150(1-\varepsilon)^2 \mu_g v_g}{\varepsilon^2 d_p^2} - \frac{1.75(1-\varepsilon)\rho_g v_g^2}{\varepsilon^2 d_p} \quad \text{Eq. (35)}$$

Eq. (34) allowed us to estimate the pressure variation along the reactor by accounting for the physical properties of the gaseous mixture (μ_g and ρ_g), the geometry of the reactor (ε is the void fraction), the fluid dynamics of the system (v_g is the superficial velocity of the gaseous stream) and the properties of the catalyst particle (d_p is the particle diameter).

Void Fraction

The void fraction was calculated with reference to the mean void correlations for FBR elaborated by Benyahia and O'Neill [180]. The authors developed a set of predictive mean voidage correlations incorporating a particle shape factor and aimed at estimating the void fraction as a function of the ratio

between the tube and the particle diameter ($^{d_t}/_{d_p}$), either considering the actual diameter or an equivalent sphere diameter (d_{pe}) for particles of different shapes (**Figure 18**). The bed porosity and, therefore, the catalyst loading, were assumed to be constant along the bed. We also assume a constant porosity and catalyst loading along the bed, and negligible catalyst deactivation over the time scale considered.

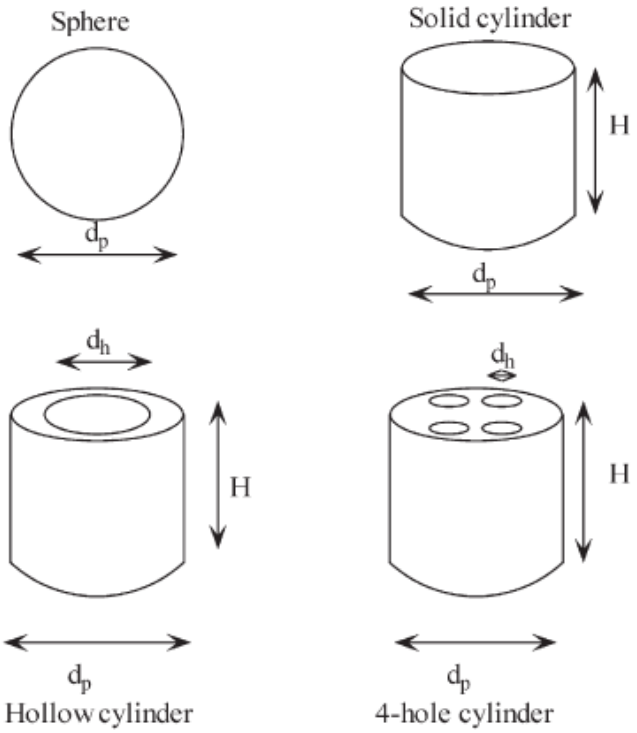

Figure 18 Basic geometries of particles employed in fixed-bed reactors [180].

Table 24 Mean void correlations for FBR [180].

Shape	Correlation	Range of d_t/d_p
Spherical	$0.390 + \frac{1.740}{(d_t/d_p + 1.140)^2}$	$1.5 \leq d_t/d_{pe} \leq 50$
Solid cylinders	$0.373 + \frac{1.703}{(d_t/d_{pe} + 0.611)^2}$	$1.7 \leq d_t/d_{pe} \leq 26.3$
Hollow cylinders	$0.465 + \frac{2.030}{(d_t/d_{pe} + 1.033)^2}$	$1.9 \leq d_t/d_{pe} \leq 14.5$
4-hole cylinders	$0.595 + \frac{0.082}{(d_t/d_{pe} + 1.244)^2}$	$1.9 \leq d_t/d_{pe} \leq 8.4$

3.2.4 Parameters Estimation

Estimates of the physicochemical parameters

The main physicochemical parameters in the balance equations (these being density, specific heat, and viscosity) are significantly influenced by temperature, pressure, and composition. Nonetheless, most of the reviewed modelling studies neglected this influence by considering an ideal gas behaviour. In the MT-HER reactor, however, steep temperature and pressure gradients and strongly variable composition lead to significant non-ideal behaviour of the gaseous mixture, mandating to adopt a rigorous real-gas model to properly depict real world behaviour Therefore, prior to implementing the model, a set of equations has been chosen to properly describe the main physicochemical properties of the gaseous mixture as functions of temperature, concentration and pressure alongside the reactor. First, the properties majorly affecting the mass transfer phenomena (i.e., density, diffusivity, and viscosity) have been considered. The molar density of the mixture has been evaluated by using the modified Peng-Robinson equation proposed by Alkhatib et al. [181] (Eq. (36)-(39)).

$$P = \frac{R}{v-b} - \frac{a(T)}{v(v+b)+b(v-b)} \qquad \text{Eq. (36)}$$

$$a(T) = 0.45724\frac{(RT_c)^2}{P_c}\alpha(T) \qquad \text{Eq. (37)}$$

$$b = 0.0778\frac{RT_c}{P_c} \qquad \text{Eq. (38)}$$

$$\alpha(T) = \left(\frac{T}{T_c}\right)^{\frac{N}{M-1}} exp\left(L\left(1-\left(\frac{T}{T_c}\right)^{NM}\right)\right) \qquad \text{Eq. (39)}$$

The viscosity of the gaseous stream (μ_g) was computed through the Wilke mixing rule, which can be applied at both low and high pressures and is given by Eq. (40) [134].

$$\mu_g = \sum_i \frac{\mu_i}{1+\frac{1}{y_i}\sum_{j\neq i}\frac{y_j\left[1+\left(\frac{\mu_i}{\mu_j}\right)^{(1/2)}\left(\frac{M_j}{M_i}\right)^{(1/4)}\right]^2}{2\sqrt{2}\left(1+\frac{M_i}{M_j}\right)^{(1/2)}}} \qquad \text{Eq. (40)}$$

Heat Transfer Modelling

The overall heat transfer coefficient was computed by considering the difference between the gas and the shell temperature, according to Eq. (41) [171].

$$\frac{1}{U_t} = \frac{1}{U_{t,eff}} + \frac{OD_t}{2k_{steel}}\ln\left(\frac{OD_t}{ID_t}\right) + \frac{A_i}{A_o}\frac{1}{h_{shell}} \qquad \text{Eq. (41)}$$

The heat transfer coefficient in the shell (h_{shell}) is computed based on the pressure of the shell side and the atmospheric pressure as reported by De Falco et al. [182].

$$h_{shell} = 7.96(T - T_{shell})^3 \left(\frac{T_{shell}}{P_{atm}}\right)^{0.4} \quad \text{Eq. (42)}$$

To adequately investigate the heat transfer phenomena, a temperature-dependant relation was used to compute the specific heat of the gaseous mixture (c_{p_g}), as described by Eq. (43)-(44).

$$c_{p_{gas}} = \sum_i c_{p_i} y_i \quad \text{Eq. (43)}$$

$$c_{p_i} = A_i + B_i T + C_i T^2 + D_i T^3 \quad \text{Eq. (44)}$$

Table 25 Parameters for the polynomial relation to estimate the specific heat capacity of the components in the gaseous phase [183].

	A	B	C	D
CO_2	5.316	$1.4285 \cdot 10^{-2}$	$-0.8362 \cdot 10^{-5}$	$1.7840 \cdot 10^{-9}$
H_2	6.952	$-0.04576 \cdot 10^{-2}$	$0.09563 \cdot 10^{-5}$	$-0.2079 \cdot 10^{-9}$
CH_4	4.750	$1.2 \cdot 10^{-2}$	$0.303 \cdot 10^{-5}$	$-2.63 \cdot 10^{-9}$
H_2O	7.700	$0.04594 \cdot 10^{-2}$	$0.2521 \cdot 10^{-5}$	$-0.8587 \cdot 10^{-9}$

The thermal conductivity of the mixture (λ_g) has been obtained through (Eq. (45)) by weighting the thermal conductivity of each component (λ_i), assessed by means of Eq. (46) [178].

$$\lambda_g = \sum_{i=1}^{n} \frac{y_i \lambda_i}{\sum_{j-1}^{n} y_j A_{ij}} \quad \text{Eq. (45)}$$

$$\lambda_i = 3.6\mu_i \left(c_{p_i} + \frac{2.5}{M_i}\right) \quad \text{Eq. (46)}$$

Concerning the effective radial thermal conductivity (λ_{er}), it was computed according to Eq. (47) to account for the gaseous and solid phases as a single homogeneous one. of the system was estimated by Eq. (48)-(51)[150].

$$\lambda_{er} = {\lambda_{er}}^0 + 0.111\lambda_g \frac{Re_p Pr^{1/3}}{1 + 46\left(d_p / OD_t\right)^2} \quad \text{Eq. (47)}$$

$$Pr = \frac{c_p \mu_g}{\lambda_g} \quad \text{Eq. (48)}$$

$$\lambda_{er}{}^{0} = \varepsilon\left(\lambda_g + 0.95\alpha_{ru} d_p\right) + \frac{0.95(1-\varepsilon)}{\frac{2}{3\lambda_s} + \frac{1}{10\lambda_g + \alpha_{rs} d_p}} \quad \text{Eq. (49)}$$

$$\alpha_{ru} = \frac{0.8171\left(\frac{T}{100}\right)^3}{1 + \frac{\varepsilon}{2(1-\varepsilon)}\left(\frac{1-\sigma}{\sigma}\right)} \quad \text{Eq. (50)}$$

$$\alpha_{rs} = 0.8171\left(\frac{\sigma}{2-\sigma}\right)\left(\frac{T}{100}\right)^3 \quad \text{Eq. (51)}$$

Effectiveness Factor

The effectiveness factor (η) represents the ratio between the observed reaction rate (that involves all the active particle) and the reaction rate over the surface of the catalyst only. The incorporation of the effectiveness factor increases model accuracy as it represents a way to partially account for intraparticle transport limitations. As reported by De Falco et al. [184], the effectiveness factor depends on both temperature and species concentration, and it is useful to include analytical expression to properly account for its changes and influence on the reaction rate. Considering both catalysts as available in the form of a spherical pellets, η was computed by means of Eq. (52), assuming a first-order kinetic for the limiting species.

$$\eta = \frac{3}{\phi}\left(\frac{1}{\tanh\phi} - \frac{1}{\phi}\right) \quad \text{Eq. (52)}$$

Previous works reported that this approach ensures a sufficient degree of accuracy, as the estimated values agree with the ones obtained by considering a detailed transport model. The Thiele modulus (ϕ) can be estimated by assuming that hydrogen diffuses faster than CO_2 into the catalyst pellets, and therefore CO_2 can be considered as the limiting species for intraparticle mass transport. Therefore, Eq. (53) was used to describe ϕ.

$$\phi = \frac{d_p}{2}\sqrt{\frac{M_{CO_2} r_{CO_2}}{D_{CO_2}^{eff} \rho_{CO_2}}} \quad \text{Eq. (53)}$$

The evaluation of the effective diffusivity (D_i^{eff}) accounts for both the molecular diffusion ($D_{i,mix}$) and the Knudsen diffusion ($D_{i,Kn}$) to account for molecule-wall interactions, given the porous nature of the catalytic particles. $D_{CO_2}^{eff}$ was therefore evaluated by means of the Bosanquet formula (Eq. (54)):

$$\frac{1}{D_i^{eff}} = \frac{\tau_p}{\varepsilon_p} \cdot \left(\frac{1}{D_{i,mix}} + \frac{1}{D_{i,Kn}} \right) \qquad \text{Eq. (54)}$$

where particle porosity (ε_p) refers to the fraction of the catalyst pellet volume occupied by pores and thus accessible to gas diffusion, whereas the particle tortuosity (τ_p) accounts for the real path length inside the pore network. Coherently with the approach adopted by Miguel et al. [178], a value of 4 was chosen for τ_p, and a value of 0.67 was assumed for ε_p. Concerning the diffusivity of the *i*-th component in the mixture ($D_{i/mix}$), the approach of Wilke Eq. (55) was used, while the diffusivity of the *i*-th component in a binary mixture ($D_{i,j}$) has been computed using the formulation proposed by Fuller et al. (Eq. (56))

$$D_{i/mix} = \frac{(1 - y_i)}{\sum_{j \neq i} \frac{y_i}{D_{i/j}}} \qquad \text{Eq. (55)}$$

$$D_{i/j} = \frac{0.00143 T^{1.75} \left[\frac{1}{M_j} + \frac{1}{M_j} \right]^{0.5}}{P\left({v_i}^{(1/3)} + {v_j}^{(1/3)} \right)^2} \qquad \text{Eq. (56)}$$

The term M_i is the molecular weight of the *i*-th component, while v_i is the molecular diffusion volume of the *i*-th component.

Table 26 Diffusion volumes of the involved components.

Hydrogen	Carbon Dioxide	Water	Methane
7.07	26.09	12.7	24.42

Finally, the Knudsen diffusion ($D_{i,Kn}$) was estimated through Eq. (57).

$$D_{i,Kn} = \frac{d_p}{2} \sqrt{\frac{8RT}{\pi M_i}} \qquad \text{Eq. (57)}$$

3.2.5 Numerical Solution Strategy

The HER model comprises a system of ordinary differential equations (ODEs) complemented by with a boundary condition reporting the value of each process parameter at the inlet section of the reactor. The

obtained ODEs set was solved using the fourth-order Runge-Kutta (RK) method defining the reactor configuration and the initial condition. The RK method was applied to solve the ODE system as it provides a proper consideration of the changes occurring in some properties along the reactor axis. Indeed, by calculated the approximate solutions of the Cauchy problem in the nodes *z(i)*, $i = 1, 2, ..., n+1$ contained in the interval $[z_0, z_{max}]$. The vector problem is composed by Eqs. (58)-(62):

$$y'(z) = f\big(z, y(z)\big) \quad \text{Eq. (58)}$$

$$y(z_0) = y_0, \qquad z \in [z_0, z_{max}] \quad \text{Eq. (59)}$$

$$y(z) = \big(y_1(z), y_2(z), \ldots, y_m(z)\big) \quad \text{Eq. (60)}$$

$$f\big(z, y(z)\big) = \Big(f_1\big(z, y(z)\big), f_2\big(z, y(z)\big), \ldots, f_m\big(z, y(z)\big)\Big) \quad \text{Eq. (61)}$$

$$y(z_0) = \big(y_1(z_0), y_2(z_0), \ldots, y_m(z_0)\big) = (y_1^0, y_2^0, \ldots, y_m^0) = y_0 \quad \text{Eq. (62)}$$

The solution is a matrix of dimension $(n+1)\cdot m$, whose *i*-th row of length m contains the approximation of the solution calculated in the node *z(i)* (*n* is the number of sub-intervals [*z(i)*, *z(i+1)*], $i = 1, ..., n$ into which the interval $[z_0, z_{max}]$ is divided). The solution calculated at the node $i+1$ is given by Eq. (63):

$$Y(i+1) = Y(i) + \frac{delta}{6}(k_1 + 2k_2 + 2k_3 + k_4) \quad \text{Eq. (63)}$$

$$delta = \frac{z_0 - z_{max}}{n} \quad \text{Eq. (64)}$$

$$k_1 = f(z, y) \quad \text{Eq. (65)}$$

$$k_2 = f\left(z + \frac{delta}{2}, y + delta \cdot \frac{k_1}{2}\right) \quad \text{Eq. (66)}$$

$$k_3 = f\left(z + \frac{delta}{2}, y + delta \cdot \frac{k_2}{2}\right) \quad \text{Eq. (67)}$$

$$k_4 = f(z + delta, y + delta \cdot k_3) \quad \text{Eq. (68)}$$

The RK method ensure a good trade-off in terms of precision and computational efforts if an equidistant step size (i.e., the cell size along the reactor) of 0.001 m and a relative error tolerance of 10^{-1} are assumed. Concerning the relative error tolerance, it refers to the considered significance of digits for the computation of the ODEs.

3.2.6 Plant Configuration

The SNG production plant layout consists of a series of MT-HERs with interstage condensation to remove the water produced as byproduct, in a configuration resembling that of the multi-CECU process investigated for DME production [136]. The MT-HERs have been simulated in MATLAB environment by using the reactor

model described in **Section 3.2.3**, which has been continuously adapted in terms of inlet composition and pressure, while maintaining a constant inlet temperature. The multi-CECU process has been implemented in Aspen Hysys to enable a real-time streamline of the final design, readapting a procedure already adopted by De Falco et al. [135]. A further reaction stage has been incorporated into the process whenever the anhydrous gas resulting from the previous reactor did not comply with the network specifications, an approach adopted also by Colelli et al. [72]. To facilitate intermediate condensation, the product gas was subjected to a cooling process that brought it to a temperature of 15°C. The resulting mixture was then separated in a simple flash unit, where the liquid–vapor equilibrium was established. To accurately estimate the stream compositions and calculate phase equilibria, an NRTL thermodynamic model was implemented. Before entering the subsequent reaction stage, the gaseous stream leaving the separator was preheated by recovering heat from the product gas of the preceding reactor and brought to the reaction temperature (see **Figure 17**). The primary assumptions concerning the feedstock and operating conditions are outlined in **Table 27**.

Table 27 Input parameters for the simulation of the multi-CECU process.

	Hydrogen	Carbon Dioxide	MT-HER
Flowrate [kmol h^{-1}]	180	45	-
Temperature [°C]	30	30	230
Pressure [bar]	10	1	10

The choice of the operating pressure is guided by the findings of **Chapter 2** as well as state-of-the-art considerations. Schaaf et al. [68] identified 20 bar as an effective threshold to achieve a conversion above 90% at high temperatures (450°C), noting that further increases provide no significant improvement in yield. Furthermore, Colelli et al. [72] recommended operating slightly above the target set pressure to account for pressure losses and to avoid the need for recompressing the gas mixture. This approach is particularly suitable for the investigated scheme, which does not include recycling and aims to push the reaction as far as possible to produce pipeline-grade SNG.

3.2.7 Grid Compliance Evaluation

The quality of the SNG streams exiting each methanation reactor stage has been assessed with reference to the technical specifications for injection into the Italian gas grid, ensuring compliance with both national standards and end-user requirements (see **Synthetic Natural Gas (SNG) Grid Requirements**). The need to account for this issue is related to the potential costs arising from non-compliance and the related extra processing steps, beside the possibility of constrained operations. Given the intended integration of the produced SNG into the existing gas network, particular emphasis has to be placed on the interchangeability features and the presence of residual quantities of hydrogen, CO_2, and water [185]. The Wobbe Index (WI) was selected as the primary metric for the evaluation of interchangeability with pipeline-quality natural gas, as it reflects the combined effects of gas composition and density on heat delivery. Since its

introduction as a quality criterion in the 1920s, the WI has become central to ensuring consistent combustion behaviour of gaseous fuels, facilitating the progressive introduction of substitute gaseous fuels that do not require requiring adjustments to burners, ignition systems, or flame stabilisation parameters. Investigating the progressive introduction of hydrogen in the Dutch gas grid, Zachariah-Wolff et al. [186] stressed the crucial role of the WI in facilitating the transition, arguing that while WI standards might appear restrictive, they also preserve system flexibility by enabling controlled integration of alternative fuels. The authors outlined that compatibility and interchangeability parameters such as the WI are essential to develop a uniform interface and ensure that the transition towards low-emission gases can be executed in an incremental manner whilst ensuring the preservation of the safety and efficiency of the system. This is mostly because gaseous fuels with identical WI deliver equivalent energy input under identical operating conditions, as the WI accounts for both the Higher Heating Value (HHV) and the specific gravity relative to air [187]. Conversely, Franco and Rocca [63] have critiqued the overreliance on the WI to determine the effective replacement potential in cases of increasing hydrogen percentages, emphasising that the WI alone is inadequate in capturing the effects of these alterations. However, despite the potential for moderate variations in the volumetric energy content, explosion limits and knock resistance of the mixture, the WI remains a reliable criterion for assessing interchangeability. Indeed, the similarity between SNG and fossil NG is such that maintaining the WI is considered sufficient to ensure end-user compliance and to minimise the risk associated with unstable flames, flashback and inefficient heat transfer. The parameters listed in **Synthetic Natural Gas (SNG) Grid Requirements** have been obtained directly from the Aspen Hysys process simulation.

3.3 Results and discussion

3.3.1 Reactor Simulation

The designed MT-HER has been simulated at pressure ranging from 5 to 15 bar at three gas hourly space velocities (GHSV) of 1000, 5000, and 10,000 h^{-1} to investigate its applicability for industrial-scale deployments. For each of the investigate pressure, reactor internals are kept identical at given GHSV and reactor length (i.e., 1 m length), resulting in the configurations reported in **Table 28**.

Table 28 Outcomes for the MT-HER design at the different GHSV investigated.

Parameter	1,000 h^{-1}	5000 h^{-1}	10,000 h^{-1}
Number of tubes	3,047	610	305
Shell Diameter [m]	3.66	1.73	1.23

As expected, while temperature and conversion profile are qualitatively similar across pressures, the results demonstrate that the effectiveness of the modelled reactor is mostly dependent on the residence time. As

the GHSV increase, the temperature peak shifts downstream and broadens, though remaining constantly below 500 °C for all the investigated cases (the highest peaks observed are at approximately 480 °C). The outlet temperature is constantly between 260 and 370 °C, signalling the effectiveness of the heat transfer modelling in both managing the occurrence of the thermal hotspot and guarantee outlet temperatures compatible with downstream processing. CO_2 conversion on the GHSV. On the other hand, a systematic, positive pressure effect is observed at fixed GHSV. From 5 to 15 bar the CO_2 per-pass conversion increases modestly yet consistently, and the outlet temperature decreases slightly at the highest GHSV. The trend is thermodynamically coherent with the Sabatier reaction, which is shifted toward methane at higher total pressure within the investigated temperature span. As the adopted kinetic predicts a positive dependence on reactant partial pressures in the 250-350 °C range [178], this is congruent with the observed incremental gains. Overall, with reference to the outcomes in **Table 29**, it can be stated that at fixed pressure, conversion decreases monotonically with increasing GHSV while outlet temperature rises, reflecting the reduction in shorter time for heat removal per unit length. On the other hand, at fixed GHSV, increasing pressure from 5 to 15 bar yields a consistent improvement in conversion and methane production, with the relative gain most visible at 10,000 h^{-1} and a small decrease in outlet temperature at high GHSV. Despite the high exothermicity, all temperature profiles remain below the critical regime associated with rapid deactivation of Ni catalysts, while the early-bed temperature spikes characteristic of adiabatic or poorly cooled beds [26,155] have not been observed. As the profiles are similar for the three investigated case, the outcomes in terms of process variable trends throughout the reactor are reported in **Figure *19*** for the mid-case (i.e., 10 bar), which is then used to perform the plant-scale simulation.

Table 29 Simulation outcomes at 5, 10 and 15 bar.

Parameter	**5 bar**			**10 bar**			**15 bar**		
	1,000 h^{-1}	**5000 h^{-1}**	**10,000 h^{-1}**	**1,000 h^{-1}**	**5000 h^{-1}**	**10,000 h^{-1}**	**1,000 h^{-1}**	**5000 h^{-1}**	**10,000 h^{-1}**
CO_2 conversion [%]	77.91	50.79	37.38	78.77	52.20	39.74	79.15	52.79	40.66
Outlet Temp [°C]	259.95	326.37	370.78	260.38	323.24	363.46	260.57	322.09	360.54
CH_4 Production [$Nm^3\ h^{-1}$]	785.82	512.25	376.99	794.52	526.53	400.8	798.29	532.45	410.13

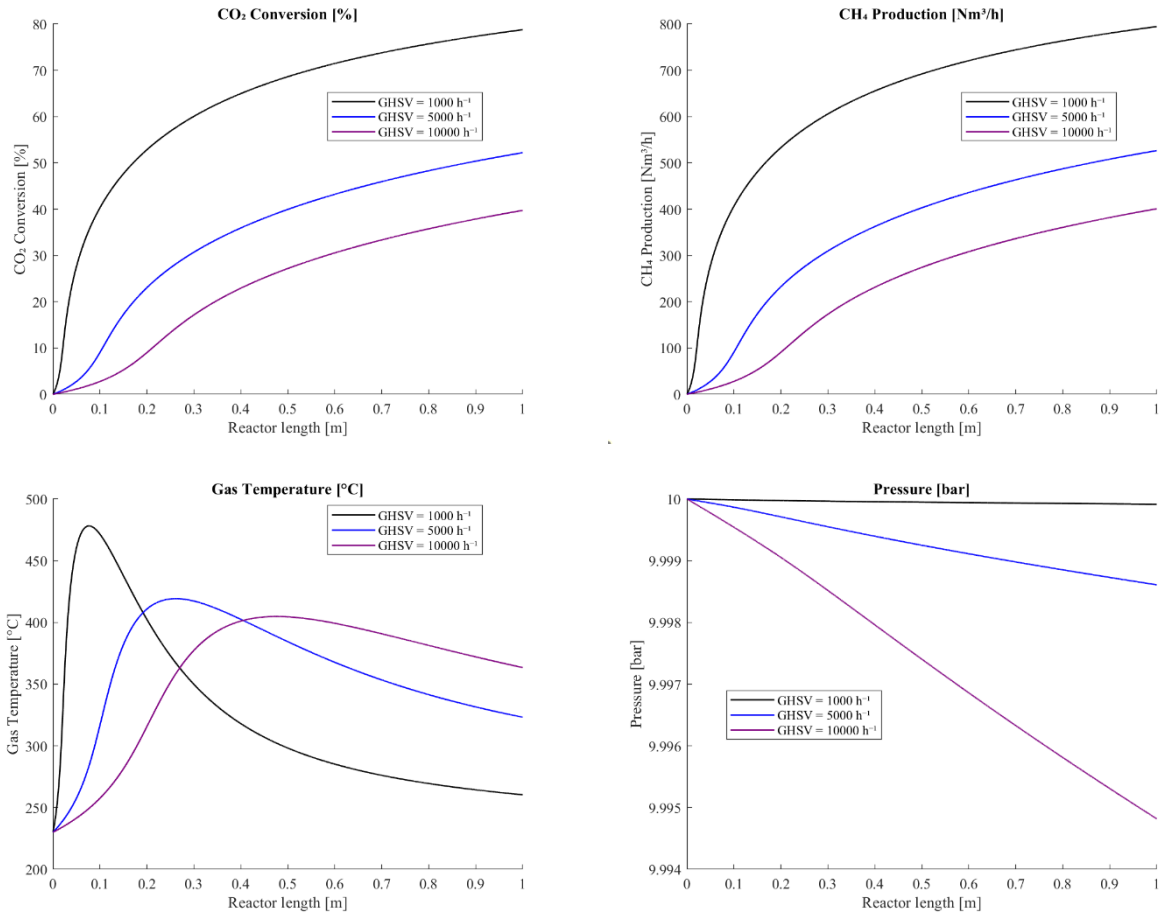

Figure 19 Simulation outcomes at 10 bar.

Eventually, it must be noted that industrial scale operations are commonly performed at GHSV of the order of 5,000-10,000 h^{-1} [154] and it is therefore necessary to overcome the issue of low-conversion by acting at a plant level. Therefore, 10 bar and 5,000 h^{-1} GHSV has been selected as input parameters to proceed with the simulation and assessment at the plant-scale, discussed in the next section.

3.3.2 Plant Simulation

The performed process simulation had the objective of identifying the minimum number of reactors needed to enhance CO_2 conversion and be compliant with Italian gas grid specification (see **Synthetic Natural Gas (SNG) Grid Requirements**). Nonetheless, as reported in **Table 30** and **Table 31**, while developing the reaction section of the plant through the multi-CECU approach enables to achieve a 97.1% CO_2 conversion and the production of 977.5 Nm^3 h^{-1} of methane, the obtained SNG does not comply with gas grid regulations, mostly due to an inadequate WI driven by the presence of non-negligible traces of water and a substantial amount of residual hydrogen.

Table 30 MT-HERs performance indicators.

	BED-1	BED-2	BED-3	BED-4	BED-5	BED-6	BED-7
CO_2 Conversion Bed [%]	54.06	51.46	47.27	39.2	30.54	25.32	21.93
CO_2 Conversion Bed [%]	54.06	77.75	88.28	92.88	95.06	96.31	97.13
CH_4 Production [$Nm^3\ h^{-1}$]	545.2	783	888.9	935.2	956.9	969.4	977.5
Outlet Temperature [°C]	321.3	315.5	307	289.4	267.6	254.3	246.5

Moreover, it must be stressed that a conversion higher than 90% is already obtainable by developing a 4-stage reaction train, as the fourth MT-HER of the series boost CO_2 conversion up to 92.9% at plant scale. Indeed, it is worth noting that beyond the fourth stage the addition of a further reactor is uniquely functional to abate the amount of unreacted CO_2 and drive and increase in the WI and the HHV, while it has no beneficial effects in terms of compliance. Therefore, the train made up of BED-5 to BED-7 should be considered as an alternative scheme to the amine scrubbing approach proposed by Tripodi et al. [159] rather than an integral part of the reaction section (only 4.3% increase in conversion with respect to the SNG stream leaving BED-4).

Table 31 Compliance assessment for the multi-CECU methanation process. Data are referred to outlet streams.

Parameter	BED-1	SEP-1	BED-2	SEP-2	BED-3	SEP-3	BED-4	SEP-4	BED-5	SEP-5	BED-6	SEP-6	BED-7	SEP-7
CO_2 concentration [mol.%]	11.72	16.14	9.39	11.72	6.95	7.94	5.14	5.51	3.96	4.10	3.12	3.19	2.52	2.56
H_2 concentration [mol.%]	46.89	64.66	37.77	37.72	028.10	32.11	20.97	22.47	16.28	16.87	12.94	13.23	10.58	10.73
CH_4 concentration [mol.%]	13.79	19.02	32.76	32.76	52.27	59.74	67.02	71.80	76.04	78.78	81.54	0.27	85.21	86.43
H_2O concentration [mol.%]	27.59	0.19	20.13	0.20	12.68	0.21	6.86	0.23	3.72	0.24	2.39	83.32	1.69	0.28
Higher Heating Value [MJ m^{-3}]	11.45	14.88	17.42	21.19	23.31	26.43	28.07	29.57	30.87	31.72	32.61	33.03	33.54	34.03
Wobbe Index [MJ m^{-3}]	16.88	23.83	25.14	31.94	33.30	38.35	39.30	42.24	42.81	44.42	44.80	45.80	46.07	46.74
Specific Gravity	0.46	0.39	0.48	0.44	0.49	0.4751	0.51	0.49	0.52	0.51	0.53	0.52	0.53	0.53

Based on these findings, it is evident that the presence of unreacted hydrogen and the residual moisture of the produced SNG represent the main hinderances for the deployment of a simple multi-CECU process intended to attain pipeline grade SNG. Leveraging the conventional purification processes of fossil NG, the inclusion of a dehydration unit could be beneficial to abate the residual moisture and met the grid requirements in terms of DP. As reported by Colelli et al. [72], the presence of non-negligible traces of water within the SNG resulting from the last reactor would require complex and expensive post-treatment technologies to achieve the required DP. The authors stress that it is unlikely that moisture removal can be obtained by solely prompting condensation at low temperature, as the presence of non-condensable compounds leads to a decrease in condensation temperature decrease. Indeed, Perna et al. [156] included a dehydration membrane with 90% efficiency while Lee et al. [188] included a triethylene glycol (TEG) based absorption process to abate water content to ppm, leveraging a process that is widely used in NG processing which is, however, substantially energy-intensive given the large amount of heat to be supplied to the reboiler [189]. On the other hand, as mentioned, Tripodi et al. [159]suggested that residual hydrogen could be removed by integrating a tailored PSA section that could lead to the implementation of further intensification strategies such as recycling or internal heat recovery.

3.4 Conclusions

The design of CO_2 methanation reactor is one of the most crucial challenges to face in order to enable the deployment of Power-to-Methane (PtM) at scale. Among the different methanation concepts, the Multi Tubular Heat Exchange Reactor (MT-HER) has emerged as a conventional yet robust technology for implementing this highly exothermic reaction on a large scale. The MT-HER integrates a packed-bed catalytic reactor into a shell-and-tube heat exchanger design, allowing the heat of reaction to be efficiently removed via cooling media in the shell side. The objective of the present chapter was to design and analyse the performance of an MT-HER under industrially relevant conditions, with a view to exploring the effects of gas hourly space velocity (GHSV) and operating pressure on reactor performance (CO_2 conversion, temperature profiles, methane production, and reactor compactness). The simulation results clearly demonstrate the dominance of GHSV in shaping the thermal field, reflecting the relative magnitudes of the effective Damköhler number and the axial Péclet number under efficient external heat removal. Increasing GHSV decreases the residence time and increases the convective enthalpy flux, broadening and shifting the temperature increase downstream without causing the emergence of thermal hotspots. The absence of peaks above 480 °C across all cases is technically significant for Ni stability, as literature identifies accelerated sintering and support-metal interfacial changes above 500 °C in the presence of steam [154]. The simulations demonstrate that, within 5-15 bar and 1,000–10 000 h^{-1}, the MT-HER achieves stable thermal behaviour without the occurrence of dangerous hot spots, delivering per-pass performance governed predominantly by space velocity (pressure provides a modest but measurable benefit). On the other hand, the obtainable conversion is limited at the considered space velocities, which have been investigated considering industrial deployment [154]. Operating at 5,000 h^{-1} and 10 bar represent a trade-off between

the need to obtain high conversions and avoid excessive expenses for reactants compressors. Indeed, at this condition it is possible to achieve a per-pass CO_2 conversion of approximately 52%, which represents a starting point for the implementation of the multi-CECU process. The performed plant scale simulation has confirmed the beneficial effect of staging and intermediate condensation in shifting the reaction equilibria towards methane formation, with conversions higher than 90% obtained by deploying four MT-HER of 1 m each. On the other hand, it must be emphasised that the application of this concept to methanation is not sufficient to deliver pipeline-grade SNG, mostly due to the residual presence of both hydrogen and moisture. Nonetheless, the adopted grid compliance assessment methodology enabled the detection of deviations from acceptable gas-quality parameters during intermediate stages and clarified the impact of interstage condensation and residual reactants on overall SNG quality. Although the WI remains the primary performance metric, parameters such CO_2 and hydrogen concentrations, as well as water dew points, are essential to be assessed in order to drive improvements in process design and guarantee full compliance with injection standards.

From the model perspective, some inherent limitations should be noted, which also highlight directions for further research. First, the main limitation of the proposed model lies into the absence of a proper accounting of carbon monoxide (CO) formation due to Reverse Water Gas-Shift (RWGS) reaction. Nonetheless, it must be noted that most of the investigations that included RWGS adopted the kinetic model of steam methane reforming over the Ni/Al_2O_3 catalyst, since those kinetic expressions account for the reversibility of the reforming and water gas shift reactions and were supposed to fit well also for modelling the CO_2 methanation reaction system [155]. Moreover, as originally reported by Lunde and Kester [82], working under controlled temperature and pressure conditions ensure that the RWGS reaction is limited and it is therefore reasonable to neglect its occurrence. Nonetheless, a recent investigation performed by Krammer et al. [154] stressed the importance of considering the whole set of reactions in case of CO/CO_2 feed gases, as the combined reaction mechanisms influence the overall process performance. Indeed, the authors stated that while CO methanation is kinetically limited, CO_2 methanation is substantially influence by the occurrence of the RWGS reaction. Second, the current model assumes steady-state operation with uniform radial and axial temperature and concentration fields, corrected only for intraparticle diffusion via an effectiveness factor. In practice, the strong exothermicity of CO_2 methanation often induces substantial temperature and concentration gradients within the catalyst bed, especially at low GHSV and high pressures. These gradients can promote hot spots and affect kinetics and thermodynamics locally, mandating the need to increase the level of details and maybe adopting a bi-dimensional model [155]. Third, the kinetic model, derived from laboratory-scale studies, has been extrapolated beyond its validated range, and the impact of catalyst deactivation, flow maldistribution, and non-ideal packing at small tube-to-particle diameter ratios is not accounted for [178].

From the plant perspective, the present investigation is based on the use of high purity, but in an industrial context these might contain residual oxygen, which must be limited to below approximately 6 mol.% for

grid injection. Pipeline-derived CO_2 is typically free of oxygen, while pathways such as biomass-to-SNG may introduce it, though its effects on conversion have not been widely explored yet [190]. On the other hand, some electrolysis technologies such as ALK produce hydrogen streams that frequently contains trace amounts of oxygen, necessitating additional purification to meet the stringent grid or end-use fuel specifications. As demonstrated by Mazzeo et al. [191], a compelling solution has been found in the form of catalytic recombination of hydrogen and O_2 over Pd/Al_2O_3, which was found to allow for the achievement of oxygen levels compatible with fuel-cell applications (down to ~5 ppm). The integration of a catalytic recombiner stage upstream of the methanation unit could thus prove essential to ensure compliance in real-world operations.

Beyond the technical perspective, performing a techno-economic assessment (TEA) is essential to evaluate the actual feasibility of deploying a PtM solution [79,192], as it allows to gain insights on the overall performance of the process and select the best process configurations and technologies to be integrated to comply with the comprehensive requirements of efficiency and cost-effectiveness. Some critiques have emerged in recent times, as the expected benefits in the field of GHGs emission reduction are not believed sufficient to sustain this pathway due to the excessive costs and issues throughout the value chain [27,193]. Therefore, future works should leverage the constructed methodological framework to thoroughly address the financial profile of the investigated system and drive advancements from a more holistic perspective. Indeed, the present chapter provides a valuable first order understanding of the design space, though further investigation using bi- dimensional models, as well as experimental validation, is required before confidently adopting such designs for industrial deployment [154]. As for the process, the integration of further handling units in the scheme should be pursue only on a complementary basis with respect to an advanced assessment and further simulation of the multi-CECU process.

Chapter 4. Conclusions

The production of Synthetic Natural Gas (SNG) in a PtM/Carbon Capture Utilisation and Storage (CCUs) framework represents a promising option to drive multiple-system decarbonisation by levering its system integration potential [38,185]. The development of the SNG production process has been driven by the necessity of reducing the reliance of the United States from natural gas (NG), as the geopolitical tensions and the increase in NG demand generated concerns of possible shortages [9]. The current socio-economic and geopolitical context share strong similarities with those times.

First, the conflict in Eastern Europe had a dramatic impact on the prices of fossil fuels in the European Union (EU), with the spikes in NG prices having led to a generalized increase in electricity bills for both household and non-household consumers [32]. The energy crisis particularly affected countries such as Italy where most of the electricity demand was supplied by NG power plants but was harsh also in countries where NG share in the electricity mix was minimal, as the price of electricity and of NG are inherently interconnected within the EU energy market [194,195]. Beside reaffirming the need to reduce third-party dependencies in energy procurement, the Eastern Europe crisis and the more recent Middle East ones mandates the need to rethink what sustainable development means for our societies and shift from a purely *environment-leading* approach to a *competitiveness* and *self-sufficiency* once. European countries are severely dependent on third-party imports for the energy and industrial sectors and considering the current geopolitical scenario this approach is recognised as being no longer conceivable.

To promote this paradigm shift, the focus of research activities should move accordingly and consider not only the immediate environmental benefits a technology under development could lead, but also the value chain and life cycle implications of an innovative technology once transferred to the industry. Within this context, the present dissertation deals with a thorough analysis of the SNG production processes, starting from the design and assessment of a novel catalytic system and passing through the design of the reactor unit and the whole process considering a commercial scale. Moreover, coherently with the methodological approach theorized by De Falco and Capocelli [196], the thesis contains the preliminary outcomes of a collegial work aimed at developing and implementing at scale a comprehensive methodology to model and investigate the performance of innovative technologies in the field of PtG and CCUS. This multifaceted approach combines conventional methods rooted in thermodynamic and kinetic modelling with a more holistic perspective that accounts for the maximum exploitation based on its quality assessment (*exergy analysis*) and for the environmental implications of a product/process [197].

The present dissertation discussed the outcomes related to the start of a testing campaign on a Ni/CeO_2-ZrO_2 catalyst synthesized via solution combustion synthesis (SCS) and conducted at CNR-ITAE. The catalyst

exhibited outstanding activity, selectivity, and stability for CO_2 methanation under industrially relevant conditions (the tests were executed at 12,000 h^{-1} and at various pressures). The advanced CeO_2-ZrO_2 support enhances oxygen vacancy formation and Ni reducibility, enabling high conversion and methane yield even at moderate temperatures and pressures (conversions up to 90% were obtained around 300 °C). Furthermore, a comparative Life Cycle Assessment (LCA) revealed that, despite higher impacts during synthesis, the superior performance of the catalyst reduces the overall environmental burden per unit of methane produced (1 Nm^3), emphasizing the importance of considering the full value chain in catalyst development. As the activities performed are part of more extensive work aimed at determining the intrinsic kinetics of the catalyst, future perspectives include obtaining a thorough understanding of the fundamental mechanisms underlying the conversion of reactants into methane to proceed with effective scaling up and transfer to industry. On the other hand, the present dissertation discusses the need to complement conventional technical performance assessment with a wider characterisation framework that encompasses both environmental and economic metrics. Future efforts should focus on harmonizing performance assessments, evaluating long-term stability, and addressing the sourcing risks of rare-earth materials. In parallel, the modelling and simulation of a Multi-Tubular Heat Exchange Reactor (MT-HER) revealed trade-offs between CO_2 conversion, methane yield, reactor compactness and thermal management. Moderate pressures (10 bar) and space velocities (5,000 h^{-1}) were identified as an optimal compromise between performance and operational feasibility. Limitations in the modelling approach suggest that further detailed modelling, experimental validation and the exploration of mitigation strategies (e.g. staged feed, gas recirculation and catalyst dilution) could foster the predictive capability and scale-up aiding capacity of the developed model. On the other hand, the *proof of concept* of the application of the multi-CECU process [136] for methanation has demonstrated the necessity to include further downstream processing units to meet grid requirements, with main reference to water abatement and hydrogen handling. As for the latter, it must be noted that, as outlined in **Section 1.2**, the threshold for hydrogen blending might vary from each country and is subject to constant scrutiny to foster the implementation of an hydrogen based economy [53]. On the other hand, the energy transition is moving faster than the actual development of its enabling technologies, these mostly belonging to the framework of energy storage systems [198]. The fast-paced deployment of RES alongside end-use electrification has significantly outpaced the capacity of the European electricity grid, which was originally designed for centralized, fossil fuel-based generation [199,200]. Therefore, PtM should be designed to guarantee the seamless integration with the energy generation sources and future assessment should be account for this issue. In an off-grid setting, the variable hydrogen load represents one of the main bottlenecks in PtM operation, with changes in the feed flow rate being considered as the major threat to the safe operation of the methanation reactor. Therefore, the whole system should be designed to operate in a dynamic manner and accommodate load variations, as stressed by several authors who investigated the dynamic behaviour of either the reactor or the whole plant during its start-up, transient operation, steady-state and shut-down phases [25,72,151,179].

In conclusion, considering the outcomes of our activities during the last 3 year, it emerged how the adoption of the above-mentioned multifaceted approach is essential to properly assess technological, environmental, economic and value chain related criticisms and obtain an effective understanding of the processes under investigation. This is of outmost importance while considering that research efforts are expected to be transferred to both industrial players and decision-makers, to whom it must be delivered a comprehensive set of information to guide the pathway towards the establishment of a sustainable economic model. Furthermore, recognising the need to transfer knowledge across the different stakeholders in this field, the outcomes of the present research line are set to be delivered to international journals in the near future. On other hand, part of the outcomes of **Chapter 2** have already been shared by attending to the first International Congress on Sustainable Energy and related Technologies (ICSET) held in June 2025 by presenting the work under the title *The life cycle implications of the catalyst synthesis method on CO_2 methanation*.

Annex

Life Cycle Assessment (LCA)

Life Cycle Assessment (LCA) has its roots in the late 1960s and 1970s, a period characterised by mounting concerns regarding environmental degradation and the energy crisis [201]. These concerns motivated scientists and companies to conduct thorough assessments of the resource and energy demands associated with products and processes. Early studies focused primarily on estimating energy consumptions, generated emissions and waste, such as the case of the *Resource and Environmental Profile Analysis* (REPA) conducted by Midwest Research Institute (MRI) for the Coca Cola Company in 1969, which entailed the comparison between glass and plastic materials for beverage containers [201,202]. Then, several pioneering studies were performed, mostly devoted to the comparison of alternative production processes and the quantification of the cumulative environmental impacts across the entire life cycle of products. The concept of Life Cycle Thinking (LCI) emerged as an approach aimed at considering a product (or a process) as part of a more extensive value chain that starts from the extraction of the raw materials and ends with the end-of-life disposal, therefore looking the product from a *cradle-to-grave* perspective [202,203].

In the 1990s, the need for a common LCA approach became urgent, as the considerable number of studies published in that periods were not considered reliable due to the absence of a common methodological [202]. A first attempt at standardisation was made by the Society of Environmental Toxicology and Chemistry (SETAC), which published one of the first books on the topic titled Code of Practice in 1997 [204]. There, SETAC defined LCA as *an objective process of assessing energy and environmental loads related to a product/process/activity, carried out through the identification of energy and materials used and waste released into the environment*, with reference to *the entire life cycle of the product/process/activity, including extraction and treatment of raw materials, manufacturing, transportation, distribution, use, reuse, recycling, and final disposal* [204]. Subsequently, in 1997, the International Organization for Standardization (ISO) published the ISO 14042 standard on impact assessment [205], which was updated in 2006 with the currently adopted standards ISO 14040 [123] and ISO 14044 [122]. Those standards delineated LCA as a methodical, cradle-to-grave evaluation of all inputs (energy, materials) and outputs (emissions, waste) of a product or process and the established framework provided researchers and companies with a shared terminology and procedure, facilitating the comparison of studies and the sharing of data.

Consequently, LCA gained credibility and rapidly increased in usage, becoming the main tool for assessing the environmental impact of products and processes, being also incorporated in regulatory recommendations. LCT approaches are widely mentioned in the legislation and acts of European institutions, starting with the 1992 Ecolabel Regulation and the ending up with the more recent European

Green Deal [12]. The Integrated Product Policy (IPP) of European Commission (EC) considered LCA is regarded the best framework for assessing the potential environmental impacts of products, though addressing the need for a more consistent data and consensus LCA methodologies [206]. Later, LCA was made mandatory to evaluate the environmental profile of products and certify them through the Environmental Product Declaration (EPD), an environmental declaration regulated by the standard ISO 14025 [207] and based on guidelines called Product Category Rules (PCRs). Sala et al. [208] reported that, considering the period between 1990 and 2020 as a reference, around 300 documents were drafted by European Union (EU) bodies in which explicit reference is made to LCT approaches, confirming the EU's ambition to become a pioneer and leader in the field. European policies have laid the foundations for a close and fruitful collaboration between the scientific community and the legislature, establishing centres such as the *European Commission-Joint Research Centre* (EC-JRC) to promote the implementation and development of LCA methodologies or platforms such as *The European Platform of Life Cycle Assessment* (EPLCA) to support the development and optimisation of Product Environmental Footprint (PEF) and Organisation Environmental Footprint (OEF) impact assessment methodologies.

Currently, LCA represents the most adopted methodology to perform an environmental assessment of a product or a process throughout its life cycle, besides being a well-established decision-making tool. Indeed, LCA critically orients both researchers, industrials and decision-makers, as it allows to simultaneously evaluate different scenarios of a process or a product and identify the one leading to the lowest possible environmental burdens. Therefore, companies and governments routinely use LCA to compare different options and guide procurement and regulatory decisions, as LCA is also an instrument to thoroughly understand value chain related risks, as it allows for a regionalized analysis of the generated impact, a tool that could also serve in a more and more demanded assessment of the value chain exposure risks.

LCA Methodology

As abovementioned, LCA is an internationally standardized methodology which is regulated by two main standards providing the basic principles [123] and the requirements [122] of the developed framework. The methodological approach is constituted by four interconnected stages (see **Figure *20***). The assessment should be performed iteratively, given that the collected data and information might necessitate modification of the scope in order to ensure that the analysis remains consistent with the initial objectives.

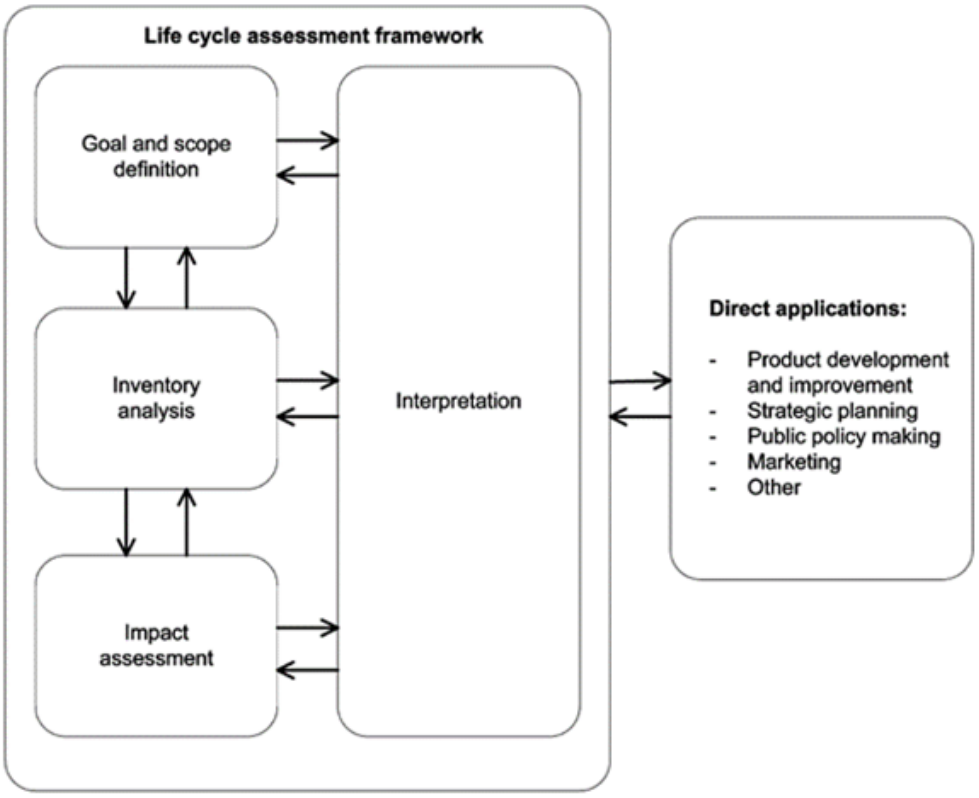

Figure 20 Framework for Life Cycle Assessment [122,123].

Table 32 Phases of a Life Cycle Assessment [122,123].

Stage	Description
Goal and Scope Definition	Goal and scope definition aims to unambiguously establish what the intended application is, the motivation for carrying out the study and the context for which it is intended. This phase is divided into the subsequent sub-activities: 1. **Goal Definition**. The first activity to perform is the formulation of the rationales for conducting the investigation, the intended application, and the intended audience. The object of the study is defined as the product system, representing the collection of processes (defined as activities that transform inputs into outputs) that constitute the value chain. 2. **Scope Definition**. This activity is related to the definition of the coverage of the LCA study by specifying technological, temporal, and geographical aspects. Moreover, a scope definition delineates the modus operandi of the analysis and the analytical sophistication of the study. The primary outcomes of this stage are: a. **Functional Unit**. The product system must be described according to its functional aspects, which is defined by the functional unit. The latter defines

and quantifies the primary functions fulfilled by a given product system, standardizing the inventory data and therefore providing a reference for the assessment. It must be noted that the selection of the functional unit should be made to ease the comparison among different processes and different studies. Moreover, the definition of the functional unit must be a clear justifiable statement deriving from surveys, questionnaire and data gathering and analysis.

b. **System Boundaries**. A system boundary could be defined as a conceptual boundary delimiting the product system under study, which can be described by means of system balance diagrams. Apart from the cradle-to-grave approach previously described, the study could be performed adopting both a cradle-to-gate boundary (that means partially assessing the product life cycle impact setting the upper limit of the boundary to the factory gate, therefore neglecting both the use and disposal phases) and cradle-to-cradle whenever the end-of-life disposal step for the product is a recycling process.

c. **Allocation Procedure**. The computed impacts must be properly referred to the inputs and outputs of the product system. In case of co-production, it is crucial to establish the allocation of these impacts and solve the multifunctionality problem following the hierarchy proposed by ISO 14044.

d. **Impact Assessment Categories**. It is necessary to identify the impact categories of interest in compliance with the stated goals of the study, beside the selected methodology which would be used to estimated them.

Life Cycle Inventory

Life Cycle Inventory (LCI) is a method of modelling a product system and collecting and verifying environmental intervention data, including emissions to air and water, waste generation and resource consumption. As previously mentioned, once these data have been acquired, they must be related to the functional unit defined in the previous stage. Furthermore, it should be noted that other activities within the LCI stage, such as cut-off, data estimation and data validation, are of crucial importance. These activities are fundamental to the consistent selection of the number and type of data required from the analyst while filling the gap, if it is not possible to track all the processes from cradle to grave.

Due to the need of gathering a huge number of data, referred to the entire life cycle of the product system, the LCI is the most time-consuming stage of the analysis. Among the factors affecting both the time requirements for LCI and the correctness of the results, the quantity and quality of the data collected plays a major role. While modelling the product systems, data should be classified as:

- **Foreground Data**. These data specifically refer to the product system under investigation and are essential to perform the assessment. Therefore, the collection of foreground data requires an in-depth knowledge of the processes constituting the core activities of the product system.

- **Background Data**. Background data are referred to all the processes which are not typical of the investigated product system but still are relevant to the production of materials, energy and waste management. These data are mostly generic and typically obtained from databases and literature material.

It must be noted that both foreground and background data used in the LCA investigation must be methodologically consistent and met the quality requirements. Furthermore, the current standards also distinguish primary data from secondary data, with the former being referred to the specific process under investigation and measured at the operating site, and the latter being obtained through publications, open literature, software, LCA libraries and similar. Secondary data are mostly adopted while modelling the background processes, such as electricity production, taking advantage of the availability of national and international databases containing the market average data.

Life Cycle Impact Assessment

Once the inventory is compiled and documented after the LCI, an impact assessment is performed considering the three main areas of protection, these being: human health, natural environment, and natural resource depletion. Life Cycle Impact Assessment (LCIA) is the stage in which indicators of environmental pressures are estimated in terms of selected impact categories that could be associated with the environmental interventions attributable to the life cycle of a product. Throughout impact assessment, the data collected within the inventory are translated into environmental impact scores, which should be firstly selected according to the stated goals of the study. In addition to the selection of impact category, the execution of two mandatory activities and three optional tasks is necessary in order to perform the impact assessment. These are:

- **Classification**. According to the data obtained from the LCI, the classification step consists of identifying environmental concerns suggested by the inventory analysis flows, assigning to each of the selected impact categories all the elementary flows that influence them.
- **Characterisation**. Characterization involves the quantification of the qualitatively assigned elementary flows in terms of a common unit for each category, with the objective of aggregating them as indicator results that describe the product environmental profile. The conversion factors reflect pressures per unit emission or resource consumed in the context of each impact category, thus facilitating a proper comparison in terms of single indicator. Characterization concerns also the selection of the perspective of interest between midpoint impacts, which are located somewhere along the cause-impact pathway, and endpoint impacts that allows reflecting damages at one of the three areas of protection.
- **Normalisation**. Normalisation is the process of calculating the magnitude of category indicators relative to reference information. It has been argued that this could be a necessary step to gain further insights and help decision-makers avoid decision mistakes caused by a lack of knowledge.

	• **Grouping**. Impact categories can be aggregated with category indicators, which can then be ranked and stored. The procedure is regarded as highly subjective and, consequently, the retrieved recommendations could be inconsistent. • **Weighting**. Weighting is a process that involves the modification of the results of category indicators according to their relative importance. This modification is achieved by the application of a weighting factor that is based on value judgements (and, therefore, is not suggested). Finally, it is important to emphasise that several LCIA methodologies are currently available on the market (such as ReCiPe, TRACI, CML) and ISO does not specify any recommendation of these. Therefore, the selection of both impact categories and impact assessment method is contingent upon the objectives of the study and, to a greater extent, the geographic area of interest. It should be noted that most impact assessment methodologies are predominantly associated with the European region and the United States.
Life Cycle Interpretation	Life cycle interpretation is the final phase of the LCA, during which the results from the inventory analysis and impact assessment are discussed in relation to the objectives that were previously defined, with the aim of developing appropriate recommendations according to the conclusions that were reached. It is imperative that the interpretation procedures are subject to a critical review of the results of the analysis and an appropriate evaluation of their sensitivity, consistency (particularly regarding the assumptions and methods selected) and completeness. This is essential to ensure that the suggestions made, or any conclusions drawn from a given comparison are valid and consistent with the purpose of the study performed.

LCIA Method

Concerning impact categories selection and LCIA methods, The International Reference Life Cycle Data System (ILCD) Handbook [209] provides a list of environmental categories and respective assessment methods on a global perspective. The main indicators recommended by the EC-JRC [210] are listed in **Table 33**, alongside the level of recommendation assigned to each of them. However, these recommendations were developed in the early stage of the European project for a common framework on LCA and, therefore, it is more appropriate to refer to sector-specific guidelines or expert opinion to select indicators and methodologies consistent with the goal and scope of the performed assessment.

Table 33 Impact categories recommended for mid-point assessment according to the EC-JRC [210].

Impact Category	Indicator	Unit of Measure	Description	Recommendation Level
Climate Change	GWP 100	kg CO_2 eq.	Estimation of the contribution of climate-altering gases to the increase	I

			in the mean global temperature over a period of 100 years	
Ozone Depletion	ODP	kg CFC-11 eq.	Estimate of the impact of emissions on the degradation of the stratospheric ozone layer, which is mainly caused by chlorofluorocarbon (CFCs)	I
Particulate Matter and Inorganic Substances	–	Kg $PM_{2.5}$ eq.	Estimation of adverse impacts on human health caused by the dispersion of particulate matter and its inorganic precursors	I
Ionizing Radiation – Human Health Effects	-	kg U^{235} eq.	Estimation of human health effects caused by exposure to radioactive substances	II
Photochemical Ozone Formation	–	Kg NMVOC eq.	Estimation of potential tropospheric ozone formation by photo-oxidation of volatile organic compounds (VOCs) of non-methane nature	II
Acidification	AP	mol H^+ eq.	Estimation of environmental consequences caused by the dispersion of acidifying substances into air, soil, and watersheds	II
Eutrophication – Terrestrial, Freshwater, and Marine	EP	mol N eq. kg P eq. kg N eq.	Estimation of nutrient accumulation in soils and water bodies, causing overgrowth of vegetation and subsequent depletion of oxygen resources	II
Human Toxicity – Carcinogenic and Non-Carcinogenic Effects	–	Comparative Toxic Unit for humans (CTU_h)	Estimation of adverse human health consequences caused by airborne, dietary or dermal intake of toxic substances of carcinogenic or non-carcinogenic nature	II/III
Resource Depletion – Mineral and Fossil	AD	kg Sb eq.	Estimated consumption of mineral and fossil resources	II
Water Resource Depletion	WS	m^3 water eq.	Estimation of water resource consumption	III

Land Use	LU	–	Estimation of land transformation and occupation by human activities	III
Ecotoxicity	–	Comparative Toxic Unit for ecosystems (CTU_e)	Estimated impacts of toxic nature on the ecosystem considered of species and functions	II/III

Concerning with recommendation levels, these are described as follows: level I for *recommended and sufficient* categories, level II for *recommended but for which improvement is required* and level III for *recommended but to be applied with caution*.

LCA for the Energy System

As mentioned, LCA is a globally recognised methodology that employs a holistic approach to evaluate the environmental impacts associated with the entire life cycle of a product or service and facilitates the identification of significant sources of impact, thereby enabling the formulation of sustainable strategies to mitigate adverse outcomes. The recourse to LCA is essential to detect and avert the rise of burden shifts throughout the value chain, a phenomenon which occurs when an action which reduces the environmental impact of a product or a process in one part of its life cycle (or in one impact category) unintentionally increases impacts in other areas. Recognising the need to identify a trade-off that goes beyond the techno-economic performance of a process and effectively assess the externalities related to its deployment, our research group has consistently integrated LCA in studies related to the decarbonisation of the energy system. This is indeed a priority, driven by EU targets of achieving carbon neutrality by 2050 and reducing greenhouse gas (GHG) emissions by 55% by 2030 [13] and, to this end, Power-to-Gas (PtG) technologies and Carbon Capture Utilisation and Storage (CCUS) have been proposed to complement the deployment of renewables [18]. Within this context, our research group performed LCA studies to thoroughly address the environmental implication of these pathways, with the investigation performed by Bellocchi et al. [65] aimed at examining the impact of the hydrogen-blending in the Italian natural gas grid, and the one of Facchino et al. [128] devoted to a comparative assessment of CCUS routes in Italy and Poland. Both studies represent a significant contribution of our research group, as they demonstrated that a detailed scenario modelling coupled with a comprehensive assessment is essential to detect critical shifts in burden. Besides, the outcomes of both investigations showed that though the integration of renewable energies and alternative fuels are effective in driving GHGs reduction, their introduction is likely to shifts pressure into resource and toxicity categories, sparce through the value chain. These analyses confirmed the validity of our approach and established the need to identify the synergies and trade-offs of decarbonisation measures to effectively guide decision-making processes. An overview of the studies is reported in **Table 34** and **Table 35**.

Table 34 Hydrogen Blending in the Italian Natural Gas Grid: Scenario Analysis and LCA [65].

Goal Definition	The primary goal was to evaluate the environmental impact of injecting hydrogen derived from renewable sources into the Italian gas grid in the context of ambitious renewable energy targets. More specifically, the objective was to quantify the obtainable benefits in terms of CO_2 emission reduction resulting from blending up to 20 vol.% hydrogen produced by means of Proton Electrolyte Membrane (PEM) electrolysers fed with renewable electricity. Three scenario cases were defined for the Italian energy system: • BASELINE (2019). The current grid mix with 31.6 GW i-RES and existing fossil plants. • MID-SCENARIO. A high-renewables future with 158.2 GW total i-RES and green hydrogen injection up to 20% molar in the gas grid. • END-SCENARIO. The maximum technical potential, with 272.1 GW RES correspondingly larger hydrogen production and grid blending.
Scope Definition	The system was analysed with respect to the production of 1 TWh of gross national electricity in Italy. The product system was analysed as a cradle-to-gate electricity supply, including fuel extraction, plant construction, operation, and electricity generation mix (including imports). Secondary markets for renewables and electrolysers included whereas the implication of electricity use were outside of the scope. The energy system was modelled through EnergyPLAN calibrated to 2019 Italy, ecoinvent 3.8 was used for background data while electrolyser and storage parameters from literature and hourly demand profiles from previous studies. Key categories analysed were Global Warming Potential ($CO_{2,eq}$), Stratospheric Ozone Depletion, $PM_{2.5}$ formation, Photochemical Ozone Formation (Human Health), Acidification, Freshwater and Marine Eutrophication, Fossil Resource Scarcity (kg oil-eq), and Mineral Resource Scarcity (kg Cu-eq). The analysis assumed hydrogen injection as part of the energy vector and there were therefore no co-products beyond electricity. All life-cycle stages above 1% contribution were included, following ILCD guidelines. Small auxiliary processes were neglected due to literature evidence of minor impact.
Impact Assessment Method	ReCiPe 2016 (H) mid-point
Results	The LCA showed substantial reductions in climate and resource impacts under high-renewable scenarios. For the electricity generation mix, global warming impact falled by ~57% in the MID-

	SCENARIO and ~66% in the END-SCENARIO relative to 2019. Most midpoint impacts declined markedly with more hydrogen and renewables (e.g. acidification –20%, fine PM –24% from base to end). A notable trade-off is Fossil Resource Scarcity, which decreased of 77%, reflecting the replacement of gas and especially coal. Conversely, mineral resource scarcity increased due to the materials for solar photovoltaic, wind, and electrolysers.
Interpretation	The results demonstrate a clear GHG mitigation benefit of hydrogen blending and renewable expansion confirming that green hydrogen, derived from surplus renewable electricity, can effectively decarbonize Italy's energy system, especially at high renewable penetration. However, significant burden shifts are evident and are referred to the surge in mineral resource demand driven by the resource-intensive nature of both i-RES and electrolysers and outlining the need to find suitable strategies to mitigate these issues.

Table 35 The Environmental Impacts of Carbon Capture Utilization and Storage on the Electricity Sector: A Life Cycle Assessment Comparison between Italy and Poland [128].

Goal Definition	The main objective was to investigate the environmental impacts rising from the retrofitting of a Natural Gas Combined Cycle (NGCC) power plant in a CCUS framework. The study entailed two possible routes, these being: • CO_2 capture and underground storage under supercritical conditions • CO_2 capture and conversion into Dimethyl Ether (DME) and CO_2 underground storage Both routes were benchmarked against a reference without capture, considering the specific context of the country in question (Italian vs Polish electricity mixes). The aim was to determine the impact of adding CCS or CCUS on the life cycle of electricity produced by the NGCC and DME production, to inform decarbonisation strategies and avoid burden shifting between categories.
Scope Definition	• In case of the CCS scenario, the functional unit was established as 1 kWh of high-voltage electricity generated through an NGCC plant. • In case of the CCUS scenario, the functional unit was established as 1 kWh of high-voltage electricity and 0.55 kg of dimethyl ether produced. These functional units were chosen to reflect the multifunctional nature of CCUS systems (electricity and chemical production) and ensure comparability between scenarios, consistently with ISO 14040/44 and prior LCA studies on similar topics. The study adopts a gate-to-gate system boundary, encompassing: • Natural gas extraction, transport, and combustion in NGCC. • Operation of CO_2 capture (post-combustion, with MDEA solvent). • Compression, transport, and underground storage of CO_2. • Production of dimethyl ether and hydrogen (for CCUS route). • Production of renewable electricity used in CCUS processes. The construction and end-of-life of plants were excluded due to lack of reliable data, as well as the long-term monitoring and maintenance of storage sites. In both Italy and Poland, the same system boundaries were applied to ensure comparability. ecoinvent v3.8 database was used for background flows while core process inventories derived from Aspen Plus simulations and literature (e.g. coal/gas composition, solvent data). Country-specific electricity and gas supply mixes were adjusted to 2020 statistics. The study evaluated environmental impacts in the following categories, selected for their relevance to the energy sector and CCUS technologies, following EC-JRC and literature guidelines: • Global Warming Potential (GWP, kg $CO_{2,eq}$), core mitigation target. • Abiotic Depletion (fossil fuels, MJ) reflects resource use.

- Acidification Potential (AP, kg $SO_{2,eq}$), important for air quality.
- Eutrophication Potential (EP, kg $PO_{4,eq}$), nutrient pollution.
- Ozone Depletion Potential (ODP, kg CFC-11-eq), stratospheric ozone.

The choice of these categories was aimed at capturing both intended benefits (GWP) and unintended burdens (others). The CML baseline method was used, given its widely application in European LCA studies and alignment with the selected impact categories and regional data.

The study addressed multifunctionality (electricity and dimethyl ether production) by system expansion, consistent with ISO standards. The CCUS scenario included avoided burdens from conventional DME production.

Processes contributing less than 1% of mass, energy, or environmental burden were excluded, ensuring focus on significant contributors.

Impact Assessment Method	CML Baseline 2016 method (Institute of Environmental Sciences, Leiden)
Results	Adding CCS to the NGCC plant led to dramatic GWP benefits but notable trade-offs in other impacts. In Italy, on a per-kWh basis, the reference plant emits about 0.715 kg $CO_{2,eq}$, while the NGCC coupled with CCS had a GWP of 0.076 kg $CO_{2,eq}$ (~89% reduction). In Poland the corresponding drop was from 0.695 to 0.021 kg (~97% reduction) due to the cleaner electricity mix in Italy's grid. On the other hand, when the captured CO_2 was used for DME (CCUS), the GWP reduction resulted to be smaller, with emissions of 0.303 kg $CO_{2,eq}$ per kWh in Italy and 0.236 kg $CO_{2,eq}$ per kWh (Poland) (~58% and ~68% below the reference). All other studied impacts increase when CCS/CCUS is implemented. For example, AD rose by 67% in Italy (66% in Poland) for both CCS and CCUS scenarios, because the energy penalty of capture requires more fuel. Similarly, Ozone Depletion (g CFC-11-eq) increases by ~74–75% due to solvent losses and added electricity consumption. AP and EP also worsened (though confidence for these categories was low).

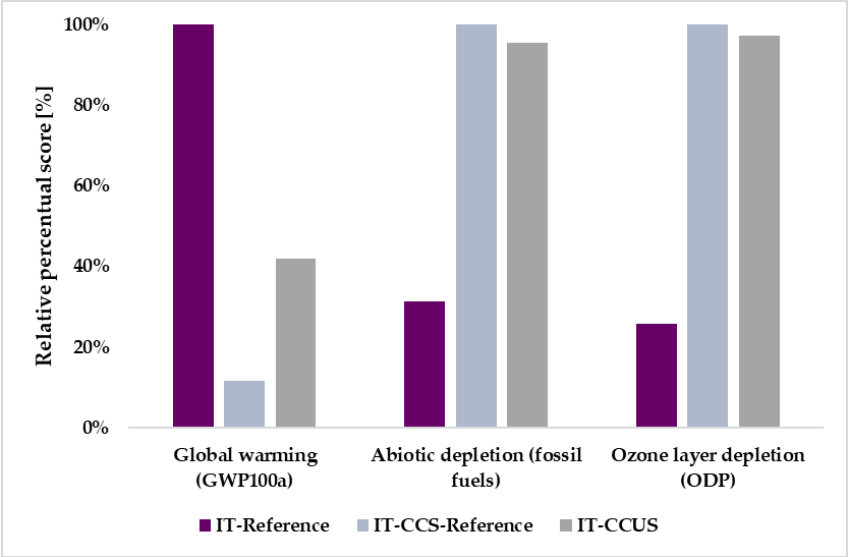

Figure 21 Impact categories scores for the Italian case study in CCUS scenario considering a comparable CCS reference scenario.

Interpretation	The CCS scenario achieves the largest GWP reduction (~89% in Italy and ~97% in Poland), while CCUS achieves lower reductions (~58% and ~68%, respectively). Both scenarios exhibited significant increases in other impact categories due to higher energy and material demands, particularly from natural gas extraction, solvent production, and renewable energy inputs. The results highlighted the severe risk of burden shifting, since while GHG emissions decrease substantially, impacts like acidification and resource depletion increased markedly. Scenario analysis showed that renewable electricity is better allocated to displace fossil-based electricity than to produce hydrogen for CCUS in terms of GWP reduction.

The above reported LCA studies, though dealing with different systems, consistently illustrate burden-shifting phenomena in the path to decarbonization. Both studies show tangible climate benefits from the proposed technologies, with hydrogen blending bringing substantial reduction in the national electricity GHGs emissions and CCUS abating roughly 90–97% of plant emissions. However, each study also warns that other impact categories suffer. In Bellocchi et al. [65], we demonstrated that the mineral depletion category triples due to the need for metals and silicon in large solar photovoltaic, wind, and electrolyser fleets. In Facchino et al. [128], we showed that adding CCS/CCUS roughly doubles fossil depletion and ozone depletion impacts. Methodologically, the studies adopted either a national energy-system perspective or a process-engineering perspective, comparing plant-level options in two national contexts. Yet, both studies pointed to the same insight: achieving massive CO_2 abatement often incurs trade-offs (resource demand, energy use for capture) and there is therefore the urgent need to spread the adoption of LCA to ensure that EU decarbonization pathways are evaluated holistically, so that one environmental benefit does not mask another burden.

Synthetic Natural Gas (SNG) Grid Requirements

Synthetic natural gas (SNG) has gained significant attention as an energy storage pathway throughout Europe. In Italy, the regulatory framework has been slightly modified in recent times to pave the way for the injection of both biomethane and SNG into the gas grid [211]. The Italian Ministerial Decree of 18 May 2018 updated the technical standards for gas quality to allow for the injection of biomethane, thereby ensuring that SNG meets the necessary safety and interchangeability requirements. SNG can therefore be supplied to the existing gas infrastructure for use in domestic and industrial applications, or as vehicle fuel (compressed natural gas, CNG), via existing CNG stations. The introduction of biomethane, SNG, and the expansion of the Liquefied Natural Gas (LNG) purchases made it necessary to establish more stringent and comprehensive quality specifications to ensure that the gas handled within the grid is compatible with the existing infrastructure and end-use devices [212]. The present annex provides a brief overview of the technical specifications that SNG must satisfy in the Italian context, covering legislative standards, gas quality parameters, and purification processes to be considered to ensure compliance. As discussed in **Section 1.2**., the Wobbe Index (WI) is the primary metric to be assess for the evaluation of interchangeability with pipeline-quality NG, as it reflects the combined effects of gas composition and density on heat delivery [186,187]. However, the injection of any SNG produced via CO_2 methanation into the NG grid is contingent upon the satisfaction of stringent quality and injection requirements, listed in **Table 36**.

Table 36 Standards for SNG injection [72].

Parameter	Technical Code	UNI EN 16726 grid
Higher Heating Value (HHV) [MJ Sm^{-3}]	34.95-45.28	n.s.
Specific Gravity	0.555-0.7	0.555-0.7
Wobbe Index [MJ Sm^{-3}]	47.31-52.33	47.31-52.33
Water Dew Point [°C]	≤ -5	≤ -8
Gas Composition	• O_2 lower than 6 mol.% • CO_2 lower than 2.5 mol.% • H_2 lower than 2 mol.% • H_2S lower than 5 mg Sm^{-3}	• O_2 lower than 6 mol.% • CO_2 lower than 2.5 mol.% • H_2 lower than 0.5 mol.% • H_2S lower than 5 mg Sm^{-3}

The HHV is defined as the amount of heat released by the complete combustion with oxygen of a specific amount of gas, such that the pressure at which the reaction takes place remains constant, and all products of combustion are restored to the same specific temperature as the reactants. It differs from the Lower Heating Value (LHV) in that this parameter considers the amount of heat resulting from the condensation of water at the reference temperature, while the remaining products remain in the gaseous state. Alongside the specific gravity (defined as the ratio between the gas density and dry air at reference temperature and composition), these are measured in accordance with UNI EN ISO 6976. Water Dew Point and gas composition are measured in accordance with UNI EN ISO 14532.

The injection of the produced SNG into the national gas grid mandates the implementation of specific conditioning steps downstream of the methanation reactor to ensure compliance with grid specifications. Among these:

- **Cooling and Dehydration** The water content in SNG is a crucial factor to deal with prior to the injection into the grid, as it is strictly regulated from the gas quality standards[7]. Pipelines must be free of excessive moisture and heavy hydrocarbons to prevent condensation. The presence of water in the gas stream could in fact lead to severe issues related to the formation of hydrates and cause blockages throughout the pipelines. Beyond threshold concentrations of water could also negatively affect the quality, value and effectiveness of SNG by lowering its calorific value, increasing transportation and distributions costs, and damaging some components of the final user processes. Furthermore, given the presence of acidic gases, an increase in water content is likely to prompt corrosion phenomena [189,213,214].
- **Impurities Polishing**. Impurities such as CO_2, CO and hydrogen could influence the resulting WI for the SNG stream. Therefore, should their concentration exceed the threshold limits set for the dedicate infrastructure, a proper treatment has to be included to abate their concentration in the product stream. Other strategies could be applied as well, spanning from membrane separation to PSA for CO_2 and hydrogen handling [159]. As for the case investigated in **Chapter 3**, it should be noted that the main objective is that of maximising CO_2 conversion by the multi-CECU process, and none of these purification processes has been considered as assumed to be redundant. On the other hand, a dedicated hydrogen removal process is mostly necessary in all PtM plants, both to recover the unreacted portion (therefore decreasing the related operating expenditures) and to attain grid specification. Nonetheless, it should be noted that the limit in hydrogen concentration is highly country dependant (some European countries allow up to 10 vol.% hydrogen content) and are also subject to continued scrutiny to foster the implementation of an hydrogen economy (see **Section 1.2**).
- **Compression and Injection**. NG transportation in Italy is usually made through a network of high-pressure pipelines for national distribution and most of the grid is controlled and operated by Snam, as it is the major national Transmission System Operator (TSO). Snam infrastructure is made up of high-pressure transmission lines aimed at supplying medium- and low-pressure distribution networks. Strategic interconnection points, such as the Trans Adriatic Pipeline (TAP), delivering gas from the Caspian region to Italy, operates at different pressures along its route, with the onshore

[7] Pipeline quality standards could slightly differ for the different gas networks in Europe based on climate and geographic-specific features. For instance, NG dehydration is more essential in case of colder climates where the occurrence of hydrates formation could be more frequent.

segments utilising 48-inch pipes that function at 95 bar and the offshore segments employing 36-inch pipes that function at 145 bar. The GreenStream pipeline, which connects North Africa to Sicily, has been engineered to withstand even higher pressures, with a maximum allowable operating pressure of 212 bar. The pressure regime in the Italian transmission grid typically spans 50-75 bar, with regional pipelines such as the Poggio Renatico–Cremona line operating specifically at 75 bar (Snam Rete Gas, Technical Data Sheet, 2021) [212].

Bibliography

[1] H. Liu, I. Khan, A. Zakari, M. Alharthi, Roles of trilemma in the world energy sector and transition towards sustainable energy: A study of economic growth and the environment, Energy Policy 170 (2022) 113238. https://doi.org/10.1016/J.ENPOL.2022.113238.

[2] L. Marti, R. Puertas, Sustainable energy development analysis: Energy Trilemma, Sustainable Technology and Entrepreneurship 1 (2022) 100007. https://doi.org/https://doi.org/10.1016/j.stae.2022.100007.

[3] Global Carbon Budget Project, Global Carbon Budget, 2024. https://globalcarbonbudget.org/ (accessed September 26, 2025).

[4] J.R. Fleming, Joseph Fourier, the 'greenhouse effect', and the quest for a universal theory of terrestrial temperatures, Endeavour 23 (1999) 72–75. https://doi.org/10.1016/S0160-9327(99)01210-7.

[5] J. Tyndall, XXVII. On radiation through the earth's atmosphere, The London, Edinburgh, and Dublin Philosophical Magazine and Journal of Science 25 (1863) 200–206. https://doi.org/10.1080/14786446308643443.

[6] S. Arrhenius, XXXI. On the influence of carbonic acid in the air upon the temperature of the ground, The London, Edinburgh, and Dublin Philosophical Magazine and Journal of Science 41 (1896) 237–276. https://doi.org/10.1080/14786449608620846.

[7] T.M.L. Wigley, P.D. Jones, Detecting CO2-induced climatic change, Nature 292 (1981) 205–208. https://doi.org/10.1038/292205a0.

[8] G.J.J. and J.J.E. J.T. Houghton, The IPCC Scientific Assessment (1990), 1990.

[9] P. Šprajc, M. Bjegović, B. Vasić, Energy security in decision making and governance - Methodological analysis of energy trilemma index, Renewable and Sustainable Energy Reviews 114 (2019) 109341. https://doi.org/https://doi.org/10.1016/j.rser.2019.109341.

[10] United Nations Framework Convention on Climate Change (UNFCCC), The Paris Agreement, 2016.

[11] European Commission, Communication from The Commission to The European Parliament, The European Council, the Council, The European Economic and Social Committee and The Committee of The Regions "The European Green Deal," (2019).

[12] The European Parliament, Regulation (EU) 2021/1119 Of The European Parliament and of The Council of 30 June 2021 establishing the framework for achieving climate neutrality and amending

Regulations (EC) No 401/2009 and (EU) 2018/1999 ('European Climate Law'), Official Journal of the European Union (2021).

[13] European Commission, Communication from the Commission to the European Parliament, the European Council, the Council, the European Economic and Social Committee and the Committee of The Regions "REPowerEU Plan," (2022).

[14] M. Tommasi, S.N. Degerli, G. Ramis, I. Rossetti, Advancements in CO2 methanation: A comprehensive review of catalysis, reactor design and process optimization, Chemical Engineering Research and Design 201 (2024) 457–482. https://doi.org/10.1016/J.CHERD.2023.11.060.

[15] J. Twitchell, K. DeSomber, D. Bhatnagar, Defining long duration energy storage, J Energy Storage 60 (2023) 105787. https://doi.org/10.1016/J.EST.2022.105787.

[16] G. Liu, T. Guo, P. Wang, H. Jiang, H. Wang, X. Zhao, X. Wei, Y. Xu, Economic analysis of hydrogen energy systems: A global perspective, Heliyon 10 (2024) e36219. https://doi.org/10.1016/J.HELIYON.2024.E36219.

[17] S. Bellocchi, M. De Falco, M. Gambini, M. Manno, T. Stilo, M. Vellini, Opportunities for power-to-Gas and Power-to-liquid in CO2-reduced energy scenarios: The Italian case, Energy 175 (2019) 847–861. https://doi.org/10.1016/J.ENERGY.2019.03.116.

[18] International Energy Agency (IEA), About CCUS, Paris, 2021. https://www.iea.org/reports/about-ccus (accessed August 5, 2022).

[19] I. Majchrzak-Kucęba, P. Szymanek, CCU Technologies in the Green Economy, Engineering and Protection of Environment 21 (2018) 261–271. https://doi.org/10.17512/ios.2018.3.5.

[20] K. Ghaib, F.Z. Ben-Fares, Power-to-Methane: A state-of-the-art review, Renewable and Sustainable Energy Reviews 81 (2018) 433–446. https://doi.org/10.1016/J.RSER.2017.08.004.

[21] C. Mebrahtu, F. Krebs, S. Abate, S. Perathoner, G. Centi, R. Palkovits, Chapter 5 - CO2 Methanation: Principles and Challenges, in: S. Albonetti, S. Perathoner, E.A. Quadrelli (Eds.), Stud Surf Sci Catal, Elsevier, 2019: pp. 85–103. https://doi.org/https://doi.org/10.1016/B978-0-444-64127-4.00005-7.

[22] T. Schaaf, J. Grünig, M.R. Schuster, T. Rothenfluh, A. Orth, Methanation of CO2 - storage of renewable energy in a gas distribution system, Energy Sustain Soc 4 (2014) 2. https://doi.org/10.1186/s13705-014-0029-1.

[23] O.E. Medina, A.A. Amell, D. López, A. Santamaría, Comprehensive review of nickel-based catalysts advancements for CO2 methanation, Renewable and Sustainable Energy Reviews 207 (2025) 114926. https://doi.org/10.1016/J.RSER.2024.114926.

[24] J. Bremer, K.H.G. Rätze, K. Sundmacher, CO2 methanation: Optimal start-up control of a fixed-bed reactor for power-to-gas applications, AIChE Journal 63 (2017) 23–31. https://doi.org/https://doi.org/10.1002/aic.15496.

[25] D. Sun, D.S.A. Simakov, Thermal management of a Sabatier reactor for CO2 conversion into CH4: Simulation-based analysis, Journal of CO2 Utilization 21 (2017) 368–382. https://doi.org/10.1016/J.JCOU.2017.07.015.

[26] C. Tregambi, P. Bareschino, D.P. Hanak, E. Mancusi, F. Montagnaro, F. Pepe, Techno-economic assessment of a synthetic methane production process by hydrogenation of carbon dioxide from direct air capture, Int J Hydrogen Energy 48 (2023) 37594–37606. https://doi.org/10.1016/J.IJHYDENE.2023.06.289.

[27] R. De Paolis, V. Bernardini, L.G. Campana, M. V. Ermini, M. Verna, G. Raimondi, G. Spazzafumo, Techno-economic and climate finance assessment of a methanation plant with green hydrogen production and CO2 recycling in Italy, Int J Hydrogen Energy 137 (2025) 939–947. https://doi.org/10.1016/J.IJHYDENE.2024.07.137.

[28] M. De Falco, M. Capocelli, Process analysis and plant simulation in a sustainable economy, Stud Surf Sci Catal 179 (2020) 121–140. https://doi.org/10.1016/B978-0-444-64337-7.00008-2.

[29] C. Gürsan, V. de Gooyert, The systemic impact of a transition fuel: Does natural gas help or hinder the energy transition?, Renewable and Sustainable Energy Reviews 138 (2021) 110552. https://doi.org/10.1016/J.RSER.2020.110552.

[30] R. Viscardi, C. Bassano, G. Nigliaccio, P. Deiana, The potential of E-fuels as future fuels, Pianeta Idrogeno e Speciale Progetti ENEA (2021). https://doi.org/10.12910/EAI2021-022.

[31] O. Dybiński, Ł. Szabłowski, A. Martsinchyk, A. Szczęśniak, J. Milewski, A. Grzebielec, P. Shuhayeu, Overview of the e-Fuels Market, Projects, and the State of the Art of Production Facilities, Energies (Basel) 18 (2025). https://doi.org/10.3390/en18030552.

[32] M. Genovese, O. Corigliano, F. Piraino, P. Fragiacomo, E-fuels infrastructures for heavy-duty applications: Case study of a refueling facility based on green hydrogen, Int J Hydrogen Energy 144 (2025) 1367–1382. https://doi.org/10.1016/J.IJHYDENE.2025.03.423.

[33] H. Singh, C. Li, P. Cheng, X. Wang, Q. Liu, A critical review of technologies, costs, and projects for production of carbon-neutral liquid e-fuels from hydrogen and captured CO2, Energy Adv. 1 (2022) 580–605. https://doi.org/10.1039/D2YA00173J.

[34] M. Götz, J. Lefebvre, F. Mörs, A. McDaniel Koch, F. Graf, S. Bajohr, R. Reimert, T. Kolb, Renewable Power-to-Gas: A technological and economic review, Renew Energy 85 (2016) 1371–1390. https://doi.org/10.1016/J.RENENE.2015.07.066.

[35] J. Kopyscinski, T.J. Schildhauer, S.M.A. Biollaz, Production of synthetic natural gas (SNG) from coal and dry biomass – A technology review from 1950 to 2009, Fuel 89 (2010) 1763–1783. https://doi.org/10.1016/J.FUEL.2010.01.027.

[36] P. Sabatier, J.B. Senderens, Direct hydrogenation of oxides of carbon in presence of various finely divided metals, C. R. Acad. Sci. 134 (1902) 689 – 691. https://www.scopus.com/inward/record.uri?eid=2-s2.0-77952105813&partnerID=40&md5=cfd787e0597903bb49f1453613906cb2.

[37] B.C. Brodie, II. Note on the synthesis of marsh-gas and formic acid, and on the electric decomposition of carbonic oxide, Proceedings of the Royal Society of London 21 (1997) 245–247. https://doi.org/10.1098/rspl.1872.0052.

[38] J. Kopyscinski, T.J. Schildhauer, S.M.A. Biollaz, Production of synthetic natural gas (SNG) from coal and dry biomass – A technology review from 1950 to 2009, Fuel 89 (2010) 1763–1783. https://doi.org/10.1016/J.FUEL.2010.01.027.

[39] S. Rönsch, J. Schneider, S. Matthischke, M. Schlüter, M. Götz, J. Lefebvre, P. Prabhakaran, S. Bajohr, Review on methanation – From fundamentals to current projects, Fuel 166 (2016) 276–296. https://doi.org/https://doi.org/10.1016/j.fuel.2015.10.111.

[40] M. Bailera, P. Lisbona, L.M. Romeo, S. Espatolero, Power to Gas projects review: Lab, pilot and demo plants for storing renewable energy and CO2, Renewable and Sustainable Energy Reviews 69 (2017) 292–312. https://doi.org/10.1016/J.RSER.2016.11.130.

[41] L. Mazzeo, A. Signorini, G. Lembo, I. Bavasso, L. Di Palma, V. Piemonte, In Situ Bio-Methanation Modelling of a Randomly Packed Gas Stirred Tank Reactor (GSTR), Processes 9 (2021). https://doi.org/10.3390/pr9050846.

[42] M. Steurer, U. Fahl, A. Voß, P. Deane, Curtailment: An Option for Cost-Efficient Integration of Variable Renewable Generation?, Europe's Energy Transition: Insights for Policy Making (2017) 97–104. https://doi.org/10.1016/B978-0-12-809806-6.00015-8.

[43] M.K. Khan, M. Raza, M. Shahbaz, U. Farooq, M.U. Akram, Recent advancement in energy storage technologies and their applications, J Energy Storage 92 (2024) 112112. https://doi.org/10.1016/J.EST.2024.112112.

[44] M.E. Ölmez, I. Ari, G. Tuzkaya, A comprehensive review of the impacts of energy storage on power markets, J Energy Storage 91 (2024) 111935. https://doi.org/10.1016/J.EST.2024.111935.

[45] J.O. Bockris, Hydrogen, Materials 4 (2011) 2073–2091. https://doi.org/10.3390/ma4122073.

[46] J.O.M. Bockris, The hydrogen economy: Its history, Int J Hydrogen Energy 38 (2013) 2579–2588. https://doi.org/10.1016/J.IJHYDENE.2012.12.026.

[47] International Energy Agency (IEA), Global Hydrogen Review 2024, Paris, 2024. https://www.iea.org/reports/global-hydrogen-review-2024 (accessed July 14, 2025).

[48] D. De Cata, L. Mazzeo, V. Piemonte, A. Giaconia, Electrified steam methane reforming as efficient pathway for sustainable hydrogen production and industrial decarbonization: A critical review, Int J Hydrogen Energy 105 (2025) 31–44. https://doi.org/10.1016/J.IJHYDENE.2025.01.202.

[49] International Renewable Energy Agency, Green Hydrogen Cost Reduction: Scaling Up Electrolyseres To Meet The 1.5°C Climate Goal, 2020. www.irena.org/publications.

[50] L. Vidas, R. Castro, Recent Developments on Hydrogen Production Technologies: State-of-the-Art Review with a Focus on Green-Electrolysis, Applied Sciences 11 (2021). https://doi.org/10.3390/app112311363.

[51] P. Afanasev, A. Askarova, T. Alekhina, E. Popov, S. Markovic, A. Mukhametdinova, A. Cheremisin, E. Mukhina, An overview of hydrogen production methods: Focus on hydrocarbon feedstock, Int J Hydrogen Energy 78 (2024) 805–828. https://doi.org/10.1016/J.IJHYDENE.2024.06.369.

[52] B.S. Zainal, P.J. Ker, H. Mohamed, H.C. Ong, I.M.R. Fattah, S.M.A. Rahman, L.D. Nghiem, T.M.I. Mahlia, Recent advancement and assessment of green hydrogen production technologies, Renewable and Sustainable Energy Reviews 189 (2024) 113941. https://doi.org/10.1016/J.RSER.2023.113941.

[53] M. Capocelli, M. De Falco, Enriched Methane: A Ready Solution for the Transition Towards the Hydrogen Economy, in: M. De Falco, A. Basile (Eds.), Enriched Methane: The First Step Towards the Hydrogen Economy, Springer International Publishing, Cham, 2016: pp. 1–21. https://doi.org/10.1007/978-3-319-22192-2_1.

[54] S. Bellocchi, M. De Falco, M. Facchino, M. Manno, Hydrogen blending in Italian natural gas grid: Scenario analysis and LCA, J Clean Prod 416 (2023) 137809. https://doi.org/10.1016/J.JCLEPRO.2023.137809.

[55] J. Gao, Y. Wang, Y. Ping, D. Hu, G. Xu, F. Gu, F. Su, A thermodynamic analysis of methanation reactions of carbon oxides for the production of synthetic natural gas, RSC Adv 2 (2012) 2358–2368. https://doi.org/10.1039/C2RA00632D.

[56] M.A. Vannice, The Catalytic Synthesis of Hydrocarbons from Carbon Monoxide and Hydrogen, Catalysis Reviews 14 (1976) 153–191. https://doi.org/10.1080/03602457608073410.

[57] L. Zhang, Z. Li, Y. Gao, Q. Li, Z. Deng, B. Miao, H. He, C.K. Poh, L. Zhang, S.H. Chan, Recent advances in supported metal catalysts for CO2 methanation: mechanisms, materials design, and the promise of perovskite-based supports, Energy Conversion and Management: X 27 (2025) 101066. https://doi.org/10.1016/J.ECMX.2025.101066.

[58] G. Garbarino, D. Bellotti, P. Riani, L. Magistri, G. Busca, Methanation of carbon dioxide on Ru/Al2O3 and Ni/Al2O3 catalysts at atmospheric pressure: Catalysts activation, behaviour and stability, Int J Hydrogen Energy 40 (2015) 9171–9182. https://doi.org/10.1016/J.IJHYDENE.2015.05.059.

[59] L. Falbo, M. Martinelli, C.G. Visconti, L. Lietti, C. Bassano, P. Deiana, Kinetics of CO2 methanation on a Ru-based catalyst at process conditions relevant for Power-to-Gas applications, Appl Catal B 225 (2018) 354–363. https://doi.org/10.1016/J.APCATB.2017.11.066.

[60] R.-Y. Chein, C.-C. Wang, Experimental Study on CO2 Methanation over Ni/Al2O3, Ru/Al2O3, and Ru-Ni/Al2O3 Catalysts, Catalysts 10 (2020). https://doi.org/10.3390/catal10101112.

[61] K. Stangeland, D.Y. Kalai, H. Li, Z. Yu, Active and stable Ni based catalysts and processes for biogas upgrading: The effect of temperature and initial methane concentration on CO2 methanation, Appl Energy 227 (2018) 206–212. https://doi.org/10.1016/J.APENERGY.2017.08.080.

[62] S. Kuhaudomlap, A. Srifa, W. Koo-Amornpattana, C. Fukuhara, S. Ratchahat, Insight and comprehensive study of Ni-based catalysts supported on various metal oxides for CO2 methanation, Sci Rep 14 (2024) 23149. https://doi.org/10.1038/s41598-024-73848-0.

[63] G. Zhou, H. Liu, K. Cui, A. Jia, G. Hu, Z. Jiao, Y. Liu, X. Zhang, Role of surface Ni and Ce species of Ni/CeO2 catalyst in CO2 methanation, Appl Surf Sci 383 (2016) 248–252. https://doi.org/10.1016/J.APSUSC.2016.04.180.

[64] M. V Konishcheva, D.I. Potemkin, S.D. Badmaev, P. V Snytnikov, E.A. Paukshtis, V.A. Sobyanin, V.N. Parmon, On the Mechanism of CO and CO2 Methanation Over Ni/CeO2 Catalysts, Top Catal 59 (2016) 1424–1430. https://doi.org/10.1007/s11244-016-0650-7.

[65] A. Cárdenas-Arenas, A. Quindimil, A. Davó-Quiñonero, E. Bailón-García, D. Lozano-Castelló, U. De-La-Torre, B. Pereda-Ayo, J.A. González-Marcos, J.R. González-Velasco, A. Bueno-López, Isotopic and in situ DRIFTS study of the CO2 methanation mechanism using Ni/CeO2 and Ni/Al2O3 catalysts, Appl Catal B 265 (2020) 118538. https://doi.org/10.1016/J.APCATB.2019.118538.

[66] M. Younas, L. Loong Kong, M.J.K. Bashir, H. Nadeem, A. Shehzad, S. Sethupathi, Recent Advancements, Fundamental Challenges, and Opportunities in Catalytic Methanation of CO2, Energy & Fuels 30 (2016) 8815–8831. https://doi.org/10.1021/acs.energyfuels.6b01723.

[67] J.A. Dumesic, G.W. Huber, M. Boudart, Principles of Heterogeneous Catalysis, in: Handbook of Heterogeneous Catalysis, 2008. https://doi.org/https://doi.org/10.1002/9783527610044.hetcat0001.

[68] S. Abate, K. Barbera, E. Giglio, F. Deorsola, S. Bensaid, S. Perathoner, R. Pirone, G. Centi, Synthesis, Characterization, and Activity Pattern of Ni–Al Hydrotalcite Catalysts in CO2 Methanation, Ind Eng Chem Res 55 (2016) 8299–8308. https://doi.org/10.1021/acs.iecr.6b01581.

[69] F. Song, Q. Zhong, Y. Yu, M. Shi, Y. Wu, J. Hu, Y. Song, Obtaining well-dispersed Ni/Al2O3 catalyst for CO2 methanation with a microwave-assisted method, Int J Hydrogen Energy 42 (2017) 4174–4183. https://doi.org/10.1016/J.IJHYDENE.2016.10.141.

[70] S. Wang, Q. Pan, J. Peng, T. Sun, D. Gao, S. Wang, CO2 methanation on Ni/Ce0.5Zr0.5O2 catalysts for the production of synthetic natural gas, Fuel Processing Technology 123 (2014) 166–171. https://doi.org/10.1016/J.FUPROC.2014.01.004.

[71] J. Ashok, M.L. Ang, S. Kawi, Enhanced activity of CO2 methanation over Ni/CeO2-ZrO2 catalysts: Influence of preparation methods, Catal Today 281 (2017) 304–311. https://doi.org/10.1016/J.CATTOD.2016.07.020.

[72] B. Miao, S.S.K. Ma, X. Wang, H. Su, S.H. Chan, Catalysis mechanisms of CO2 and CO methanation, Catal Sci Technol 6 (2016) 4048–4058. https://doi.org/10.1039/C6CY00478D.

[73] L. He, Q. Lin, Y. Liu, Y. Huang, Unique catalysis of Ni-Al hydrotalcite derived catalyst in CO2 methanation: cooperative effect between Ni nanoparticles and a basic support, Journal of Energy Chemistry 23 (2014) 587–592. https://doi.org/10.1016/S2095-4956(14)60144-3.

[74] C. Italiano, J. Llorca, L. Pino, M. Ferraro, V. Antonucci, A. Vita, CO and CO2 methanation over Ni catalysts supported on CeO2, Al2O3 and Y2O3 oxides, Appl Catal B 264 (2020) 118494. https://doi.org/10.1016/J.APCATB.2019.118494.

[75] A. Vita, C. Italiano, L. Pino, M. Laganà, M. Ferraro, V. Antonucci, High-temperature CO2 methanation over structured Ni/GDC catalysts: Performance and scale-up for Power-to-Gas application, Fuel Processing Technology 202 (2020) 106365. https://doi.org/10.1016/J.FUPROC.2020.106365.

[76] C. Italiano, G. Drago Ferrante, L. Pino, M. Laganà, M. Ferraro, V. Antonucci, A. Vita, Silicon carbide and alumina open-cell foams activated by Ni/CeO2-ZrO2 catalyst for CO2 methanation in a heat-exchanger reactor, Chemical Engineering Journal 434 (2022) 134685. https://doi.org/10.1016/J.CEJ.2022.134685.

[77] A.I. Tsiotsias, N.D. Charisiou, C. Italiano, G.D. Ferrante, L. Pino, A. Vita, V. Sebastian, S.J. Hinder, M.A. Baker, A. Sharan, N. Singh, K. Polychronopoulou, M.A. Goula, Ni-noble metal bimetallic catalysts for improved low temperature CO2 methanation, Appl Surf Sci 646 (2024) 158945. https://doi.org/10.1016/J.APSUSC.2023.158945.

[78] S. Specchia, C. Galletti, V. Specchia, Solution Combustion Synthesis as intriguing technique to quickly produce performing catalysts for specific applications, Stud Surf Sci Catal 175 (2010) 59–67. https://doi.org/10.1016/S0167-2991(10)75008-4.

[79] S. Specchia, C. Galletti, V. Specchia, Solution Combustion Synthesis as intriguing technique to quickly produce performing catalysts for specific applications, Stud Surf Sci Catal 175 (2010) 59–67. https://doi.org/10.1016/S0167-2991(10)75008-4.

[80] S. Specchia, G. Ercolino, S. Karimi, C. Italiano, A. Vita, Solution combustion synthesis for preparation of structured catalysts: A mini-review on process intensification for energy applications and pollution control, International Journal of Self-Propagating High-Temperature Synthesis 26 (2017) 166–186. https://doi.org/10.3103/S1061386217030062.

[81] A. Vita, C. Italiano, C. Fabiano, M. Laganà, L. Pino, Influence of Ce-precursor and fuel on structure and catalytic activity of combustion synthesized Ni/CeO2 catalysts for biogas oxidative steam reforming, Mater Chem Phys 163 (2015) 337–347. https://doi.org/10.1016/J.MATCHEMPHYS.2015.07.048.

[82] C. Italiano, A. Vita, C. Fabiano, M. Laganà, L. Pino, Bio-hydrogen production by oxidative steam reforming of biogas over nanocrystalline Ni/CeO2 catalysts, Int J Hydrogen Energy 40 (2015) 11823–11830. https://doi.org/10.1016/J.IJHYDENE.2015.04.146.

[83] A. Zhao, W. Ying, H. Zhang, H. Ma, D. Fang, Ni–Al2O3 catalysts prepared by solution combustion method for syngas methanation, Catal Commun 17 (2012) 34–38. https://doi.org/10.1016/J.CATCOM.2011.10.010.

[84] P. Summa, M. Gajewska, L. Li, C. Hu, B. Samojeden, M. Motak, P. Da Costa, Solution combustion synthesis as an alternative synthesis route for novel Ni-Mg-Al mixed-oxide catalyst for CO2 methanation, Journal of CO2 Utilization 60 (2022) 101983. https://doi.org/10.1016/J.JCOU.2022.101983.

[85] P. Summa, K. Świrk Da Costa, J. Gopakumar, B. Samojeden, M. Motak, M. Rønning, W. Van Beek, P. Da Costa, Optimization of Co-Ni-Mg-Al mixed-oxides CO2 methanation catalysts with solution combustion synthesis: On the importance of Co incorporation and basicity, Appl Mater Today 32 (2023) 101795. https://doi.org/10.1016/J.APMT.2023.101795.

[86] Y. He, D. Mao, Q. Guo, J. Yu, Ru/CeO2 catalyst derived from Ce-based MOF for highly efficient catalytic CO2 methanation integrated with renewable hydrogen, Fuel Processing Technology 259 (2024) 108101. https://doi.org/10.1016/J.FUPROC.2024.108101.

[87] S. Sharma, K.B. Sravan Kumar, Y.M. Chandnani, V.S. Phani Kumar, B.P. Gangwar, A. Singhal, P.A. Deshpande, Mechanistic Insights into CO2 Methanation over Ru-Substituted CeO2, The Journal of Physical Chemistry C 120 (2016) 14101–14112. https://doi.org/10.1021/acs.jpcc.6b03224.

[88] B. Agarski, V. Nikolić, Ž. Kamberović, Z. Anđić, B. Kosec, I. Budak, Comparative life cycle assessment of Ni-based catalyst synthesis processes, J Clean Prod 162 (2017) 7–15. https://doi.org/10.1016/J.JCLEPRO.2017.06.012.

[89] T. Kar, H.P. Veluswamy, To nip it or let it bloom: Life cycle assessment of lab-scale catalysts used in low-TRL CCUS technologies, Sustainable Chemistry for Climate Action 6 (2025) 100057. https://doi.org/10.1016/J.SCCA.2025.100057.

[90] R. Aromaa-Stubb, M. Rinne, M. Lundström, Life Cycle Assessment of Cobalt Catalyst Production and Recycling, Journal of Sustainable Metallurgy 10 (2024) 1795–1806. https://doi.org/10.1007/s40831-024-00897-0.

[91] M. Heberl, C. Withelm, A. Kaul, D. Rank, M. Sterner, Prospective Life Cycle Assessment of Biological Methanation in a Trickle-Bed Pilot Plant and a Potential Scale-Up, Energies (Basel) 17 (2024). https://doi.org/10.3390/en17092206.

[92] A. Navajas, T. Mendiara, L.M. Gandía, A. Abad, F. García-Labiano, L.F. de Diego, Life cycle assessment of power-to-methane systems with CO2 supplied by the chemical looping combustion of biomass, Energy Convers Manag 267 (2022) 115866. https://doi.org/10.1016/J.ENCONMAN.2022.115866.

[93] N. Gerloff, Comparative Life-Cycle Assessment Analysis of Power-to-Methane Plants Including Different Water Electrolysis Technologies and CO2 Sources While Applying Various Energy Scenarios, ACS Sustain Chem Eng 9 (2021) 10123–10141. https://doi.org/10.1021/acssuschemeng.1c02002.

[94] E. Vega Puga, G. Moumin, N.C. Neumann, M. Roeb, A. Ardone, C. Sattler, Holistic View on Synthetic Natural Gas Production: A Technical, Economic and Environmental Analysis, Energies (Basel) 15 (2022). https://doi.org/10.3390/en15051608.

[95] F. Federici, J. Puna, T.M. Mata, A.A. Martins, Life cycle analysis of a combined electrolysis and methanation reactor for methane production, Energy Reports 8 (2022) 554–560. https://doi.org/10.1016/J.EGYR.2022.01.042.

[96] X. Wang, M. Yang, X. Zhu, L. Zhu, S. Wang, Experimental study and life cycle assessment of CO2 methanation over biochar supported catalysts, Appl Energy 280 (2020) 115919. https://doi.org/10.1016/J.APENERGY.2020.115919.

[97] A. Sayyah, E. Mahmoudi, S. Farhoudi, G. Behmenyar, A.Z. Turan, S.R. Nabavi, A. Niaei, Environmental assessment of carbon dioxide methanation process using mixed metal oxide and zeolite-supported

catalysts by life cycle assessment methodology, J Clean Prod 362 (2022) 132529. https://doi.org/10.1016/J.JCLEPRO.2022.132529.

[98] A. Sayyah, M. Ahangari, J. Mostafaei, S.R. Nabavi, A. Niaei, Machine learning-based life cycle optimization for the carbon dioxide methanation process: Achieving environmental and productivity efficiency, J Clean Prod 426 (2023) 139120. https://doi.org/10.1016/J.JCLEPRO.2023.139120.

[99] The International Organization for Standardization (ISO), ISO 14044:2006 Environmental management - Life cycle assessment - Requirements and guidelines, (2006). https://www.iso.org/standard/38498.html (accessed July 5, 2023).

[100] The International Organization for Standardization (ISO), ISO 14040:2006 Environmental management - Life cycle assessment - Principles and framework, (2006). https://www.iso.org/standard/37456.html (accessed July 5, 2023).

[101] D. Ratthanapra, U. Suwanmanee, Life Cycle Assessment of Separation Methods of Cerium Oxide from Monazite Ore, Chem Eng Trans 74 (2019) 907–912. https://doi.org/10.3303/CET1974152.

[102] N. Sanchez, R. Ruiz, A. Rödl, M. Cobo, Life cycle inventory data for power production from sugarcane press-mud, Data Brief 37 (2021) 107194. https://doi.org/10.1016/J.DIB.2021.107194.

[103] A. Sayyah, M. Ahangari, J. Mostafaei, S.R. Nabavi, A. Niaei, Machine learning-based life cycle optimization for the carbon dioxide methanation process: Achieving environmental and productivity efficiency, J Clean Prod 426 (2023) 139120. https://doi.org/10.1016/J.JCLEPRO.2023.139120.

[104] A. Sayyah, E. Mahmoudi, S. Farhoudi, G. Behmenyar, A.Z. Turan, S.R. Nabavi, A. Niaei, Environmental assessment of carbon dioxide methanation process using mixed metal oxide and zeolite-supported catalysts by life cycle assessment methodology, J Clean Prod 362 (2022) 132529. https://doi.org/10.1016/J.JCLEPRO.2022.132529.

[105] M. Facchino, P. Popielak, M. Panowski, D. Wawrzyńczak, I. Majchrzak-Kucęba, M. De Falco, The Environmental Impacts of Carbon Capture Utilization and Storage on the Electricity Sector: A Life Cycle Assessment Comparison between Italy and Poland, Energies (Basel) 15 (2022). https://doi.org/10.3390/en15186809.

[106] M.A.J. Huijbregts, Z.J.N. Steinmann, P.M.F. Elshout, G. Stam, F. Verones, M. Vieira, M. Zijp, A. Hollander, R. van Zelm, ReCiPe2016: a harmonised life cycle impact assessment method at midpoint and endpoint level, Int J Life Cycle Assess 22 (2017) 138–147. https://doi.org/10.1007/s11367-016-1246-y.

[107] J.A. Onrubia-Calvo, A. Quindimil, A. Davó-Quiñonero, A. Bermejo-López, E. Bailón-García, B. Pereda-Ayo, D. Lozano-Castelló, J.A. González-Marcos, A. Bueno-López, J.R. González-Velasco, Kinetics, Model

Discrimination, and Parameters Estimation of CO2 Methanation on Highly Active Ni/CeO2 Catalyst, Ind Eng Chem Res 61 (2022) 10419–10435. https://doi.org/10.1021/acs.iecr.2c00164.

[108] A. Cárdenas-Arenas, A. Quindimil, A. Davó-Quiñonero, E. Bailón-García, D. Lozano-Castelló, U. De-La-Torre, B. Pereda-Ayo, J.A. González-Marcos, J.R. González-Velasco, A. Bueno-López, Design of active sites in Ni/CeO2 catalysts for the methanation of CO2: tailoring the Ni-CeO2 contact, Appl Mater Today 19 (2020) 100591. https://doi.org/10.1016/J.APMT.2020.100591.

[109] A. Alarcón, J. Guilera, R. Soto, T. Andreu, Higher tolerance to sulfur poisoning in CO2 methanation by the presence of CeO2, Appl Catal B 263 (2020) 118346. https://doi.org/10.1016/J.APCATB.2019.118346.

[110] D. Schlereth, O. Hinrichsen, A fixed-bed reactor modeling study on the methanation of CO2, Chemical Engineering Research and Design 92 (2014) 702–712. https://doi.org/10.1016/J.CHERD.2013.11.014.

[111] A. Bertino, L. Mazzeo, V. Piemonte, Shell and Tube Water-Cooled Reactor for Methanol Synthesis, Comprehensive Methanol Science: Production, Applications, and Emerging Technologies: First Edition, Volume 1-4 2 (2025) 461–494. https://doi.org/10.1016/B978-0-443-15740-0.00020-3.

[112] M. De Falco, M. Capocelli, A. Basile, Selective membrane application for the industrial one-step DME production process fed by CO2 rich streams: Modeling and simulation, Int J Hydrogen Energy 42 (2017) 6771–6786. https://doi.org/10.1016/J.IJHYDENE.2017.02.047.

[113] M. De Falco, M. Capocelli, A. Giannattasio, Membrane Reactor for one-step DME synthesis process: Industrial plant simulation and optimization, Journal of CO2 Utilization 22 (2017) 33–43. https://doi.org/10.1016/J.JCOU.2017.09.008.

[114] A. D'Ambrosio, M. Facchino, S. Tatarelli, V. Piemonte, M. Capocelli, M. De Falco, Carbon capture utilization through a novel multistage configuration for dimethyl ether synthesis, J Clean Prod 490 (2025) 144658. https://doi.org/10.1016/J.JCLEPRO.2025.144658.

[115] W.J. Lee, C. Li, H. Prajitno, J. Yoo, J. Patel, Y. Yang, S. Lim, Recent trend in thermal catalytic low temperature CO2 methanation: A critical review, Catal Today 368 (2021) 2–19. https://doi.org/10.1016/J.CATTOD.2020.02.017.

[116] K. Ghaib, K. Nitz, F.-Z. Ben-Fares, Chemical Methanation of CO2: A Review, ChemBioEng Reviews 3 (2016) 266–275. https://doi.org/https://doi.org/10.1002/cben.201600022.

[117] L. Kiewidt, J. Thöming, Predicting optimal temperature profiles in single-stage fixed-bed reactors for CO2-methanation, Chem Eng Sci 132 (2015) 59–71. https://doi.org/10.1016/J.CES.2015.03.068.

[118] M. Gruber, P. Weinbrecht, L. Biffar, S. Harth, D. Trimis, J. Brabandt, O. Posdziech, R. Blumentritt, Power-to-Gas through thermal integration of high-temperature steam electrolysis and carbon dioxide

methanation - Experimental results, Fuel Processing Technology 181 (2018) 61–74. https://doi.org/10.1016/J.FUPROC.2018.09.003.

[119] Store&Go, (n.d.). https://www.storeandgo.info/index.html (accessed March 17, 2023).

[120] R. Schlautmann, H. Böhm, A. Zauner, F. Mörs, R. Tichler, F. Graf, T. Kolb, Renewable Power-to-Gas: A Technical and Economic Evaluation of Three Demo Sites Within the STORE&GO Project, Chemie Ingenieur Technik 93 (2021) 568–579. https://doi.org/https://doi.org/10.1002/cite.202000187.

[121] C. Bassano, P. Deiana, L. Lietti, C.G. Visconti, P2G movable modular plant operation on synthetic methane production from CO2 and hydrogen from renewables sources, Fuel 253 (2019) 1071–1079. https://doi.org/10.1016/J.FUEL.2019.05.074.

[122] P. Deiana, L. Colelli, C. Bassano, Y. De Pra, G. Testa, N. Verdone, G. Vilardi, Power to Gas Pilot Plant for CO2 Methanation with a Ni-Based Catalyst, Ind Eng Chem Res 64 (2025) 3886–3901. https://doi.org/10.1021/acs.iecr.4c03289.

[123] G. Pintér, The development of global power-to-methane potentials between 2000 and 2020: A comparative overview of international projects, Appl Energy 353 (2024) 122094. https://doi.org/10.1016/J.APENERGY.2023.122094.

[124] European Biogas Association (EBA), Mapping e-methane plants and technologies, 2024. https://www.europeanbiogas.eu/mapping-e-methane-plants-and-technologies-2/ (accessed September 27, 2025).

[125] A.G. Dixon, An improved equation for the overall heat transfer coefficient in packed beds, Chemical Engineering and Processing: Process Intensification 35 (1996) 323–331. https://doi.org/10.1016/0255-2701(96)80012-2.

[126] M. De Falco, L. Di Paola, L. Marrelli, Heat transfer and hydrogen permeability in modelling industrial membrane reactors for methane steam reforming, Int J Hydrogen Energy 32 (2007) 2902–2913. https://doi.org/10.1016/J.IJHYDENE.2007.04.014.

[127] M. Gruber, D. Wiedmann, M. Haas, S. Harth, A. Loukou, D. Trimis, Insights into the catalytic CO2 methanation of a boiling water cooled fixed-bed reactor: Simulation-based analysis, Chemical Engineering Journal 406 (2021) 126788. https://doi.org/10.1016/J.CEJ.2020.126788.

[128] D. Sun, F.M. Khan, D.S.A. Simakov, Heat removal and catalyst deactivation in a Sabatier reactor for chemical fixation of CO2: Simulation-based analysis, Chemical Engineering Journal 329 (2017) 165–177. https://doi.org/10.1016/J.CEJ.2017.06.160.

[129] T. Tsuboi, S. Yasuda, C. Choi, W. Zhang, H. Machida, K. Norinaga, T. Yajima, Y. Kawajiri, Modeling and estimating kinetic parameters for CO2 methanation from fixed bed reactor experiments, J Adv Manuf Process 5 (2023) e10145. https://doi.org/https://doi.org/10.1002/amp2.10145.

[130] A. Krammer, K. Salbrechter, M. Lehner, High-capacity CO/CO2 methanation reactor design strategy based on 1D PFR modelling and experimental investigation, Journal of CO2 Utilization 80 (2024) 102661. https://doi.org/10.1016/J.JCOU.2023.102661.

[131] R.T. Zimmermann, J. Bremer, K. Sundmacher, Optimal catalyst particle design for flexible fixed-bed CO2 methanation reactors, Chemical Engineering Journal 387 (2020) 123704. https://doi.org/10.1016/J.CEJ.2019.123704.

[132] A. Perna, L. Moretti, G. Ficco, G. Spazzafumo, L. Canale, M. Dell'Isola, SNG Generation via Power to Gas Technology: Plant Design and Annual Performance Assessment, Applied Sciences 10 (2020). https://doi.org/10.3390/app10238443.

[133] S. Szima, C.-C. Cormos, CO2 Utilization Technologies: A Techno-Economic Analysis for Synthetic Natural Gas Production, Energies (Basel) 14 (2021). https://doi.org/10.3390/en14051258.

[134] F. Salomone, E. Giglio, D. Ferrero, M. Santarelli, R. Pirone, S. Bensaid, Techno-economic modelling of a Power-to-Gas system based on SOEC electrolysis and CO2 methanation in a RES-based electric grid, Chemical Engineering Journal 377 (2019) 120233. https://doi.org/10.1016/J.CEJ.2018.10.170.

[135] A. Tripodi, F. Conte, I. Rossetti, Carbon Dioxide Methanation: Design of a Fully Integrated Plant, Energy & Fuels 34 (2020) 7242–7256. https://doi.org/10.1021/acs.energyfuels.0c00580.

[136] C. Faria, C. Rocha, C. Miguel, A. Rodrigues, L.M. Madeira, Process intensification concepts for CO2 methanation – A review, Fuel 386 (2025) 134269. https://doi.org/10.1016/J.FUEL.2024.134269.

[137] P. Bareschino, G. Piso, F. Pepe, C. Tregambi, E. Mancusi, Numerical modelling of a sorption-enhanced methanation system, Chem Eng Sci 277 (2023) 118876. https://doi.org/10.1016/J.CES.2023.118876.

[138] L. Gómez, I. Martínez, M. V. Navarro, T. García, R. Murillo, Sorption-enhanced CO and CO2 methanation (SEM) for the production of high purity methane, Chemical Engineering Journal 440 (2022) 135842. https://doi.org/10.1016/J.CEJ.2022.135842.

[139] J. van Kampen, J. Boon, F. van Berkel, J. Vente, M. van Sint Annaland, Steam separation enhanced reactions: Review and outlook, Chemical Engineering Journal 374 (2019) 1286–1303. https://doi.org/10.1016/J.CEJ.2019.06.031.

[140] H. Ohya, J. Fun, H. Kawamura, K. Itoh, H. Ohashi, M. Aihara, S. Tanisho, Y. Negishi, Methanation of carbon dioxide by using membrane reactor integrated with water vapor permselective membrane and its analysis, J Memb Sci 131 (1997) 237–247. https://doi.org/10.1016/S0376-7388(97)00055-0.

[141] A. Catarina Faria, C. V Miguel, A.E. Rodrigues, L.M. Madeira, Modeling and Simulation of a Steam-Selective Membrane Reactor for Enhanced CO2 Methanation, Ind Eng Chem Res 59 (2020) 16170–16184. https://doi.org/10.1021/acs.iecr.0c02860.

[142] S.E. Hashemi, K.M. Lien, M. Hillestad, S.K. Schnell, B. Austbø, Thermodynamic Insight in Design of Methanation Reactor with Water Removal Considering Nexus between CO2 Conversion and Irreversibilities, Energies (Basel) 14 (2021). https://doi.org/10.3390/en14237861.

[143] J. Uebbing, L.K. Rihko-Struckmann, K. Sundmacher, Exergetic assessment of CO2 methanation processes for the chemical storage of renewable energies, Appl Energy 233–234 (2019) 271–282. https://doi.org/10.1016/J.APENERGY.2018.10.014.

[144] A. Fache, F. Marias, V. Guerré, S. Palmade, Optimization of fixed-bed methanation reactors: Safe and efficient operation under transient and steady-state conditions, Chem Eng Sci 192 (2018) 1124–1137. https://doi.org/10.1016/J.CES.2018.08.044.

[145] J. Ducamp, A. Bengaouer, P. Baurens, Modelling and experimental validation of a CO2 methanation annular cooled fixed-bed reactor exchanger, Can J Chem Eng 95 (2017) 241–252. https://doi.org/https://doi.org/10.1002/cjce.22706.

[146] Shell-and-Tube Heat Exchangers, in: Kern's Process Heat Transfer, 2019: pp. 289–380. https://doi.org/https://doi.org/10.1002/9781119364825.ch7.

[147] The Heat Transfer Equation, in: Kern's Process Heat Transfer, 2019: pp. 159–216. https://doi.org/https://doi.org/10.1002/9781119364825.ch5.

[148] A. Campari, F. Ustolin, A. Alvaro, N. Paltrinieri, A review on hydrogen embrittlement and risk-based inspection of hydrogen technologies, Int J Hydrogen Energy 48 (2023) 35316–35346. https://doi.org/10.1016/J.IJHYDENE.2023.05.293.

[149] The American Society of Mechanical Engineers (ASME), Hydrogen Piping and Pipelines, 2020. https://www.asme.org/codes-standards/find-codes-standards/b31-12-hydrogen-piping-pipelines (accessed March 17, 2023).

[150] P.J. Lunde, F.L. Kester, Rates of methane formation from carbon dioxide and hydrogen over a ruthenium catalyst, J Catal 30 (1973) 423–429. https://doi.org/10.1016/0021-9517(73)90159-0.

[151] G.D. Weatherbee, C.H. Bartholomew, Hydrogenation of CO2 on group VIII metals: II. Kinetics and mechanism of CO2 hydrogenation on nickel, J Catal 77 (1982) 460–472. https://doi.org/10.1016/0021-9517(82)90186-5.

[152] L. Marrelli, Reattori chimici. Teoria elementare ed applicazioni, Second Edition, 2017.

[153] F. Celoria, F. Salomone, A. Tauro, M. Gandiglio, D. Ferrero, I. Champon, G. Geffraye, R. Pirone, S. Bensaid, Kinetic study and deactivation phenomena for the methanation of CO2 and CO mixed syngas on a Ni/Al2O3 catalyst, Chemical Engineering Journal 512 (2025) 162113. https://doi.org/10.1016/J.CEJ.2025.162113.

[154] J. Xu, G.F. Froment, Methane steam reforming, methanation and water-gas shift: I. Intrinsic kinetics, AIChE Journal 35 (1989) 88–96. https://doi.org/https://doi.org/10.1002/aic.690350109.

[155] F. Koschany, D. Schlereth, O. Hinrichsen, On the kinetics of the methanation of carbon dioxide on coprecipitated NiAl(O)x, Appl Catal B 181 (2016) 504–516. https://doi.org/10.1016/J.APCATB.2015.07.026.

[156] I. Champon, A. Bengaouer, A. Chaise, S. Thomas, A.C. Roger, Carbon dioxide methanation kinetic model on a commercial Ni/Al2O3 catalyst, Journal of CO2 Utilization 34 (2019) 256–265. https://doi.org/10.1016/J.JCOU.2019.05.030.

[157] C. V. Miguel, A. Mendes, L.M. Madeira, Intrinsic kinetics of CO2 methanation over an industrial nickel-based catalyst, Journal of CO2 Utilization 25 (2018) 128–136. https://doi.org/10.1016/J.JCOU.2018.03.011.

[158] K.L. Fischer, M.R. Langer, H. Freund, Dynamic Carbon Dioxide Methanation in a Wall-Cooled Fixed Bed Reactor: Comparative Evaluation of Reactor Models, Ind Eng Chem Res 58 (2019) 19406–19420. https://doi.org/10.1021/acs.iecr.9b02863.

[159] F. Benyahia, K.E. and O'Neill, Enhanced Voidage Correlations for Packed Beds of Various Particle Shapes and Sizes, Particulate Science and Technology 23 (2005) 169–177. https://doi.org/10.1080/02726350590922242.

[160] I.I.I. Alkhatib, A. AlHajaj, A. Almansoori, L.F. Vega, Accurate Predictions of the Effect of Hydrogen Composition on the Thermodynamics and Transport Properties of Natural Gas, Ind Eng Chem Res 61 (2022) 6214–6234. https://doi.org/10.1021/acs.iecr.2c00363.

[161] M. De Falco, M. Capocelli, A. Basile, Selective membrane application for the industrial one-step DME production process fed by CO2 rich streams: Modeling and simulation, Int J Hydrogen Energy 42 (2017) 6771–6786. https://doi.org/10.1016/J.IJHYDENE.2017.02.047.

[162] D.W. Green, R.H. Perry, Perry's Chemical Engineers' Handbook, Eighth Edition, 8th ed. /, McGraw-Hill Education, New York, 2008. https://www.accessengineeringlibrary.com/content/book/9780071422949.

[163] M. De Falco, L. Di Paola, L. Marrelli, Heat transfer and hydrogen permeability in modelling industrial membrane reactors for methane steam reforming, Int J Hydrogen Energy 32 (2007) 2902–2913. https://doi.org/10.1016/J.IJHYDENE.2007.04.014.

[164] L. Colelli, C. Bassano, N. Verdone, V. Segneri, G. Vilardi, Power-to-Gas: Process analysis and control strategies for dynamic catalytic methanation system, Energy Convers Manag 305 (2024) 118257. https://doi.org/10.1016/J.ENCONMAN.2024.118257.

[165] T. Schaaf, J. Grünig, M.R. Schuster, T. Rothenfluh, A. Orth, Methanation of CO2 - storage of renewable energy in a gas distribution system, Energy Sustain Soc 4 (2014) 2. https://doi.org/10.1186/s13705-014-0029-1.

[166] J. Crane, C.-T. Dinh, Strategies for decarbonizing natural gas with electrosynthesized methane, Cell Rep Phys Sci 3 (2022). https://doi.org/10.1016/j.xcrp.2022.101027.

[167] J.L. Zachariah-Wolff, T.M. Egyedi, K. Hemmes, From natural gas to hydrogen via the Wobbe index: The role of standardized gateways in sustainable infrastructure transitions, Int J Hydrogen Energy 32 (2007) 1235–1245. https://doi.org/10.1016/J.IJHYDENE.2006.07.024.

[168] J. Klimstra, Interchangeability of Gaseous Fuels ? The Importance of the Wobbe-Index, SAE Transactions 95 (1986) 962–972. http://www.jstor.org/stable/44718173.

[169] A. Franco, M. Rocca, Industrial Decarbonization through Blended Combustion of Natural Gas and Hydrogen, Hydrogen 5 (2024) 519–539. https://doi.org/10.3390/hydrogen5030029.

[170] K. Lee, P. Sun, A. Elgowainy, K.H. Baek, P. Bobba, Techno-economic and life cycle analysis of synthetic natural gas production from low-carbon H2 and point-source or atmospheric CO2 in the United States, Journal of CO2 Utilization 83 (2024) 102791. https://doi.org/10.1016/J.JCOU.2024.102791.

[171] R. Chebbi, M. Qasim, N. Abdel Jabbar, Optimization of triethylene glycol dehydration of natural gas, Energy Reports 5 (2019) 723–732. https://doi.org/10.1016/J.EGYR.2019.06.014.

[172] E. Giglio, M. Bianco, G. Zanardi, E. Catizzone, G. Giordano, M. Migliori, Direct biogas methanation via renewable-based Power-to-Gas: Techno-economic assessment based on real industrial data, Energy Convers Manag 332 (2025) 119775. https://doi.org/10.1016/J.ENCONMAN.2025.119775.

[173] L. Mazzeo, A. Bertino, R. Lo Bianco, E. Mattei, S. Marta, F. Curioni, V. Piemonte, Kinetics of hydrogen-oxygen catalytic recombination at low oxygen levels and ambient temperature, Chemical Engineering Journal 509 (2025) 161546. https://doi.org/10.1016/J.CEJ.2025.161546.

[174] A.W. Zimmermann, J. Wunderlich, L. Müller, G.A. Buchner, A. Marxen, S. Michailos, K. Armstrong, H. Naims, S. McCord, P. Styring, V. Sick, R. Schomäcker, Techno-Economic Assessment Guidelines for CO2 Utilization, Front Energy Res 8 (2020). https://doi.org/10.3389/fenrg.2020.00005.

[175] S.S. Ravi, J. Mazumder, J. Sun, C. Brace, J.W. Turner, Techno-Economic assessment of synthetic E-Fuels derived from atmospheric CO2 and green hydrogen, Energy Convers Manag 291 (2023) 117271. https://doi.org/10.1016/J.ENCONMAN.2023.117271.

[176] Z. Lv, H. Du, S. Xu, T. Deng, J. Ruan, C. Qin, Techno-economic analysis on CO2 mitigation by integrated carbon capture and methanation, Appl Energy 355 (2024) 122242. https://doi.org/10.1016/J.APENERGY.2023.122242.

[177] Eurostat, Eurostat Energy Database, (n.d.). https://ec.europa.eu/eurostat/web/energy/database (accessed September 27, 2025).

[178] J.M. Uribe, S. Mosquera-López, O.J. Arenas, Assessing the relationship between electricity and natural gas prices in European markets in times of distress, Energy Policy 166 (2022) 113018. https://doi.org/10.1016/J.ENPOL.2022.113018.

[179] B. Zakeri, I. Staffell, P.E. Dodds, M. Grubb, P. Ekins, J. Jääskeläinen, S. Cross, K. Helin, G. Castagneto Gissey, The role of natural gas in setting electricity prices in Europe, Energy Reports 10 (2023) 2778–2792. https://doi.org/10.1016/J.EGYR.2023.09.069.

[180] M. De Falco, M. Capocelli, Process analysis and plant simulation in a sustainable economy, Stud Surf Sci Catal 179 (2020) 121–140. https://doi.org/10.1016/B978-0-444-64337-7.00008-2.

[181] M. De Falco, G. Natrella, M. Capocelli, P. Popielak, M. Sołtysik, D. Wawrzyńczak, I. Majchrzak-Kucęba, Exergetic Analysis of DME Synthesis from CO2 and Renewable Hydrogen, Energies (Basel) 15 (2022). https://doi.org/10.3390/en15103516.

[182] B. Igliński, U. Kiełkowska, K. Mazurek, S. Drużyński, M.B. Pietrzak, G. Kumar, A. Veeramuthu, M. Skrzatek, M. Zinecker, G. Piechota, Renewable energy transition in Europe in the context of renewable energy transition processes in the world. A review, Heliyon 10 (2024) e40997. https://doi.org/10.1016/J.HELIYON.2024.E40997.

[183] W. Gorman, J.M. Kemp, J. Rand, J. Seel, R. Wiser, N. Manderlink, F. Kahrl, K. Porter, W. Cotton, Grid connection barriers to renewable energy deployment in the United States, Joule 9 (2025) 101791. https://doi.org/10.1016/J.JOULE.2024.11.008.

[184] S. Saha, M.I. Saleem, T.K. Roy, Impact of high penetration of renewable energy sources on grid frequency behaviour, International Journal of Electrical Power & Energy Systems 145 (2023) 108701. https://doi.org/10.1016/J.IJEPES.2022.108701.

[185] M. and M.C. and H.M.Z. Bjørn Anders and Owsianiak, LCA History, in: R.K. and O.S.I. Hauschild Michael Z. and Rosenbaum (Ed.), Life Cycle Assessment: Theory and Practice, Springer International Publishing, Cham, 2018: pp. 17–30. https://doi.org/10.1007/978-3-319-56475-3_3.

[186] J.B. Guinée, R. Heijungs, G. Huppes, A. Zamagni, P. Masoni, R. Buonamici, T. Ekvall, T. Rydberg, Life Cycle Assessment: Past, Present, and Future, Environ Sci Technol 45 (2011) 90–96. https://doi.org/10.1021/es101316v.

[187] M. Finkbeiner, E.M. Schau, A. Lehmann, M. Traverso, Towards Life Cycle Sustainability Assessment, Sustainability 2 (2010) 3309–3322. https://doi.org/10.3390/su2103309.

[188] Society of Environmental Toxicology and Chemistry (SETAC), Guidelines for Life-Cycle Assessment: A "Code of Practice," Environmental Science and Pollution Research 1 (1993) 55. https://doi.org/10.1007/BF02986927.

[189] The International Organization for Standardization (ISO), ISO 14042:2000 Environmental management - Life cycle assessment - Life cycle impact assessment, (2000). https://www.iso.org/standard/23153.html (accessed November 25, 2022).

[190] Commission of the European Communities, Communication from the Commission to the Council and the European Parliament - Integrated Product Policy Building on Environmental Life-Cycle Thinking, 2003. http://europa.eu.int/comm/environment/ipp/ippsum.pdf.

[191] The International Organization for Standardization (ISO), ISO 14025:2006 Environmental labels and declarations - Type III environmental declarations - Principles and procedures, (2006). https://www.iso.org/standard/38131.html (accessed February 6, 2023).

[192] S. Sala, A.M. Amadei, A. Beylot, F. Ardente, The evolution of life cycle assessment in European policies over three decades, Int J Life Cycle Assess 26 (2021) 2295–2314. https://doi.org/10.1007/s11367-021-01893-2.

[193] European Commission Joint Research Centre, International Reference Life Cycle Data System (ILCD) Handbook: general guide for life cycle assessment, detailed guidance, Publications Office, 2011. https://doi.org/doi/10.2788/38479.

[194] European Commission Joint Research Centre, International Reference Life Cycle Data System (ILCD) Handbook: framework and requirements for life cycle impact assessment models and indicators, Publications Office, 2011. https://doi.org/doi/10.2788/38719.

[195] A. Giocoli, V. Motola, N. Scarlat, N. Pierro, S. Dipinto, Techno-economic viability of renewable electricity surplus to green hydrogen and biomethane, for a future sustainable energy system: Hints from Southern Italy, Renewable and Sustainable Energy Transition 3 (2023) 100051. https://doi.org/10.1016/J.RSET.2023.100051.

[196] Snam, Technical data for the network, (n.d.). https://www.snam.it/en/our-businesses/transportation/business-information/technical-data-for-the-network.html (accessed September 27, 2025).

[197] M. Netušil, P. Ditl, Natural Gas Dehydration, in: S.B. Gupta (Ed.), Natural Gas, IntechOpen, Rijeka, 2012: p. Ch. 1. https://doi.org/10.5772/45802.

[198] S. Chen, G. Chen, X. Zhao, X. Luo, H. Gao, W. Li, Z. Liang, Feasibility analysis and process simulation of CO2 dehydration using triethylene glycol for CO2 pipeline transportation, Chin J Chem Eng 40 (2021) 179–186. https://doi.org/10.1016/J.CJCHE.2020.12.025.

[199] A.J. Akande, R.O. Idem, A.K. Dalai, Synthesis, characterization and performance evaluation of Ni/Al2O3 catalysts for reforming of crude ethanol for hydrogen production, Appl Catal A Gen 287 (2005) 159–175. https://doi.org/10.1016/J.APCATA.2005.03.046.